Dear Dr. Hargraves,

Please find below comments by the executive editor (David Ham) and two reviewer's comments in blue, and my response in black. I am very thankful to the reviewers, and in particular for the in-depth review provided by the second reviewer (Dr. Marcello Vichi), that has much improved the manuscript.

Yours sincerely,

Mark Baird

Executive Editor comment.

This comment addresses the compliance of the manuscript with GMD policy on code and data availability. The issues raised here must be satisfactorily addressed before a revised manuscript can be accepted for publication. Thank you for publishing the full source of your model. The one technical issue is that GitHub, while an excellent development platform, is not a suitable persistent archive for citable code. Indeed, GitHub themselves tell you this and provide instructions as to how to obtain a citable archive of a particular release of a GitHub project using their interface to the Zenodo archive1 . Please provide a proper persistent archive of the exact version of the code you are documenting (the GitHub Zenodo integration makes this very easy).

We will retain the GitHub archive, but have also added an entry in the permanent CSIRO software collection which has the citation:

CSIRO (2019): EMS Release v1.1.1. v1. CSIRO. Software Collection. https://doi.org/10.25919/5e701c5c2d9c9.

[email advice from Dr. Ham suggested this would meet the journal's requirements].

Please also ensure that any files required to run the verification experiments are also archived (it's possible this data is already on the thredds server you currently cite, in which case simply making this explicit would suffice).

Section 13 (Section 11 in the original manuscript) provides the means to download a complete model system with all forcing and configuration files.

Reply Reviewer #1.

The manuscript provides a compilation of many individuals' past coding efforts to develop the EMS. The model, consisting of biogeochemical, optical, and sedimentary components, is within the scope of GMD and scientifically relevant. Collecting the mathematical descriptions of the major model components into a single document linked to the model code and User Guide might improve convenience for EMS users. The authors provide sufficient documentation to reproduce their results. The language is clear and the presentation is well-structured, though a spellchecker should be run on the document as there are a number of typos.

Thank you.

Most, if not all, of the material has been previously published in the peer-reviewed literature. Hence, the material cannot be considered novel, nor does the manuscript represent a substantial advance in modelling.

As pointed out by the reviewer, a number of individual process parameterisations in the model have been published before. When these published papers contain complete sections that are exactly the same as version B3p0, such as the seagrass and coral model parameterisations, we have not re-derived the model equations, but just included tables of parameter values and equations.

Many of the formulations have not been published before, or have been updated from much earlier work. But most importantly, some aspect of the model approach only become apparent, and reproducible, when the entire model is described together.

To summarise the unpublished components (numbering uses original manuscript):

Previously unpublished formulations.

- Preferential ammonia uptake that considers the physical limit to ammonia uptake due to diffusion to the uptake surface.
- Oxygen balance that includes chemical oxygen demand as well as the oxygen content of nitrate. This requires new equations for the differing implications for oxygen of anerobic versus aerobic remineralisation of organic matter.
- The zooplankton grazing on model microalgae that contain the definition of internal reserves used in EMS
- Phosphorus immobilisation.
- Gas exchange and equilibrium carbon chemistry – a combination of other studies, but also adapted to the EMS model structure.

Updated formulations building on previous work.

- Optical model. An earlier manuscript (Baird et al., 2016) described a new optical model that included some IOPs, but this work much expands the use of mineralogical-based inorganic particulate IOPs, as well as an extensive library of pigment-specific absorption coefficients.
- Further expansion of optical implications of benthic habitat, and, in particular, the role of symbionts (Eq. 212-214).
- Aragonite saturation state -depended coral calcification and dissolution (Table 33).
- Revised calcification rate calculation based on the physiological state of symbionts (Eq. 192)
- Revised phosphorus absorption-desorption model (Section 3.5.3).
- Revised nitrogen-fixing *Trichodesmium* formulation (Section 3.4).
- Differential breakdown rates of detrital and organic phosphorus when compared to nitrogen.
- Improved nitrification / denitrification model with new sigmoidal formulation for stability at the transition between oxic and anoxic conditions.

Novel aspects apparent in whole model description.

- Derivation of planktonic rates using the individual rather than the population.
- Systematic use of geometric descriptions of ecological rates.

- Process-based scientific description so that individual formulations can be easily extracted for use by other modellers.
- The details of mass balance equations of C, N, P, and O that can be dissolved, contained within particles, and that are distributed within 3D volumes of water column and porewaters, and as 2D masses on the sediment-water column interface.

Finally, readers might also find some aspects of the model presentation worth considering. For example, we used integer values for stoichiometric ratios in the equations (i.e.$\frac{16}{106}\frac{12}{14}$), consistently throughout the manuscript. I think this improves readability over a large number of stoichiometric coefficients.

Because this manuscript represents a collection of previously published work, little effort is spent explaining why parameterisations are the way they are. While methods and assumptions may be valid, they are not always clearly outlined.

I don't think this is a fair comment. The reason the manuscript is so long is because there are descriptions of why certain formulations were chosen. For example, arguably the most important functional form in the whole model, relating benthic cover to biomass, has a large section dedicated to its explanation (beginning of section 6). Another example of a basic explanation is Fig. 12, the schematic of the growth from reserves.

Nonetheless, the 2nd reviewer wanted a more thorough introduction of internal reserves, and this is now given.

References to the primary literature are given, but the manuscript cannot be understood by a non-expert reader as a stand-alone document.

Following the suggestion of the other reviewer, three new sections, "Structure of the model description", "Presentation of process equations" and "Model stoichiometry", have been added at the beginning. These hopefully provide more background for the non-expert reader.

Likewise, the model is given a perfunctory evaluation that includes no discussion of the biases. More detailed assessments are cited, but the reader of the present manuscript is left with no real understanding of why the model performs well (and what biases may be due to) in the examples provided.

I agree the model evaluation is brief. A thorough model evaluation would add much to the length of the manuscript, and repeat that already undertaken in other work, particularly Skerratt et al., 2019.

A thorough discussion of systematic biases across ecosystems could represent a major advance for the model. Included in this meta-analysis should be a description of how the many "not attributed" parameters (in the supplement) are tuned. Perhaps the authors could even go further, and address those biases by presenting an improved model.

An analysis of how a single model performs across many environments is an interesting task, and versions of this have been undertaken by, for example, studying how differing global biogeochemical models perform in different regions of the world. But the coastal environment, with its multiple habitat types make this virtually impossible.

Reviewer #2

This is an extremely in-depth review, and I greatly appreciate all of the comments by the reviewer. When submitting to this journal I was hoping for such a review to help us improve our work. Thank you so much.

This manuscript offers a description of the Environment Modelling Suite (EMS) developed over several years in Australia by CSIRO. It is based on a set of existing publications, as well as some on-line documentation. Despite the limited amount of original material included in this manuscript, I see the value of its publication, because it would offer a single point entry for new users interested in approaching such a complex suite. It would also be a supporting reference document for further scientific applications in other regions.

Thank you.

1 Main comments

I have some major concerns, that I would like the authors to address before resubmitting the manuscript

1. It is a very lengthy manuscript, that does not have distinct points of entry.

I apologise for the length. To reduce its size I have placed in the supplementary material components that lead to the calculation of remote-sensing reflectance, and thus true colour. These are essentially diagnostic variables, and therefore not necessary for the core model. I have also removed "Model User" components.

> In its current version, it needs to be read sequentially in order to appreciate the various components. I would suggest the authors to separate the pelagic from the benthic component, especially because the community of scientists is rather different, and this would also allow to clarify some aspects of the coupling with the transport processes that are a bit overlooked. This would help the referees to focus more on the original components of the model because they would be closer to their expertise, and would provide a more informed assessment.

It is true that different scientific communities often exclusively model pelagic or benthic processes. For example, benthic modellers often consider habitats and diversity rather than nutrients. However the closest model to EMS, the ERSEM model, also describes pelagic and benthic processes in the same GMD paper:

Butenschön et al., ERSEM 15.06: a generic model for marine biogeochemistry and the ecosystem dynamics of the lower trophic levels Geosci. Model Dev., 9, 1293–1339, 2016

Also, I would argue that the key innovation of this model, as stated on page 4 line 13 of the original submission, is:

"the most important consequence of using geometric constraints in the BGC model is the representation of benthic flora as two dimensional surfaces, while plankton are represented as three dimensional suspended objects"

This innovation is most apparent when the pelagic and benthic models are described together.

2. In the current state, it looks more of a hybrid combination between a user manual, a scientific model description, a technical report and a summary of model applications. I

would suggest the authors to better clarify their aims and decide which approach is the main one. In particular, it is not clear how the authors decided to include a full description of certain aspects, while for others they refer the reader to published literature in toto.

The primary aim of the paper is a scientific model description. The two sections that are referenced off in toto are the coral and seagrass sections, although the equations are retained. The rationale for this is that these two sections are described virtually exactly in the journal articles as in the software version (B3p0), and the journal they are published in, Ecological Modelling, allows full scientific descriptions.

I have moved two sections that looked 'code'-like to the supplementary material.

3. Three unique features are listed in the Introduction (pag 6), but it is not clear how innovative they are with respect to other published works (e.g. Dutkiewicz et al., 2015).

The manuscript splits the unique aspects of the model into two lists, one set derived with geometric origins (which I would argue is innovative too), and a second more generic list that this comment refers to (p6). As the reviewer points, the second list involves new equations, but some of them are approximations when others such as Dutkiewicz have equivalent, and perhaps better solutions. I have added a brief reference to the approximate nature of these features.

4. I am concerned about the lack of discussion on the model science and what differentiates it from the other available open-source models. There is a cursory introduction on how the model differs from other approaches, although they are lumped into being Fasham-like, which is actually inaccurate, since several models consider stoichiometry and the internal storage of nutrient and energy (for instance Lancelot et al., 1993,2000; Baretta et al., 1995; Vichi et al., 2007). Aumont et al., 2015 and Butenschoen et al 2016 are indeed referenced, but to remark the need for thorough description of models).

New section in the Discussion added: "Comparison with other marine biogeochemical models" (p77 of revised manuscript)

Rather strikingly, only by looking at Table 6 the (skilled) readers understands that the main currency of the model is nitrogen and that biomass is measured in N concentration units. I am not suggesting to have an additional lengthy discussion on the type of biogeochemical models, but just to make the reader aware of what are the peculiarities of this approach with respect to others.

Thank you. Upon re-reading, I agree the section on microalgae growth does not give enough context to the reader. Further that when it does come in, it follows a particular line of equation development. I have added a significant contextual start to this section before pursing the particular model I have chosen. (p24 of revised manuscript)

The scaling or geometric constraints are indeed a special feature of this modelling approach, although it should be clarified that models with multiple functional types also includes implicit size considerations in the value of the parameters.

In the modelling of plankton, geometric and size-based properties are similar concepts, and I have included a reference to size-based trait modelling. However geometric-constraints is broader than just size, as illustrated in the next section (on 2D leaves vs 3D microalgae).

> The concept that geometric description is a means to reduce parameter uncertainties (pag 4, L1-3) would also require further clarification, especially because this model implements only two size classes with generic functions, which means it has a limited range of applications in the coastal region.

Yes. Thank you. An example makes a more powerful point. The best illustration is in the relationship between benthic cover and seagrass nitrogen. I have added a few sentences when I get to this example on the next page of the manuscript. (L6, P6 of new manuscript)

> If the Si or Fe cycles would need to be resolved, or specific harmful algae, then additional parameters would be forcibly needed.

Yes, some new stoichiometric coefficients for the new elements. The EMS ecology library does contain a harmful algal bloom category, but because it is a process that can be excluded, and wasn't used in the simulations shown in the results, we have decided not to include a description here.

2 Detailed comments

P6L14-15 There should be some description on what Fig. 3 shows. Since it is used in the introduction, I would expect some more context. However, the authors suggest me to go and read Baird et al. 2016 to understand the figure (and what is GBR4 at this stage?)

I have removed this figure as true colour is a diagnostic variables and not essential.

Sec 1.1: This is the most important section when engaging with a manuscript of this size. However, it offers only a quick list of the upcoming sections, something akin to what is offered in shorter manuscripts. The authors state that descriptions are sorted by processes, but I would argue with this statements, since some processes are spread across various sections and there are several cross-references that interrupt the flow of the description.

The biogeochemical processes are distinct, as demonstrated by the fact that each table of equations conserves mass. But the reviewer might be getting at the fact that light absorption appears in two places, because it is part of the optical model and the ecological process of photosynthesis. Following suggestions elsewhere in this review, I have combined the optical model components, and now make this structure clearer from the beginning. (P11 – 23, revised manuscript)

I would also strongly advocate against the offered solution to the reader (L26-28): to combine all the various process terms to obtain the complete differential equation. This is in my opinion what makes the manuscript more difficult to read, since there is no full appreciation of the dynamics of each state variable. This approach was also followed by Vichi et al. (2007), but in that case, a specific notation was introduced and the full dynamics were presented.

The reviewer is supporting our approach of presenting partial differential equations for each processes. Looking at Vichi et al., (2007) this paper has an excellent introduction to how the model presented. I have copied this approach, adding three new subsections, "Structure of the model description", "Presentation of process equations" and "Model stoichiometry". (p10-12 of new manuscript)

Sec 2. I have a few problems with the organization of this section. The EMS biogeochemical model has not been introduced yet (while the next Fig. 4 and 5 are about the biogeochemical model and not the optics), but the reader is offered an initial description with no references of the science of IOP and AOP. I would suggest to invert the order and first illustrate the model structure, then highlighting the details of the optical model.

I mostly agree with these comment, and have re-organised the manuscript by:

1. Extracting all components of the optical model that involve calculating the light field into a separate section titled "Optical model", with subsections "Pelagic optical model", "Epibenthic optical model" and "Sediment optical model".
2. Point 1 allows for a section to describe the IOP / AOP terminology that is very familiar to optical modellers, but is only beginning to be adopted by biogeochemical modellers.
3. Removed all calculations of remote-sensing reflectance. This is a diagnostic variables, and for sake of brevity description of all diagnostic variables has been removed from the manuscript.

I have put the optical model before the BGC model because the EMS suite can be used with an optical model but no biogeochemical processes, but there can be no biogeochemical model (at least with autotrophs) without an optical model.

Otherwise, the authors can opt for a shorter manuscript that would focus on the optical model only if they consider this the most innovative component.

No, I am emphasising the BGC model. In fact, as mentioned later, I have removed the components describing the calculation of remote-sensing reflectance.

At Pag. 9 L19 microalgae are mentioned, but there is no mathematical equivalence neither an explanation of what small and large means. I recognize that there are tables later in the model where size classes are provided, but a set of ranges should be given from the beginning, especially because of the emphasis on geometric constraints.

OK. Included comment on size and function role of different plankton. (p8, L6 of new manuscript)

P10L12 The authors should state what kind of approximation they make when considering dissolved and particulate concentrations of pelagic variables affected by transport processes. The basic approximation of fluid dynamics is the continuum hypothesis, which should also be considered for biogeochemistry (e.g. O'Brien and Wroblewski, 1973; Vichi et al., 2007). I understand that this is an aspect that was overlooked in the early works (Nihoul, 1975; Fasham et al, 1990, etc), but it is nowadays essential given the increasing resolutions of hydrodynamic models.

Text add (p11 of new manuscript):

The advection-diffusion terms of Eq. 1, based on the continuum hypothesis for a fluid (Vichi et al., 2007), are solved by either an in-line advection scheme with the baroclinc timestep of the hydrodynamic model, or an offline transport scheme using a potentially much longer timestep (Gillibrand and Herzfeld, 2016). Options in EMS include mass conservative Lagrangian and flux-form schemes described in Herzfeld (2006) and Gillibrand and Herzfeld (2016).

P10L17 I would suggest the authors to give information on whether the model has been coupled with other hydrodynamic models.

Included reference to application of the plankton model coupled to the Princeton Ocean Model. (p11 of new manuscript)

P10L22 This is one of the many cases where the authors start an explanation and then drop it abruptly referring to published papers (see my main comment 2 above)

Yes, but this part is well described elsewhere, and the manuscript is already too long.

Sec 3.2. What is the difference with Sec. 2.1 and why two separate sections are needed?

Agreed. Removed.

P23L18 Please define a "function group"

I meant functional groups. Thank you.

P23L23 I think that the concept of internal reserves is an essential one to understand the equations. Nevertheless, the authors refer to Fig. 3 in another paper (see main comment 2)

My mistake. A version of this figure is actually in this paper. Cross-reference fixed.

P24 Table 4 caption: the authors should explain what they mean by cells here. Mean population characteristics? This is not introduced anywhere in the main text.

I have removed 'cells' in the Table caption. However, the concept of 'cell' vs. 'population' is important in the model formation. This even gets a mention in the abstract "A second focus has been on, where possible, the use of geometric derivations of physical limits to constrain ecological rates, which generally requires population-based rates to be derived from initially considering the size and shape of individuals."

Since the most important implications of cell vs. population are in microalgae, I have included a new section 5.1.5 in the revised manuscript. (p28 of new manuscript)

P24L7-8 and L10 The variable R* is introduced and used without any context. I would suggest to show an equation defining R* instead of a figure.

Agreed. Beginning of "Microlagae growth" now includes a section on reserves. (p24 of new manuscript)

P25L7 Menten

Spelling fixed.

Sec 3.3.3 I am struggling with this section. There is very little structure in the description. I can follow the flow because of my experience in numerical models, but to my understanding this manuscript should introduce the model to a larger audience and expand its usage beyond the group of developers (main comment 1 above). I think the authors need to make a decision on what is the narrative approach they want to have, either from the point of view of the optics or from the biogechemistry and ecosystem viewpoint.

The focus is biogeochemistry. Optics component has been scaled back to that required to calculate light field and therefore photosynthesis.

I understand that from the point of view of an optical model, the absorption cross section is independent of the physiology and definition of phytoplankton. However, treating separately eq 6 and the variable rho does make the reading more difficult. At the risk of being pedantic, I think one

should first present the dynamics in eq 37 and then illustrate the various terms. I'm particularly thinking about a student user who would like to learn the model and who may not have a full understanding of the underlying physiology.

To be helpful, I cross-reference chlorophyll synthesis as influencing intracellular concentrations in the optical model, and the role of absorption cross section in determining chlorophyll synthesis term in the BGC model. I have left the order of the manuscript the same.

P27L20 and L28 Table 6 is referenced before Table 5, which is the one listing the state variables whose dynamics is listed in Table 6.

Rearranged Table citations.

I would strongly suggest that a full list of the state variables is given at the very beginning when the biogeochemical model is introduced.

There is a full list in the Appendix. The philosophy of introducing one process at time is important to model framework, and I think also the scientific description (i.e. microalgae nutrient uptake does not depend directly on whether a seagrass community is there or not).

In P27L20, Tab 5 presents state and diagnostic variables, not equations.

Fixed.

P28L4 Please refer to the eq numbers and not just the table.

Fixed.

P30L2-3 This is an important information that should be given in the introduction, and briefly expanded upon to clarify how this models is positioned in the context of the existing theories and methodologies.

Yes, this has moved to the top of the microalgae model section. I haven't moved it into the introduction, because the introduction concentrates on the components of the model, rather than the equations.

Sec3.6. The mathematical formulation and equations are very little detailed for this component.

I have added a section referring to other saturating zooplankton grazing terms. Also, to help negotiate the equations I have cross-referenced some of the equations individually from the text. (p35 of new manuscript)

Table 14 containing the dynamics is just referenced, and there is not a single equation describing the biomass evolution.

Eq. 76 in the original manuscript is biomass evolution.

It is also not clear from the beginning that the zooplankton variable has no variable stoichiometry (or internal reserves).

OK. Made this clear at the top of the zooplankton equation description. (p35 of new manuscript)

P35L13 This is a coarse over-generalization which does not pay much attention to the model development occurred in the past 30 years. Models that use preference factors and a food matrix do not have this issue (Gentleman et al., 2003).

Yes. I looked up a range of papers, and my preconceptions were out of date. I have removed a few sentences. Thank you.

Sec 3.6.1 Grazing is actually not illustrated in this section.

Improved the model schematic in Section 2.2 to better resolve grazing interactions, showing microzooplankton eating small phytoplankton, large zooplankton eating large phytoplankton, *Trichodesmium* and microphytobenthos, and large zooplankton eating small zooplankton.

Table 15 is just mentioned but the specific terms not described. It is not much clear what is the foodweb accessed by zooplankton, apart from the first generic sentence at the beginning of sec. 3.2. How the fluxes between the state variables are actually computed is not clear.

Yes, I agree, the diets of the zooplankton were not mentioned in Sec 3.6. Fixed.

Table 12 What is the difference between variable mn in Table 7 and variable mB?

No difference. I have revised all use of m and its subscripts with the following change:

Both be $m_{B,N.}$ Looked for other terms such as m_P that I made $m_{B,N}$.

Sec. 3.8 I suggest the authors to make specific reference to the numbered equations and not to the Table containing them

I have done this in some cases.

(also check the typo at line 9 same page “zooplankton plankton”)

Typo fixed.

Sec 3.9 I would see the section on non-grazing plankton mortality to be more pertinent to plankton dynamics, and less to zooplankton grazing. Is zooplankton mentioned at L6 because this is a loss term for all the plankton? It is rather confusing, and proper structuring would be helpful.

I have replaced ‘phytoplankton mortality’ with ‘plankton mortality’, which is what was meant.

Sec 3.10 I guess the author means gas exchange at the surface of the ocean here.

Title changes to: “Air-sea gas exchange”

P41L3 The variable is u10. This is the cubic function.

Thank you. Removed power of three.

P41L18 positive

Replaced.

P41L31 This seems a fragment with no connection with the previous paragraph.

Thank you. Fragment removed.

P42L22 Please clarify what “vertical order” means.

Replaced with “from top to bottom”

P43L18 Please refer where the diffusivity values have been taken. I could not find a table with the values.

Thank you. I refer back to the Table with the first use of diffusivity coefficients, and now also reference the original source, Li and Gregory (1974).

Eq113 and other. I would suggest the authors to use named constant for the stoichiometric coefficients, to allow identifying which conversion is actually being done.

In this manuscript I have made a deliberate decision to represent stoichiometric coefficients with combinations of integers. The reviewer's suggestion, to replace these with coefficients, would follow the approach generally used by biogeochemical modellers. However, I wonder if the use of integers is better. It is, after all, the way that it is done in physical chemistry. Also, there would be three stoichiometric coefficients for each autotroph, requiring unique subscripts, challenging the readability of the equations. The slight correction required for isotopes is small (Section 7.4.1 in original manuscript) and has been accounted for in the model itself.

Also, the authors should briefly illustrate the rationale for the use of this multiple minimum function, which I guess is linked to the maintenance of the constant stoichiometry in this functional group biomass.

OK. Added (p45 of new manuscript):

We have used the commonly applied multiple minimum function (Liebig, 1840), although it is noted that others use the multiple of limitation terms (Fasham, 1993). The microalgae model described above uses dynamical reserves to determine the growth rate. The growth approximated using dynamical reserves closer approximates a multiple minimum function than a multiple of minimum terms, so it was deemed more appropriate to use a multiple minimum function for macroalgae and seagrass for which internal reserves were not resolved.

P49L1 This is another example of the main problem I have with this manuscript (main comment 2). The same can be found at L29 w=in the case of coral processes. The authors seem to have cherry-picked what should be described and what should be left for the reader to scavenge through the literature. Please explain if there is an underlying rationale or a unified criterion.

Two papers exactly describe a subset of the equations in vB3p0. For coral processes:

Baird, M. E., M. Mongin, F. Rizwi, L. K. Bay, N. E. Cantin, M. Soja-Wozniak and J. Skerratt (2018) A mechanistic model of coral bleaching due to temperature-mediated light-driven reactive oxygen build-up in zooxanthellae. Ecol. Model 386: 20-37.

And for seagrass processes:

Baird, M. E., M. P. Adams, R. C. Babcock, K. Oubelkheir, M. Mongin, K. A. Wild-Allen, J. Skerratt, B. J. Robson, K. Petrou, P. J. Ralph, K. R. O'Brien, A. B. Carter, J. C. Jarvis, M. A. Rasheed (2016) A biophysical representation of seagrass growth for application in a complex shallow-water biogeochemical model *Ecol. Mod.* 325: 13-27.

The sections of these in the original submission failed this journal's plagiarism software. It was decided because these were the most detailed, and isolatable, sections of the model (and which are not implemented in all cases) they could be referenced to.

Some of the earlier papers (Baird et al., 2013 for example) include more fragmented sets of equations, but we consider it too difficult to bring them together in a coherent model description.

P49L6-7 These are microalgae, so I wonder why the authors decided not to use the same dynamics described earlier.

Good point. The dynamics are similar but we added a few extra processes to zooxanthellae, the most important being photoadaptation and photoinhibition, to resolve coral bleaching. While photoadaptation and photoinhibition could easily be added to the other microalgae, we would need to add 5 new state variables for each microalgae, or about twenty 3D new state variables that require advecting by the transport model, a large computational cost. In contrast, because the zooxanthellae remain in the coral host, they are only 2D variables and don't require advection.

P57 How is M computed?

This manuscript does not describe the dynamics of inorganic sediments, which determine *M*. I point the reader to section 5.1, which summarises some aspects of the sediment model, and then points the reader onto published papers of the sediment model.

P58L5 With the use of coding style, the manuscript turns towards the user manual. This is the first time that code is used in the document. I am not against it if properly explained, but makes the manuscript less coherent (see main point 2).

Agreed. Wrong place for this. Removed.

P58L7-8 Make reference to Table 34 where the variables are listed.

Yes. Thank you.

Sec 5.2.1 I am a bit confused here, because light is not an environmental variable that controls the dynamics in the sediment model. What is the difference with Sec. 4.2.2?

The derivation of light capture by macroalgae (and also seagrass) considers them to be a 2D leaf. In contrast, the microalgae are considered a layer of spheres lying in the top layer of the sediment. Thus the equation 112 (in the original manuscript) is fundamentally different to equation 206.

I understand that the optical model is a major part of this manuscript, but then I would separate the biogeochemistry from the optics in two different manuscripts and make reference when needed instead of mixing the descriptions (see main point 1).

It is my hope to have one succinct manuscript containing both the optical and biogeochemical components. Also, the biogeochemical model cannot exist without the optics model (although the reverse is not true)

Equally important, the key innovation of the model derivation is the geometric origin of the equations. Often this geometric origin results in similar forms in both the optical and biogeochemical models, such as the use of absorption cross-sections in Eq. 6, 12 and 35.

Sec 5.3.1 and 5.3.2 There is no reference to equation numbers in these short sections.

Yes. Thank you. Fixed by referencing to Eqs. in Table 37 by number.

Sec. 6 I understand that section 6 collects all processes that are common to the pelagic, epibenthic and benthic processes. Therefore, I would expect to find here cross-references to the other sections where they have been described, as well as the inverse (when the dynamics are first illustrated, inform the reader that a certain term is considered a common process and found in Sec. 6).

OK. Good point. The organisation is intended such that processes are fully contained within a section. BUT, as the pointed out by the reviewer, I fail this criteria with respect to temperature dependence of ecological rates and preferential ammonium uptake that are cross process. Section 6

has now been split into two sections, one that refers to common processes, and a second that is common parameterisations. These are now extensively cross-referenced.

P68L9-11 I agree with this sentence, but this would deserve some more discussion. According to the Introduction, the model is designed to be generic, and the combination of physical and biogeochemical processes may lead to stiffness (this is cursory mentioned somewhere in the text or in the captions). The authors can refer to Butenschön et al., 2012 for an illustration of the problem. I would also ask the authors to clarify what do they mean with the "time step of the splitting"? Different time steps can be used for the various steps, but I am not familiar with a splitting time step. (Please explain what GBR1-4 mean in the table)

The Hundsdorfer and Verwer reference is a 460 page textbook on advection-diffusion-reaction equations. But I wasn't aware of the Butenschön et al. (2012) which is more focus to marine models, and it is included in the references (p67, revised manuscript). I have removed reference to GBR1/GBR4 as these are particular configurations, and just retain the values used in the results presented (from GBR4). "Time step of the splitting" is removed, and the text amended to be more explicit as to what was meant.

P68L13 The choice of a 5th order ODE should be justified, especially in the case of empirically-derived parameterizations. Please also say here which scheme is used and that it includes adaptive stepping. This information is given further below somewhere.

Our approach is to split the description of the solvers which is described in the text, with the actual choice that is given in the Table. Thus, I have added more in the text about the choices that include 1^{st} – 8^{th} order, and then give further details in the table. The justification now appears in the text. I also moved the information from below to here. (p67 of new manuscript)

P69L2-4 This justification raises some concerns. The method is explicit, which would actually lead to instabilities that would require a time step shortening. Is this what the authors mean?

Yes, the adaptive approach reduces the time-step to avoid instabilities.

P69L16 Please explain the term "between". Is this implicit or explicit?

Replaced "between the physical and ecological" with "after the physical and before the ecological"

According to Table 42,it uses the same timestep as the ecology, but not clear what light environment is used for the ecology.

Added: "The light climate used for ecological timestep is that calculated at the start time of the ecological integration."

P70L9-10 This sentence is not clear. I understand that the manuscript is not about the coupling between the physics and the ecology, but this sentence would require more context. Please refer to the table where the number of levels in the described applications are listed.

Yes, this sentence has now moved into the Section 7.1, and some more context is given. Added text: "The solution of the ecological equations are independent for each vertical column, and depend only on the layers above through which the light has propagated." (p67 of new manuscript)

Sec 8 I would argue that this manuscript does not offer any model evaluation beyond what has been already published. Is the assessment done here a technical check that version vB3p0 produces the same results as vB2p0 described in Skerratt et al. (2019)?

Yes, it is about ensuring that there are results from the published version.

Sec 9 and 10. I am not sure these sections help the manuscript concept, and they confirm my impression of the lack of coherence in the original idea of the presentation (point 1 above). I would suggest the authors to reconsider their structure and to move some sections to the appendix or to on line material.

I would be happy to move these to supplementary material, but I think they are a requirement of the journal?

Sec 11 I have some concerns about the content of this discussion. I would expect Sec 11.1 in the introduction. I cannot really see any discussion here as I have indicated in my main point 3 above.

I think the reviewer would be happier if the discussion of other biogeochemical models (that I have expanded and now is in the discussion) be in the introduction, and the explanation of the geometric descriptions (which is in the introduction) be in the discussion.

I really want the reader to appreciate that I set out to produce a biogeochemical model that was based on geometric constraints that place physical limits on ecological processes. This has been the motivation from the start. I chose this approach on the 18 May 1996, the first day of my PhD. My Master supervisor, Marlin Atkinson at the University of Hawaii, was a pioneering advocate of physical limits on nutrient uptake by coral communities, and I was pig-headedly determined to try this for a biogeochemical model, whether my new PhD supervisor (Jacqui McGlade, University of Warwick) liked it or not (she gave me a free rein to pursue it). CSIRO has since supported me in this endeavour. My point is, the model equations would not be like they are had I not, in the subsequent 24 years, always asked myself when parameterising a process was there a geometric property I could take advantage off. Thus, the geometric approach is for me not a post-implementation talking point but the fundamental motivation of the work.

But I am not so pig-headed now, so if you want these sections reversed (introducing other models in the introduction and discussing EMS's unique features in the discussion) I will oblige.

Thank you.

CSIRO Environmental Modelling Suite (EMS): Scientific description of the optical and biogeochemical models (vB3p0).

Mark E. Baird[1], Karen A. Wild-Allen[1], John Parslow[1], Mathieu Mongin[1], Barbara Robson[2], Jennifer Skerratt[1], Farhan Rizwi[1], Monika Soja-Wozniak[1], Emlyn Jones[1], Mike Herzfeld[1], Nugzar Margvelashvili[1], John Andrewartha[1], Clothilde Langlais[1], Matthew P. Adams[3], Nagur Cherukuru[4], Malin Gustafsson[5], Scott Hadley[1], Peter J. Ralph[5], Uwe Rosebrock[1], Thomas Schroeder[1], Leonardo Laiolo[1], Daniel Harrison[6], and Andrew D. L. Steven[1]

[1]CSIRO, Oceans and Atmosphere, Hobart, Australia
[2]Australian Institute of Marine Science, Townsville, Australia
[3]School of Chemical Engineering, The University of Queensland, Brisbane, Australia
[4]CSIRO, Land and Water, Canberra, Australia
[5]Plant Functional Biology and Climate Change Cluster, Faculty of Science, University of Technology Sydney, Sydney, Australia
[6]Southern Cross University, Coffs Harbour, Australia

Correspondence: Mark Baird (mark.baird@csiro.au)

Abstract.

Since the mid 1990s, Australia's Commonwealth Science Industry and Research Organisation (CSIRO) has developed a biogeochemical (BGC) model for coupling with a hydrodynamic and sediment model for application in estuaries, coastal waters and shelf seas. The suite of coupled models is referred to as the CSIRO Environmental Modelling Suite (EMS) and has been applied at tens of locations around the Australian continent. At a mature point in the BGC model's development, this paper presents a full mathematical description, as well as links to the freely available code and User Guide. The mathematical description is structured into processes so that the details of new parameterisations can be easily identified, along with their derivation. ~~The EMS BGC model~~ In the EMS the underwater light field is simulated by a spectrally-resolved optical model that calculates vertical light attenuation from the scattering and absorption of 20+ optically-active constituents. The BGC model itself cycles carbon, nitrogen, phosphorous and oxygen through multiple phytoplankton, zooplankton, detritus and dissolved organic and inorganic forms in multiple water column and sediment layers. The ~~underwater light field is simulated by a spectrally-resolved optical model that includes the calculation of water-leaving reflectance for validation with remote sensing. The~~ water column is dynamically coupled to the sediment to resolve deposition, resuspension and benthic-pelagic biogeochemical fluxes. With a focus on shallow waters, the model also includes particularly-detailed representations of benthic plants such as seagrass, macroalgae and coral polyps. A second focus has been on, where possible, the use of geometric derivations of physical limits to constrain ecological rates, which generally requires population-based rates to be derived from initially considering the size and shape of individuals. For example, zooplankton grazing considers encounter rates of one predator on a prey field based on summing relative motion of the predator with the prey individuals and the search area~~,~~ ; chlorophyll synthesis includes a geometrically-derived self-shading term~~,~~ ; and the bottom coverage of benthic plants is ~~generically-related to~~ calculated

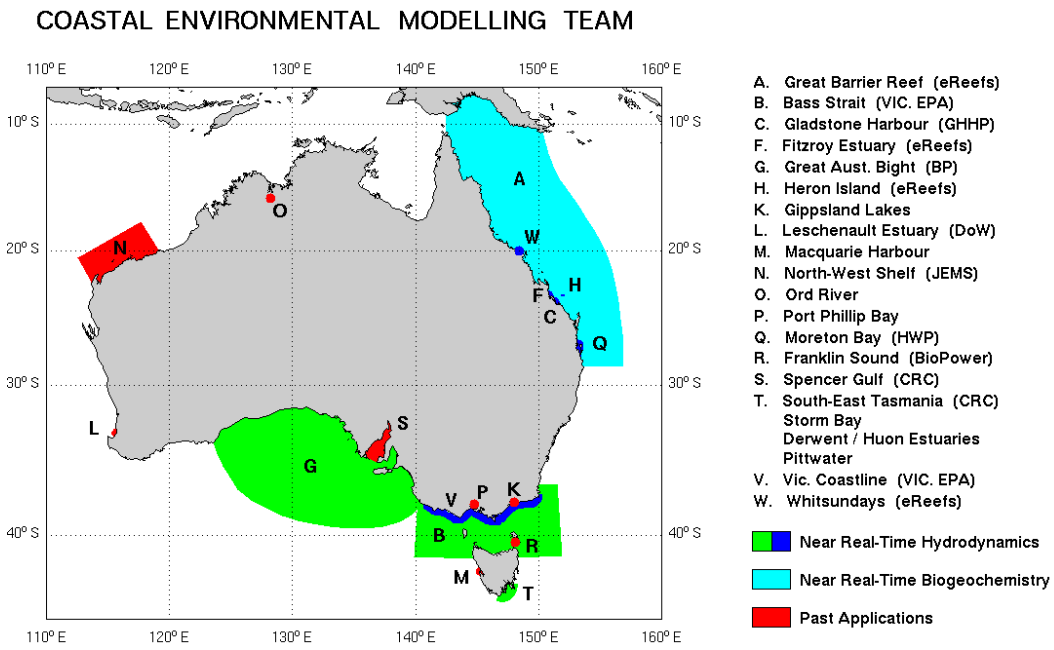

Figure 1. Model domains of the CSIRO EMS hydrodynamic and biogeochemical applications from 1996 onwards. Additionally, EMS was used for the nation-wide Simple Estuarine Response Model (SERM) ~~,~~that was applied generically around Australia's 1000+ estuaries (Baird et al., 2003). Brackets refer to specific funding bodies. EMS has also been applied in the Los Lagos region of Chile. A full list of past and current applications and funding bodies is available at: `https://research.csiro.au/cem/projects/`.

from their biomass using an exponential form derived from geometric arguments. This geometric approach has led to a more algebraically-complicated set of equations when compared to more empirical biogeochemical model formulations. But while being algebraically-complicated, the model has fewer unconstrained parameters and is therefore simpler to move between applications than it would otherwise be. The version of ~~the biogeochemistry~~ EMS described here is implemented in the eReefs project that is delivering a near real time coupled hydrodynamic, sediment and biogeochemical simulation of the Great Barrier Reef, northeast Australia, and its formulation provides an example of the application of geometric reasoning in the formulation of aquatic ecological processes.

Keywords. Great Barrier Reef, mechanistic model, geometric derivation

1 Introduction

The first model of marine biogeochemistry was ~~a~~ developed more than 70 years ago to explain phytoplankton blooms (Riley, 1947). Today the modelling of estuarine, coastal and global biogeochemical systems has been used for a wide variety of applications including coastal eutrophication (Madden and Kemp, 1996; Baird et al., 2003), shelf carbon and nutrient dynamics (Yool and Fasham, 2001; Dietze et al., 2009), plankton ecosystem diversity (Follows et al., 2007), ocean acidification (Orr et al., 2005), impact of local developments such as fish farms and sewerage treatment plants (Wild-Allen et al., 2010), fishery production (Stock et al., 2008) and operational forecasting (Fennel et al., 2019), to name a few. As a result of these varied applications, a diverse range of biogeochemical models have emerged, with some models developed over decades and being capable of investigating a suite of biogeochemical phenomena (Butenschön et al., 2016). With model capabilities typically dependent on the history of applications for which a particular model has been funded, and perhaps even the backgrounds and interests of the developers themselves, significant differences exist between models. Thus it is vital that biogeochemical models are accurately described in full (e.g. Butenschön et al. (2016); Aumont et al. (2015) and Dutkiewicz et al. (2015)), so that model differences can be understood, and, where useful, innovations shared between modelling teams.

Estuarine, coastal and shelf modelling projects undertaken over the past 20+ years by Australia's national science agency, the Commonwealth Science Industry and Research Organisation (CSIRO), have led to the development of the CSIRO Environmental Modelling Suite (EMS). ~~The~~ EMS contains a suite of hydrodynamic, transport, sediment, optical and biogeochemical models that can be run coupled or sequentially. The EMS biogeochemical model, the subject of this paper, has been applied around the Australian coastline (Fig. 1) leading to characteristics of the model which have been tailored to the Australian environment and its challenges.

Australian shelf waters range from tropical to temperate, micro- to macro-tidal, with shallow waters containing coral, seagrass or algae-dominated benthic communities. With generally narrow continental shelves, and being surrounded by two poleward-flowing boundary currents (Thompson et al., 2009), primary production in Australian coastal environments is generally limited by dissolved nitrogen in marine environments, phosphorus in freshwaters, and unlimited by silica and iron. The episodic nature of rainfall on the Australian continent, especially in the tropics, and a lack of snow cover, delivers intermittent but occasionally extreme river flows to coastal waters. With a low population density, continent-wide levels of human impacts are small relative to other continents, but can be significant locally, often due to large isolated developments such as dams, irrigation schemes, mines and ports. Global changes such as ocean warming and acidification affect all regions. The EMS BGC model has many structural features similar to other models (e.g. multiple plankton functional types, nutrient and detrital pools, an increasing emphasis on optical and carbon chemistry components). Nonetheless, the geographical characteristics of, and anthropogenic influences on, the Australian continent have shaped the development of EMS, and led to a BGC model with many unique features.

As the national science body, CSIRO needed to develop a numerical modelling system that could be deployed across the broad range of Australian coastal environments and capable of resolving multiple anthropogenic impacts. With a long coastline (60,000+ km by one measure), containing over 1000 estuaries, an Australian-wide configuration has insufficient resolution to be used for many applied environmental challenges. Thus, in 1999, the EMS biogeochemical model development was targeted to increase its applicability across a range of ecosystems. In particular, given limited resources to model a large number of

environments / ecosystems, developments aimed to minimise the need for re-parameterisation of biogeochemical processes for each application. Two innovations arose from this imperative: 1. the software development of a process-based modelling architecture, such that processes could be included, or excluded, while using the same executable file; and 2. the use, where possible, of geometric descriptions of physical limits to ecological processes as a means of reducing parameter uncertainty (Baird et al., 2003). It is the use of these geometric descriptions that has led to the greatest differences between EMS and other aquatic biogeochemical models.

In the aquatic sciences there has been a long history of experimental and process studies that use geometric arguments to quantify ecological processes, but these derivations have rarely been applied in biogeochemical models, with notable exceptions (microalgal light absorption and plankton sinking rates generally, surface area to volume considerations (Reynolds, 1984), ~~among others~~size-focused trait-based modelling (Litchman and Klausmeier, 2008)). By prioritising geometric arguments, EMS has included a number of previously-published geometric forms including diffusion limitation of microalgae nutrient uptake (Hill and Whittingham, 1955), absorption cross-sections of microalgae (Fig. 2C, Duysens (1956); Kirk (1975); Morel and Bricaud (1981)), diffusion limits to macroalgae and coral nutrient uptake (Munk and Riley, 1952; Atkinson and Bilger, 1992; Zhang et al., 2011), and encounter-rate limitation of grazing rates (Fig. 2B, Jackson (1995)).

Perhaps the most important consequence of using geometric constraints in the BGC model is the representation of benthic flora as two dimensional surfaces, while plankton are represented as three dimensional suspended objects (Baird et al., 2003). Thus leafy benthic plants such as macroalgae take up nutrients and absorb light on a 2D surface. In contrast, nutrient uptake to microalgae occurs through a 3D field while light uptake of the 3D cell is limited by the 2D projected area (Fig. 2A). These contrasting geometric properties, from which the model equations are derived, generates greater potential light absorption relative to nutrient uptake of benthic communities relative to the same potential light absorption relative to nutrient uptake in unicellular algae (Baird et al., 2004). In the most simple terms, this can be related to the surface area to projected area of a leaf being 1/4 times that of a microalgae cell (Fig. 2A). Thus the competition for nutrients, ultimately being driven by light absorption and its rate compared to nutrient uptake, is explicitly determined by the contrasting geometries of cells and leaves.

In addition to geometric constraints derived by others, a number of novel geometric descriptions have been introduced into the EMS BGC model, including:

1. Geometric derivation of the relationship between biomass, B, and fraction of the bottom covered, $A_{eff} = 1 - \exp(-\Omega B)$, where Ω is the nitrogen-specific leaf area (Sec. 6).

2. Impact of self-shading on chlorophyll synthesis quantified by the incremental increase in absorption with the increase in pigment content (Sec. 5.1.3).

3. Mass-specific absorption coefficients of photosynthetic pigments have been better utilised to determine phytoplankton absorption cross-sections (Duysens, 1956; Kirk, 1975; Morel and Bricaud, 1981) through the availability of a library of mass-specific absorption coefficients (Clementson and Wojtasiewicz, 2019), and their wavelength correction using the refractive index of the solvent used in the laboratory determinations (Fig. 5).

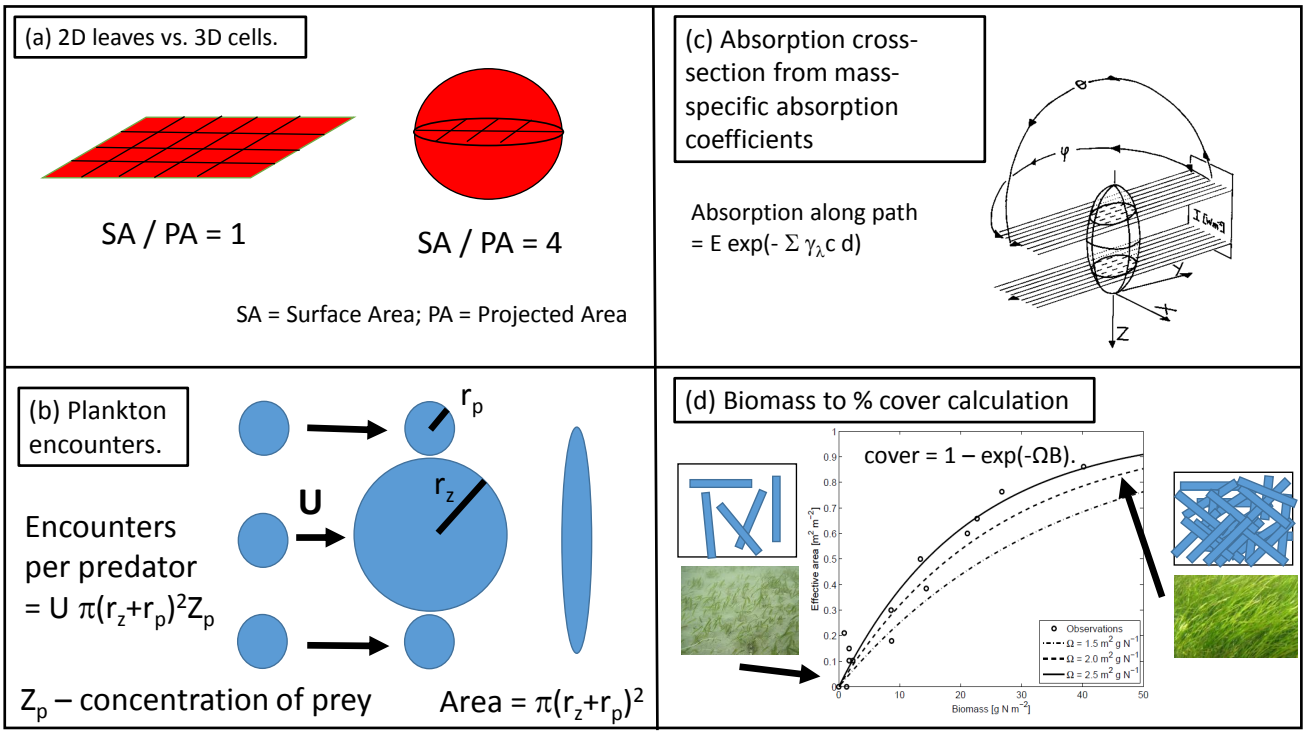

Figure 2. Examples of geometric descriptions of ecological processes. (a) The relative difference in the 2D experience to nutrient and light fields of leaves compared to the 3D experience of cells, as typified by the ratio of surface area (coloured) to projected area (hashed area); (b) The encounter rate of prey per individual predator as a function of the radius of encounter (the sum the predator and prey radii) and the relative motion and prey concentration following Jackson (1995); (c) The use of ray tracing and the mass-specific absorption coefficient to calculate an absorption cross section for a randomly oriented spheroid following (Kirk, 1975); (d) Fraction of the bottom covered as seen from above as a result of increasing the number of randomly placed leaves (Baird et al., 2016a). Based on the assumption that leaves are randomly placed, the cover reaches $1-\exp(-1) = 0.63$ when the sum of the shaded areas induced by all individual leaves equals the ground area (i.e. a Leaf Area Index of 1).

4. The space-limitation of zooxanthellae within coral polyps using zooxanthellae projected areas in a two layer gastrodermal cell anatomy (Sec. 6.3.1).

5. Preferential ammonia uptake, which is often calculated using different half-saturation coefficients of nitrate and ammonia uptake (Lee et al., 2002), is determined ~~in the EMS BGC model~~ by allowing ammonia uptake to proceed up to the diffusion limit. Should this diffusion limit not meet the required demand, nitrate uptake supplements the ammonia uptake. This representation has the benefit that no additional parameters are required to assign preference, with the same approach ~~can be~~ applied for both microalgae and benthic plants (Sec. 9.1).

To be clear, these geometric definitions have their own set of assumptions (e.g. a single cell size for a population), and simplifications (e.g. spherical shape). Nonetheless, the effort to apply geometric descriptions of physical limits across the BGC model appears to have been beneficial, as measured by the minimal amount of re-parameterisation that has been required to apply the model to contrasting environments. Of the above mentioned new formulations, the most useful and easily applied is the bottom cover calculation (Fig. 2D). In fact it is so simple, and such a clear improvement on empirical forms as demonstrated in Baird et al. (2016a), that it is likely to have been applied in other ecological / biogeochemical models, although we are unaware of any other implementation.

The geometrically-constrained relationship between bottom cover and seagrass biomass, B, is $\text{cover} = 1 - \exp(-\Omega B)$ and can be used to illustrate how geometric arguments can produce model equations with tightly-constrained parameters. This geometric relationship contains only one parameter, Ω, that is the initial slope between cover and biomass. At low biomass there is no overlapping of leaves, so the Ω is the area of leaves per unit of biomass (or nitrogen-specific leaf area), and has been determined by many authors on hundreds of types of seagrass. Comparison with data is shown in Appendix A of Baird et al. (2016a) and Fig. 2D. Thus by using geometric arguments in developing the equation, the form contains only one parameter which has a physical meaning that is tightly constrained.

In addition to using geometric descriptions, there are a few other features unique to the EMS BGC model including:

1. Calculation of ~~remote-sensing reflectance from an optical-depth weighted ratio of backscatter to absorption plus backscatter (Sec. 4.1.2).~~

2. ~~Calculation of~~ scalar irradiance from downwelling irradiance, vertical attenuation and a photon balance within a layer (Sec. 4.1.2).

3. An oxygen balance achieved through use of biological and chemical oxygen demand tracers (Sec. 10.3.2). ~~The calculation of remote-sensing reflectance, which is also undertaken in other biogeochemical modelling studies (Dutkiewicz et al., 2015) , is one example of an approach that we are pursuing to bring the model outputs closer to the observations (Baird et al., 2016b) . The most dramatical example of this is the development of simulated true colour, which renders model calculations of spectrally-resolved remote-sensing reflectance as would be expected by the human visual experience (Fig. **??**).~~

4. The stoichiometric link of excess photons to reactive oxygen production in zooxanthallae.

~~Observed (top) and simulated (bottom) true colour from simulated remote-sensing reflectance at 670, 555 and 470 nm in the GBR4 model configuration in the region of the Burdekin River. A brightening of 10 (left) and 20 (right) was applied for comparison. See Baird et al. (2016b).~~

1.1 ~~Outline~~Manuscript outline

This document provides a summary of the biogeochemical processes included in the model (Sec. 2), a ~~full description of the model equations~~ summary of the transport model that integrates the advection-diffusion and sinking terms (Sec. ~~5 - Sec. 10),~~

Figure 3. Schematic of CSIRO Environmental Modelling Suite, illustrating the biogeochemical processes in the water column, epipelagic and sediment zones, as well as the carbon chemistry and gas exchange used in vB3p0 for the Great Barrier Reef application. Orange labels represent components that scatter or absorb light.

as well as links to model evaluation 3), and full descriptions of the optical (Sec. 11) , code availability 4) and ecological (Sec. 12) and test case generation (5 - Sec. 13) 10) model equations. The description of both the optical and biogeochemical models is divided into the primary environmental zones: pelagic(Sec. 5), epibenthic (Sec. 6) and sediment(Sec. 7), epibenthic and sediment, as well as processes that are common to all zones(Sec. 8) and numerical integration details (. Sec. 10). Within these zones, descriptions are sorted by 9 details parameterisations that are common across numerous ecological processes, such as microalgae growth, coral growth, food web interactions etc.This organisation allows the model to be explained, with notation, in self-contained chunks. For each process the complete set of model equations, parameter values and state variables are given in tables.As the code itself allows the inclusion / exclusion of processes at runtime, the process-based structuring of this document aligns with the architecture of the code . To investigate the complete equation for a single state variable, such as nitrate concentration, the reader will need to combine the individual terms affecting the variable from all processes (such as nitrate uptake by each of the autotrophs, remineralisation etc.)temperature dependence, and Sec. 10 provides details of the numerical integration techniques. Further sections detail the model evaluation (Sec. 11), code availability (Sec. 12) and test case generation (Sec. 13). Section 10 gives some of the details of the numerical methods that solve the model equations. The Discussion (Sec. 14) details how past and present applications have influenced the development of the EMS BGC model, and anticipates some future developments. Finally, the Appendices gives some code details, as well as tables of state variables and parameters, with both mathematical and numerical code details.

2 Overview of the EMS biogeochemical and optical modeland biogeochemical models

2.1 Spectrally-resolved optical model

The optical model undertakes calculations at distinct wavelengths of light (say 395, 405, 415, ... 705 nm) representative of individual wavebands (say 400-410, 410-420 nm etc.) , and can be modified for the particular application. First the spectrally-resolved Inherent Optical Properties (IOPs) of the water column are calculated from the optically-active model biogeochemical state (phytoplankton biomass, particulate concentrations etc.). These include the absorption and scattering properties of clear water, coloured dissolved organic matter, suspended solids and each microalgal population.

Using the calculated IOPs, as a well as of the vertically-resolved downwelling and scalar irradiance that are used by the biogeochemical model to drive photosynthesis. The optical model includes the effect of Earth-Sun distance, sun angle, surface albedo and refraction , the on the downwelling surface irradiance. In the water column, the model attenuates light based on the spectrally-resolved light field (downwelling and scalar irradiance) is calculated for each grid cell in the model. From this light field phytoplankton absorption is calculated. The light that reaches the bottom is absorbed by epibenthic flora as a function

~~of wavelength, depending on the absorbance of each individual flora. From the calculation of the light field other apparent optical properties (AOPs), such as remote-sensing reflectance, can be determined and compared to either in situ measurements or remotely-sensed products. As AOPs can be recalculated from IOPs post-simulation, the model can be run for one set of wavelengths to optimise the integration speed and accuracy, and the AOPs re-calculated at another set of wavelengths for comparison with hyperspectral observations such as those used to calculate chlorophyll from the ocean color sensors.~~

~~The use of remote-sensing reflectance introduces a novel means of model assessment - simulated true colour. The model output can be processed to produce simulated true colour images of the water surface, with features such as bottom reflectance, river plumes, submerged coral reefs and microalgal blooms easily characterised by their colour (Baird et al., 2016b)~~total absorption and scattering of microalgae, detritus, dissolved organic matter, inorganic particles and the water itself (Fig. 3). The light reaching the bottom is further attenuated by macroalgae, seagrass, corals and benthic microalgae.

2.1 ~~Biogeochemical model~~

~~The ecological~~

The biogeochemical model is organised into 3 zones: pelagic, epibenthic and sediment. Depending on the grid formulation the pelagic zone may have one or several layers of similar or varying thickness. The epibenthic zone overlaps with the lowest pelagic layer and the top sediment layer and shares the same dissolved and suspended particulate material fields. The sediment is modelled in multiple layers with a thin layer of easily resuspendable material overlying thicker layers of more consolidated sediment.

Dissolved and particulate biogeochemical tracers are advected and diffused throughout the model domain in an identical fashion to temperature and salinity. Additionally, biogeochemical particulate substances sink and are resuspended in the same way as sediment particles. Biogeochemical processes are organized into pelagic processes of phytoplankton and zooplankton growth and mortality, detritus remineralisation and fluxes of dissolved oxygen, nitrogen and phosphorus; epibenthic processes of growth and mortality of macroalgae, seagrass and corals, and sediment based processes of plankton mortality, microphytobenthos growth, detrital remineralisation and fluxes of dissolved substances (Fig. 3).

The biogeochemical model considers four groups of microalgae (small and large phytoplankton representing the functionality of photosynthetic cyanobacteria and diatoms respectively, microphytobenthos and *Trichodesmium*), four macrophytes types (seagrass types corresponding to *Zostera*, *Halophila*, deep *Halophila* and macroalgae) and coral communities. For temperate system applications of the EMS, dinoflagellates, *Nodularia* and multiple macroalgal species have also been characterised (Wild-Allen et al., 2013; Hadley et al., 2015a)

Photosynthetic growth is determined by concentrations of dissolved nutrients (nitrogen and phosphate) and photosynthetically active radiation. Autotrophs take up dissolved ammonium, nitrate, phosphate and inorganic carbon. Microalgae incorporate carbon (C), nitrogen (N) and phosphorus (P) at the Redfield ratio (106C:16N:1P) while macrophytes do so at the Atkinson ratio (550C:30N:1P). Microalgae contain two pigments (chlorophyll *a* and an accessory pigment), and have variable carbon:pigment ratios determined using a photoadaptation model.

Micro- and meso-zooplankton graze on small and large phytoplankton respectively, at rates determined by particle encounter rates and maximum ingestion rates. Additionally large zooplankton consume small zooplankton. Of the grazed material that is not incorporated into zooplankton biomass, half is released as dissolved and particulate carbon, nitrogen and phosphate, with the remainder forming detritus. Additional detritus accumulates by mortality. Detritus and dissolved organic substances are remineralised into inorganic carbon, nitrogen and phosphate with labile detritus transformed most rapidly (days), refractory detritus slower (months) and dissolved organic material transformed over the longest timescales (years). The production (by photosynthesis) and consumption (by respiration and remineralisation) of dissolved oxygen is also included in the model and depending on prevailing concentrations, facilitates or inhibits the oxidation of ammonia to nitrate and its subsequent denitrification to di-nitrogen gas which is then lost from the system.

Additional water column chemistry calculations are undertaken to solve for the equilibrium carbon chemistry ion concentrations necessary to undertake ocean acidification (OA) studies, and to consider sea-air fluxes of oxygen and carbon dioxide. The adsorption and desorption of phosphorus onto inorganic particles as a function of the oxic state of the water is also considered.

In the sediment porewaters, similar remineralisation processes occur as in the water column (Fig. 4). Additionally, nitrogen is denitrified and lost as N_2 gas while phosphorus can become adsorbed onto inorganic particles, and become permanently immobilised in sediments.

2.1 Structure of the model description

The biogeochemical model presented in this paper is process-based. That is, the rate of change of each ecological state variable is determined by a mathematical representation of each process that moves mass between one variable and another, conserving total mass. For dissolved inorganic phosphorus, the equation in the bottom water column layer (excluding advection, diffusion and particle sinking) could be written as:

$$\begin{aligned}\frac{dP}{dt} \approx\ & -\sum^{4}\text{microaglae uptake} - \sum^{3}\text{seagrass uptake} - \text{macroalgae uptake} - \text{zooxanthallae uptake} \\ & - \text{water column / sediment porewater exchange} - \text{phosphorus adsorption/desorption} \\ & + \sum^{4}\text{microalgae respiration} + \sum^{3}\text{seagrass respiration} + \text{macroalgae respiration} + \text{zooxanthallae respiration} \\ & + \sum^{2}\text{zooplankton sloppy feeding} + \sum^{2}\text{zooplankton respiration} + \text{remineralisation of labile detritus} \\ & + \text{remineralisation of refractory detritus} + \text{remineralisation of dissolved organic matter}\end{aligned}$$

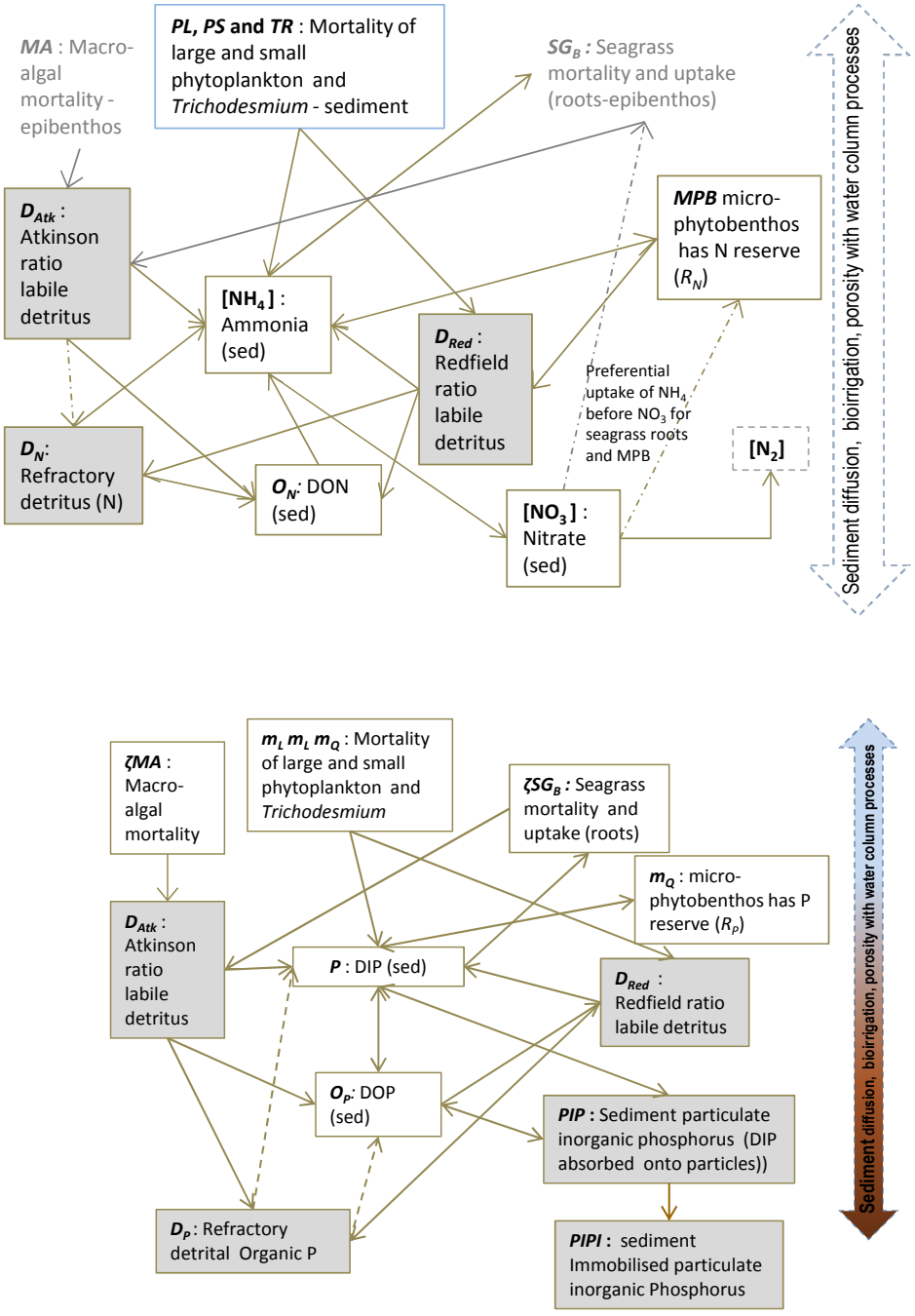

Figure 4. Schematic of sediment nitrogen and phosphorus pools and fluxes. Processes represented include phytoplankton mortality, detrital decomposition, denitification (nitrogen only), phosphorus adsorption (phosphorus only) and microphytobenthic growth.

As the number of processes in the model has grown, the representation of all the terms affecting one variables has become unworkable. Thus, instead of presenting the full equation for each state variable, we present the full set of equations for each process.

2.1.1 Presentation of process equations

In Sec. 5 - Sec. 10 descriptions are sorted by processes, such as microalgae growth, coral growth, food web interactions. This organisation allows the model to be explained, with individual notation, in self-contained chunks. For each process the complete set of model equations, parameter values and state variables are given in tables. Within each process the equations are required to conserve mass of oxygen, carbon, nitrogen and phosphorus. Furthermore each process description is independent of any other processes in the model. As the code itself allows the inclusion / exclusion of processes at runtime, the process-based structuring of the scientific description aligns with the architecture of the numerical code.

2.1.2 Model stoichiometry

The model contains state variables that quantify the mass of carbon, nitrogen, phosphorus and oxygen, as well as state variables that contain stoichiometrically-constant combinations of carbon, nitrogen, phosphorus (O:C:N:P of 110:106:16:1 for plankton and animals; 554:550:30:1 for benthic plants). While a number of state variables and parameters are specified in units of nitrogen, the model could equally be specified by carbon or phosphorus. Furthermore, while the structural material of microalgae (including benthic microalgae and zooxanthallae) is at the Redfield ratio, changing reserves in microalgae of fixed carbon, nitrogen and phosphorus mean that the microalgae have a variable stoichiometry. Furthermore, the model has separate state variables for refractory detrital carbon, nitrogen and phosphorus, meaning detritus also has a variable stoichiometry. As explained later, we also represent stoichiometric coefficients in the model equations as integers, a simple approximation to make the mathematical equations easier to read.

3 Transport model

The local rate of change of concentration of each dissolved and particulate constituent, C, contains sink/source terms, S_C, which are described in length in this document, and the advection, diffusion and sinking terms:

$$\frac{\partial C}{\partial t} + \mathbf{v} \cdot \nabla^2 C = \nabla \cdot (K \nabla C) + w_{sink} \frac{\partial C}{\partial z} + S_C \tag{1}$$

where the symbol $\nabla = \left(\frac{\partial}{\partial x}, \frac{\partial}{\partial y}, \frac{\partial}{\partial z} \right)$, $\mathbf{v}$ is the velocity field, K is the eddy diffusion coefficient which varies in space and time, and w_C is the local sinking rate (positive downwards) and the z co-ordinate is positive upwards. The calculation of $\mathbf{v}$ and K is described in the hydrodynamic model (Herzfeld, 2006; Gillibrand and Herzfeld, 2016). The advection-diffusion terms of Eq. 1, based on the continuum hypothesis for a fluid (Vichi et al., 2007), are solved by either an in-line advection scheme with the baroclinc timestep of the hydrodynamic model, or an offline transport scheme using a potentially much longer timestep

(Gillibrand and Herzfeld, 2016). Options for advection and transport schemes in EMS include mass conservative Lagrangian and flux-form approaches described in Herzfeld (2006) and Gillibrand and Herzfeld (2016).

The microalgae are particulates that contain internal concentrations of dissolved nutrients (C, N, P) and pigments that are specified on a per cell basis. To conserve mass, the local rate of change of the concentration of microalgae, B, multiplied by the content of the cell, R, is given by:

$$\frac{\partial(BR)}{\partial t} + \mathbf{v} \cdot \nabla^2(BR) = \nabla \cdot (K \nabla(BR)) + w_C \frac{\partial(BR)}{\partial z} + S_{BR} \tag{2}$$

For more information see Sec. 5.1.6 and Sec. 3.1 of Baird et al. (2004) which describes the coupling of the plankton component of the biogeochemical model to the Princeton Ocean Model.

4 Optical model

The optical model calculates the spectrally-resolved light field in each vertical column and uses it to drive the photosynthesis of phytoplankton and benthic plants in the biogeochemical model. Following the terminology of aquatic optics (Mobley, 1994), we divide the description of the model into calculations of inherent optical properties (IOPs) followed by apparent optical properties (AOPs). IOPs are properties of the medium (e.g. scattering and absoprtion) and do not depend on the ambient light field. The optical model uses the value of the optically-active state variables, and their mass-specific absorption and scattering properties, to calculate the total absoprtion and scattering. AOPs are those properties that depend both on the medium (the IOPs) and on the surface light field (e.g. downwelling and scalar irradiance). Thus the optical model uses the vertical distribution of IOPs, and the surface light field, to determine the vertical distribution of the AOPs.

4.1 Water column optical model

4.1.1 Inherent optical properties (IOPs)

Phytoplankton absorption. The model contains 4 phytoplankton types (small and large phytoplankton, benthic mircoalgae and *Trichodesmium*), each with a unique ratio of internal concentration of accessory photosynthetic pigments to chlorophyll-a. To calculate the absorption due to each pigment, we use a database of spectrally-resolved mass-specific absorption coefficients (Clementson and Wojtasiewicz, 2019). As it can be assumed that accessory pigments stay in a constant ratio to chlorophyll-*a*, the model needs only a state variable for chlorophyll-*a* for each phytoplankton type. The model then calculates the chlorophyll-*a* specific absorption coefficient due to all pigments by using the Chl-a state variable, the ratio of concentration of the accessory pigment to chlorophyll-*a*, and the mass-specific absorption coefficient of each of the accessory pigments. Thus the chlorophyll-*a* specific absorption coefficient due to all photosynthetic pigments for small phytoplankton at wavelength λ, $\gamma_{small,\lambda}$, is given by:

$$\gamma_{small,\lambda} = 1.0\gamma_{Chla,\lambda} + 0.35\gamma_{Zea,\lambda} + 0.05\gamma_{Echi,\lambda} + 0.1\gamma_{\beta-car,\lambda} + 2\gamma_{PE,\lambda} + 1.72\gamma_{PC,\lambda} \tag{3}$$

where Chla is the pigment chlorophyll-*a*, Zea is zeaxanthin, Echi is echinenone, β-car is beta-carotene, PE is phycoerithin, and PC is phycocyanin, and the ratios of chlorophyll-*a* to accessory pigment concentration are determined from Wojtasiewicz and Stoń-Egiert (2016). Note that the coefficient in Eq. 3 for Chla is 1.0 because the ratio of chlorophyll-*a* to chlorophyll-*a* is 1. The resulting chlorophyll-*a* specific absorption coefficient is shown in Fig. 5.

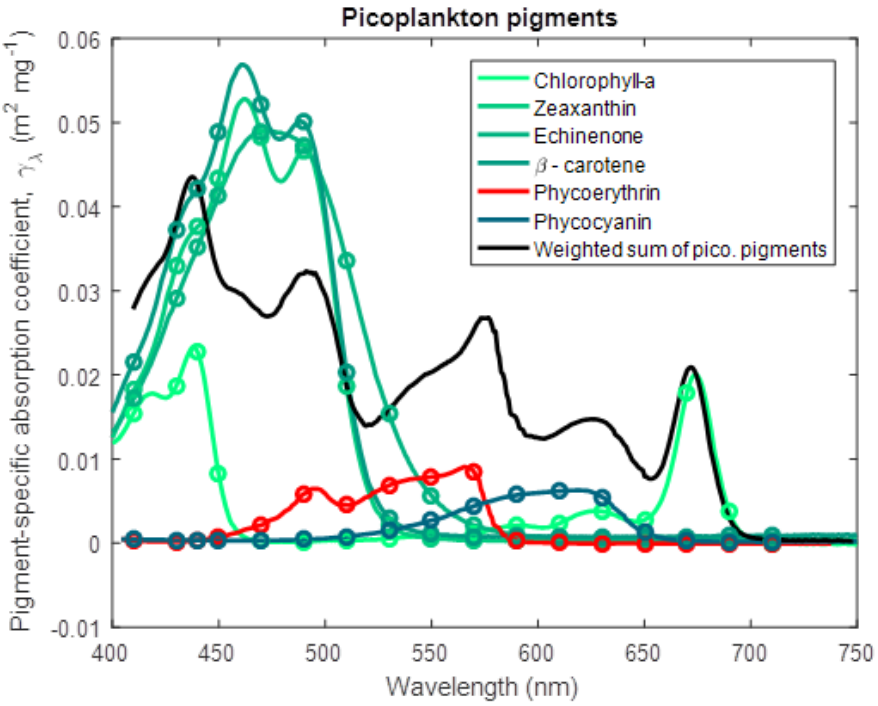

Figure 5. Pigment-specific absorption coefficients for the dominant pigments found in small phytoplankton determined using laboratory standards in solvent in a 1 cm vial. Green and red lines are photosynthetic pigments constructed from 563 measured wavelengths. Circles represent the wavelengths at which the optical properties are calculated in the simulations. The black line represents the weighted sum of the photosynthetic pigments (Eq. 3), with the weighting calculated from the ratio of each pigment concentration to chlorophyll *a*. The spectra are wavelength-shifted from their raw measurement by the ratio of the refractive index of the solvent to the refractive index of water (1.352 for acetone used with chlorophyll *a* and β-carotene; 1.361 for ethanol used with zeaxanthin, echinenone; 1.330 for water used with phycoerythrin, phycocyanin).

Similarly for large phytoplankton and microphytobenthos (Wright et al., 1996):

$$\gamma_{large,\lambda} = 1.0\gamma_{Chla,\lambda} + 0.6\gamma_{Fuco,\lambda} \tag{4}$$

where Fuco is fucoxanthin. And for *Trichodesmium* (Carpenter et al., 1993) :

$$\gamma_{Tricho,\lambda} = 1.0\gamma_{Chla,\lambda} + 0.1\gamma_{Zea,\lambda} + 0.02\gamma_{Myxo,\lambda} + 0.09\gamma_{\beta-car,\lambda} + 2.5\gamma_{PE,\lambda} \tag{5}$$

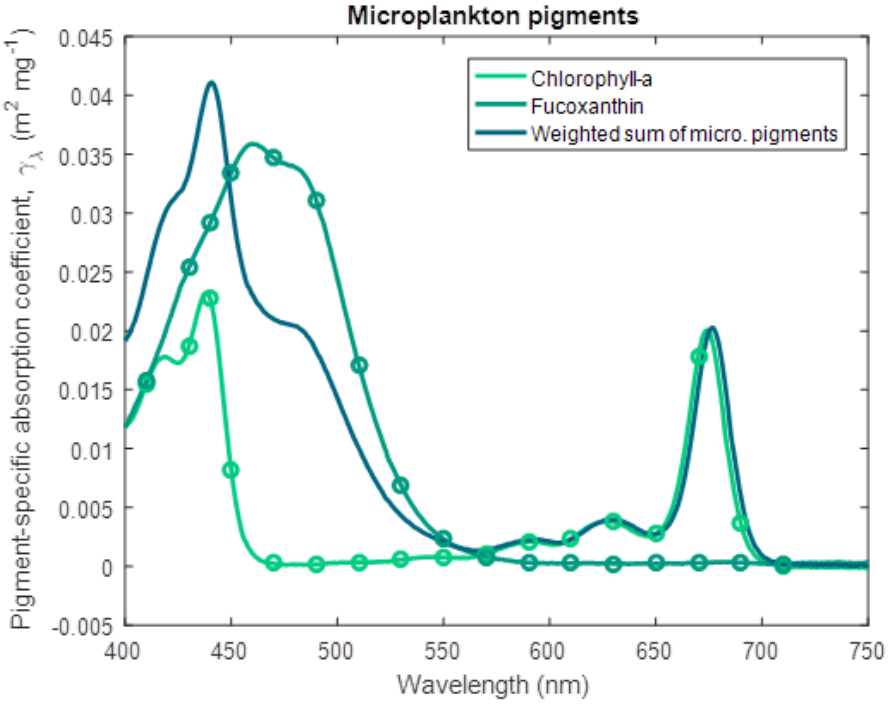

Figure 6. Pigment-specific absorption coefficients for the dominant pigments found in large phytoplankton and microphytobenthos determined using laboratory standards in solvent in a 1 cm vial. The aqua line represents the weighted sum of the photosynthetic pigments (Eq. 4), with the weighting calculated from the ratio of each pigment concentration to chlorophyll *a*. See Fig. 5 for more details. Fucoxanthin was dissolved in ethanol.

where Myxo is myxoxanthophyll.

The absorption cross-section at wavelength λ (α_λ) of a spherical cell of radius (r), chlorophyll-*a* specific absorption coefficient (γ_λ), and homogeneous intracellular chlorophyll-*a* concentration (c_i) can be calculated using geometric optics (i.e., ray tracing without considering internal scattering) and is given by (Duysens, 1956; Kirk, 1975):

$$\alpha_\lambda = \pi r^2 \left(1 - \frac{2(1-(1+2\gamma_\lambda c_i r)e^{-2\gamma_\lambda c_i r})}{(2\gamma_\lambda c_i r)^2}\right) \tag{6}$$

where πr^2 is the projected area of a sphere, and the bracketed term is 0 for no absorption ($\gamma c_i r = 0$) and approaches 1 as the cell becomes fully opaque ($\gamma c_i r \to \infty$). Note that the bracketed term in Eq. 6 is mathematically equivalent to the dimensionless efficiency factor for absorption, Q_a (used in Morel and Bricaud (1981), Finkel (2001) and Bohren and Huffman (1983)), of homogeneous spherical cells with an index of refraction close to that of the surrounding water. Note that the intracellular chlorophyll concentration, c_i, changes as a result of chlorophyll synthesis (described later in Eq. 36).

The use of an absorption cross-section of an individual cell has two significant advantages. Firstly, the same model parameters used here to calculated absorption in the water column are used to determine photosynthesis by individual cells, including

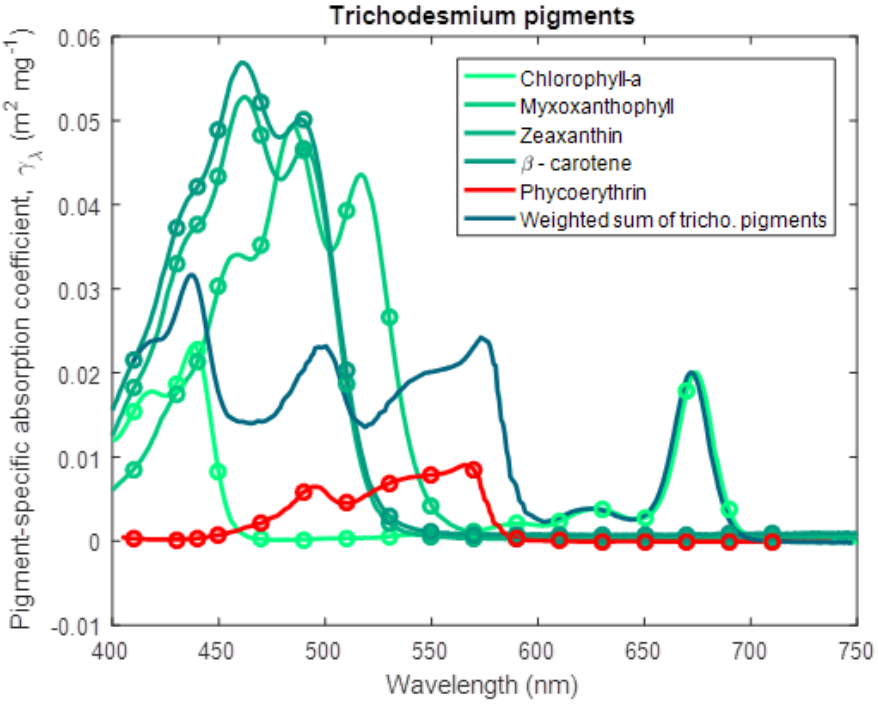

Figure 7. Pigment-specific absorption coefficients for the dominant pigments found in *Trichodesmium* determined using laboratory standards in solvent in a 1 cm vial. The aqua line represents the weighted sum of the photosynthetic pigments (Eq. 5), with the weighting calculated from the ratio of each pigment concentration to chlorophyll *a*. See Fig. 5 for more details. Myxoxanthophyll was dissolved in acetone.

the effect of packaging of pigments within cells. Secondly, the dynamic chlorophyll concentration determined later can be explicitly included in the calculation of phytoplankton absorption. Thus the absorption of a population of n cell m^{-3} is given by $n\alpha$ m^{-1}, while an individual cell absorbs αE_o light, where E_o is the scalar irradiance.

Coloured Dissolved Organic Matter (CDOM) absorption. Two equations for CDOM absorption are presently being trialled. The two schemes are:

Scheme 1. The absorption of CDOM, $a_{CDOM,\lambda}$, is determined from a relationship with salinity in the region (Schroeder et al., 2012):

$$a_{CDOM,443} = -0.0332S + 1.2336 \tag{7}$$

where S is the salinity. In order to avoid unrealistic extrapolation, the salinity used in this relationship is the minimum of the model salinity and 36. In some cases coastal salinities exceed 36 due to evaporation. The absorption due to CDOM at other wavelengths is calculated using a CDOM spectral slope for the region (Blondeau-Patissier et al., 2009):

$$a_{CDOM,\lambda} = a_{CDOM,443} \exp\left(-S_{CDOM}\left(\lambda - 443.0\right)\right) \tag{8}$$

	Symbol	Value
Constants		
Speed of light	c	2.998×10^8 m s^{-1}
Planck constant	h	6.626×10^{-34} J s^{-1}
Avogadro constant	A_V	6.02×10^{23} mol^{-1}
[a]Total scattering coefficient of phytoplankton	b_{phy}	0.2 (mg Chl a m^{-2})$^{-1}$
[b]Azimuth-independent scattering coefficient	g_i	0.402
[b]Azimuth-dependent scattering coefficient	g_{ii}	0.180
[c]CDOM-specific absorption coefficient at 443 nm	$k^*_{CDOM,443}$	0.02 m^2 mg C^{-1}
[c]Spectral slope of CDOM absorption	S_{CDOM}	0.012 nm^{-1}
[d]Linear remote-sensing reflectance coefficient	g_0	0.0895 sr^{-1}
[d]Quadratic remote-sensing reflectance coefficient	g_1	0.1247 sr^{-1}

Table 1. Constants and parameter values used in the optical model.[a] Kirk (1994).[b] Kirk (1991) using an average cosine of scattering of 0.924 (Mobley, 1994). [c] Blondeau-Patissier et al. (2009) see also Cherukuru et al. (2019). [d] Brando et al. (2012). [e] Vaillancourt et al. (2004).

	Symbol	Units
Downwelling irradiance at depth z, wavelength λ	$E_{d,z,\lambda}$	W m^{-2}
Scalar irradiance at depth z, wavelength λ	$E_{o,z,\lambda}$	W m^{-2}
In water azimuth angle	θ	rad
Fractional backscattering	u_λ	-
Below-surface remote-sensing reflectance	$r_{rs,\lambda}$	sr^{-1}
Above-surface remote-sensing reflectance	$R_{rs,\lambda}$	sr^{-1}
Thickness of model layer	h	m
Optical depth weighting function	$w_{z,\lambda}$	
Vertical attenuation coefficient	K_λ	m^{-1}
Total absorption coefficient	$a_{T,\lambda}$	m^{-1}
Total scattering coefficient	$b_{T,\lambda}$	m^{-1}
Absorption cross-section	α_λ	m^2 cell^{-1}
Concentration of cells	n	cell m^{-3}

Table 2. State and derived variables in the water column optical model.

where S_{CDOM} is an approximate spectral slope for CDOM, with observations ranging from 0.01 to 0.02 nm^{-1} for significant concentrations of CDOM. Lower magnitudes of the spectral slope generally occur at lower concentrations of CDOM (Blondeau-Patissier et al., 2009).

Scheme 2. The absorption of CDOM, $a_{CDOM,\lambda}$, is directly related to the concentration of dissolved organic carbon, D_C.

$$a_{CDOM,\lambda} = k^*_{CDOM,443} D_C \exp\left(-S_{CDOM}\left(\lambda - 443.0\right)\right) \tag{9}$$

where $k^*_{CDOM,443}$ is the dissolved organic carbon-specific CDOM absorption coefficient at 443 nm.

Both schemes have drawbacks. Scheme 2, using the concentration of dissolved organic carbon, is closer to reality, but is likely to be sensitive to poorly-known parameters such as remineralisation rates and initial detritial concentrations. Scheme 1, a function of salinity, will be more stable, but perhaps less accurate, especially in estuaries where hypersaline waters may have large estuarine loads of coloured dissolved organic matter.

Absorption due to non-algal particulate material. The waters of the Great Barrier Reef contain suspended sediments originating from various marine sources, such as the white calcium carbonate fragments generated by coral erosion, and sediments derived from terrestrial sources such as granite (Soja-Woźniak et al., 2019). The model uses spectrally-resolved mass-specific absorption coefficients (and also total scattering measurements) from a database of laboratory measurements conducted on either pure mineral suspensions, or mineral mixtures, at two ranges of size distributions (Fig. 8, Stramski et al. (2007)). In this model version we use the calcium carbonate sample CAL1 for $CaCO_3$-based particles

For the terrestrially-sourced particles we used observations from Gladstone Harbour in the central GBR (Fig. 9). These IOPs gave a realistic surface colour for the Queensland river sediment plumes (Baird et al., 2016b). In the model, optically-active non-algal particulates (NAPs) includes the inorganic particulates (such as sand and mud, see Sec. 7.1) and detritus. We assumed the optical properties of the detritus was the same as the optical properties in Gladstone Harbour, although open ocean studies have used a detritial absorption that is more like CDOM (Dutkiewicz et al., 2015).

The absorption due to calcite-based NAP is given by:

$$a_{NAP_{\mathrm{CaCO_3},\lambda}} = c_1 NAP_{\mathrm{CaCO_3}} \tag{10}$$

where c_1 is the mass-specific, spectrally-resolved absorption coefficient determine from laboratory experiments (Fig. 8). The absorption due to non-calcite NAPs, $NAP_{\mathrm{non-CaCO_3}}$, combined with detritus, is given by:

$$a_{NAP_{\mathrm{non-CaCO_3},\lambda}} = c_2 NAP_{\mathrm{non-CaCO_3}} + \left(\frac{550}{30}\frac{12}{14} D_{Atk} + \frac{106}{16}\frac{12}{14} D_{Red} + D_C\right)/10^6 \tag{11}$$

where c_2 is the mass-specific, spectrally-resolved absorption coefficient determine from field measurements (Fig. 9), $NAP_{\mathrm{non-CaCO_3}}$ is quantified in kg m^{-3}, D_{Atk} and D_{Red} are quantified in mg N m^{-3} and D_C is quantified in mg C m^{-3}.

Total absorption. The total absorption, $a_{T,\lambda}$, is given by:

$$a_{T,\lambda} = a_{w,\lambda} + a_{NAP_{\mathrm{non-CaCO_3},\lambda}} + a_{NAP_{\mathrm{CaCO_3},\lambda}} + a_{CDOM,\lambda} + \sum_{x=1}^{N} n_x \alpha_{x,\lambda} \tag{12}$$

where $a_{w,\lambda}$ is clear water absorption (Fig. 10) and N is the number of phytoplankton classes (see Table 4).

Scattering. The total scattering coefficient is given by

$$b_{T,\lambda} = b_{w,\lambda} + c_1 NAP_{\mathrm{non-CaCO_3}} + c_2 NAP_{\mathrm{CaCO_3}} + b_{phy,\lambda} \sum_{x=1}^{N} n_x c_{i,x} V_x \tag{13}$$

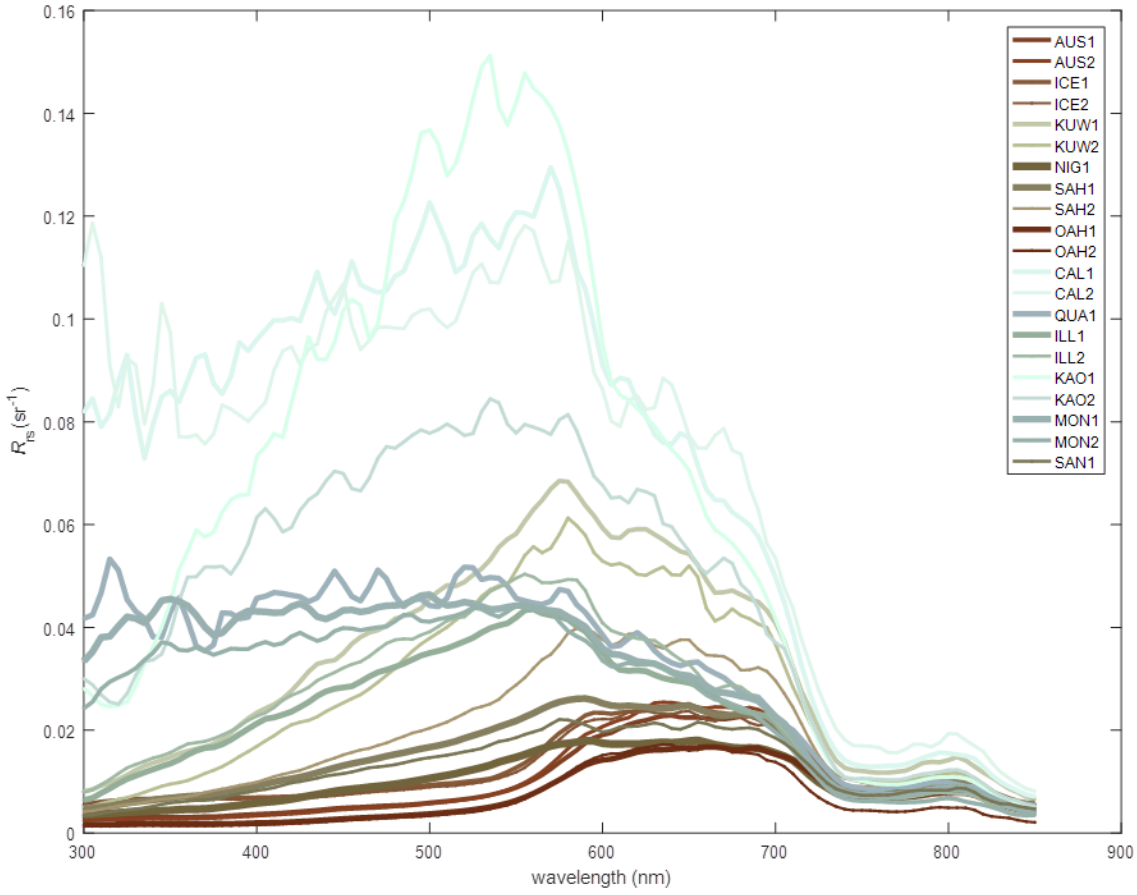

Figure 8. The remote-sensing reflectance of the 21 mineral mixtures suspended in water as measured by Stramski et al. (2007). Laboratory measurements of absorption and scattering properties are used to calculated remote-sensing reflectance (Baird et al., 2016b). Line colouring corresponds to that produced by the mineral suspended in clear water as calculated using the MODIS true color algorithm (Gumley et al., 2010). CAL1, with a median particle diameter of 2 μm, is used for $\mathrm{Mud}_{\mathrm{CaCO_3}}$.

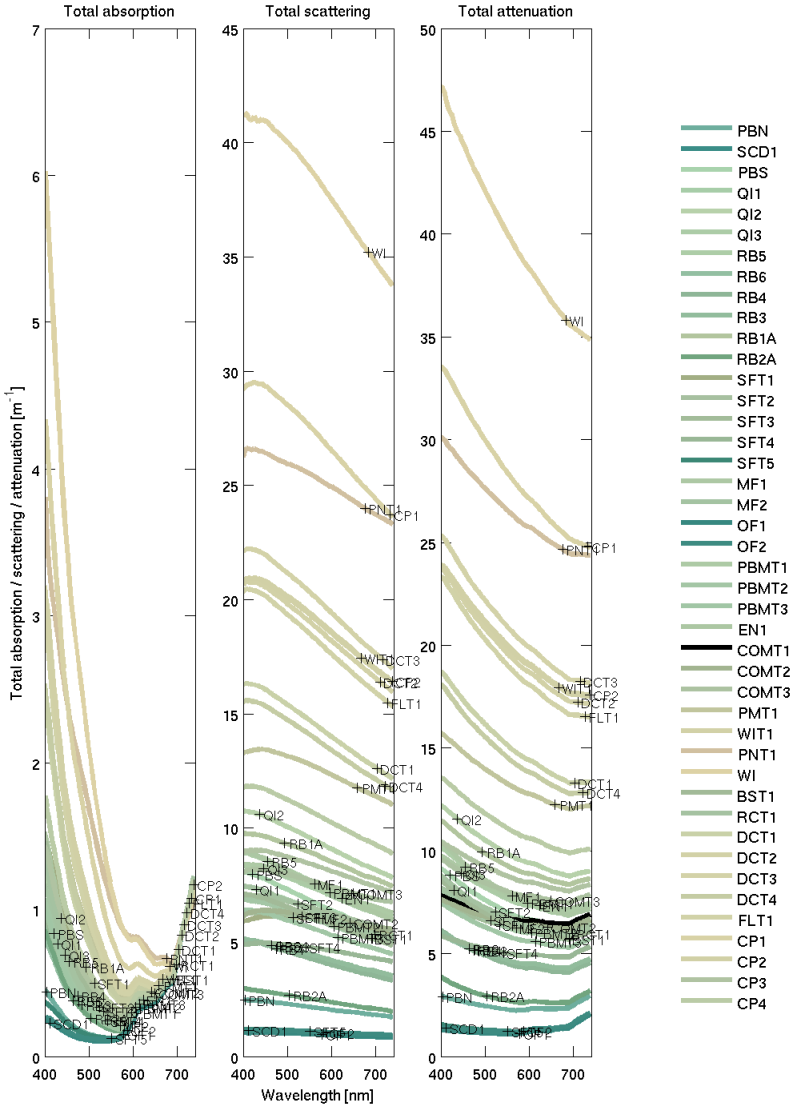

Figure 9. Inherent optical properties (total absorption and total scattering) at sample sites in Gladstone Harbour on 13-19 September 2013 (Babcock et al., 2015). The line colour is rendered like Fig. 8. The site labelling is ordered in time, from the first sample collected during neap tides at the top, to the last sample collected at spring tides on the bottom. The IOPs used for the $\mathrm{Mud}_{\mathrm{non-CaCO_3}}$ end-member is from the WIT site at the centre of the harbour, was dominated by inorganic particles. The measured concentration of NAP at the site was 33.042 mg L^{-1}, and is used to calculate mass-specific IOPs.

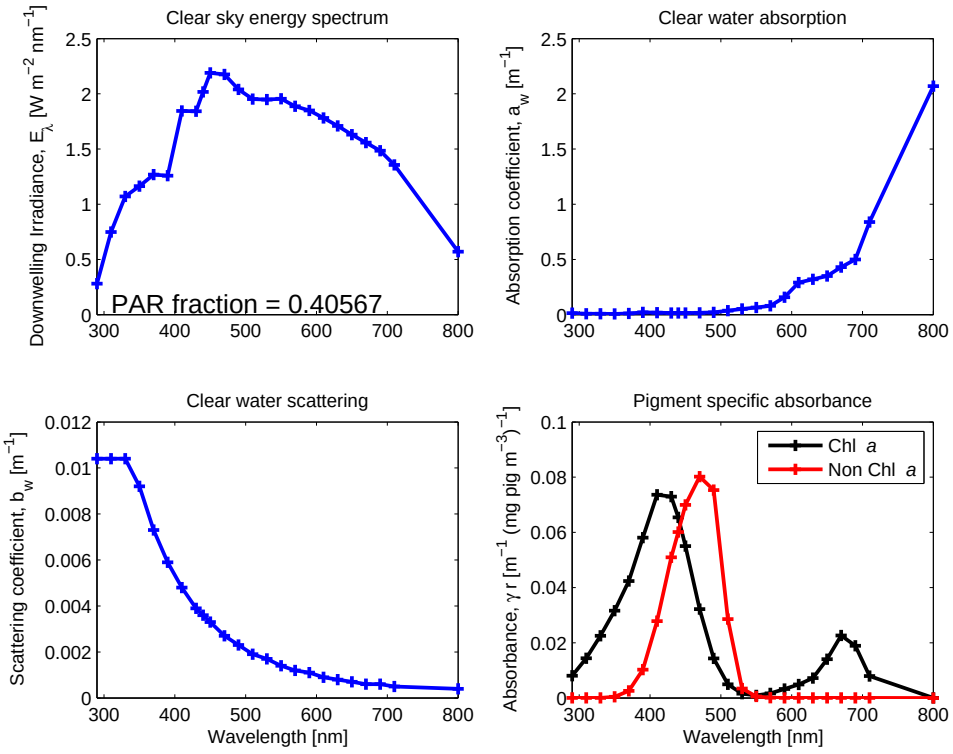

Figure 10. Spectrally-resolved energy distribution of sunlight, clear water absorption, and clear water scattering (Smith and Baker, 1981). The fraction of solar radiation between 400 and 700 nm for clear sky irradiance at the particular spectral resolution is given in the top left panel. The centre of each waveband used in the model simulations is identified by a cross on each curve. The bottom right panel shows the pigment-specific absorption of Chl *a* and generic photosynthetic carotenoids (Ficek et al., 2004) that were used in earlier versions of this model (Baird et al., 2016b) before the mass-specific absorption coefficients of multiple accessory pigments was implemented (Figs. 5, 6 & 7).

where NAP is the concentration of non-algal particulates, $b_{w,\lambda}$ is the scattering coefficient due to clear water (Fig. 10), c_1 and c_2 are the spectrally-resolved, mass-specific coefficients (Figs. 8 & 9) and phytoplankton scattering is the product of the chlorophyll-specific phytoplankton scattering coefficient, $b_{phy,\lambda}$, and the water column chlorophyll concentration of all classes, $\sum n_x c_{i,x} V_x$ (where c_i is the chlorophyll concentration in the cell, and V is the cell volume). The value for $b_{phy,\lambda}$ is set to 0.2 (mg Chl *a* m^{-2})$^{-1}$ for all wavelengths, a typical value for marine phytoplankton (Kirk, 1994). For more details see Baird et al. (2007b).

Backscattering In addition to the IOPs calculated above, the calculation of remote-sensing reflectance uses a backscattering coefficient, b_b, which has a component due to pure seawater, and a component due to algal and non-algal particulates. The backscattering ratio is a coarse resolution representation of the volume scattering function, and is the ratio of the forward and backward scattering.

The backscattering coefficient for clear water is 0.5, a result of isotropic scattering of the water molecule.

The particulate component of backscattering for phytoplankton is strongly related to cell carbon (and therefore cell size) and the number of cells (Vaillancourt et al., 2004):

$$b^*_{bphy,\lambda} = 5 \times 10^{-15} m_C^{1.002} \quad (R^2 = 0.97) \tag{14}$$

where m_C is the carbon content of the cells, here in pg cell^{-1}.

For inorganic particles, backscattering can vary between particle mineralogies, size, shape, and at different wavelengths, resulting, with spectrally-varying absorption, in the variety of colours that we see from suspended sediments. Splitting sediment types by mineralogy only, the backscattering ratio for carbonate and non-carbonate particles is given in Table 3.

	Wavelength [nm]								
	412.0	440.0	488.0	510.0	532.0	595.0	650.0	676.0	715.0
Carbonate	0.0209	0.0214	0.0224	0.0244	0.0216	0.0201	0.0181	0.0170	0.0164
Terrestrial	0.0028	0.0119	0.0175	0.0138	0.0128	0.0134	0.0048	0.0076	0.0113

Table 3. Particulate backscattering ratio for carbonate and non-carbonate minerals based on samples at Lucinda Jetty Coastal Observatory, a site at the interface on carbonate and terrestrial bottom sediment (Soja-Woźniak et al., 2019).

The backscatter due to phytoplankton is approximately 0.02. To account for a greater backscattering ratio, and therefore backscatter, at low wavelengths (Fig. 4 of Vaillancourt et al. (2004)), we linearly increased the backscatter ratio from 0.02 at 555 nm to 0.04 at 470 nm. Above and below 555 nm and 470 nm respectively the backscatter ratio remained constant.

The total backscatter then becomes:

$$b_{b,\lambda} = \tilde{b}_w b_{w,\lambda} + b^*_{bphy,\lambda} n + \tilde{b}_{b,NAP_{non-CaCO_3},\lambda} c_1 NAP_{\mathrm{non-CaCO_3}} + \tilde{b}_{b,NAP_{CaCO_3},\lambda} c_2 NAP_{\mathrm{non-CaCO_3}} NAP_{\mathrm{CaCO_3}} \tag{15}$$

where the backscatter ratio of pure seawater, $\tilde{b}_w$, is 0.5, n is the concentration of cells, and for particulate matter (NAP and detritus), $\tilde{b}_{b,NAP,\lambda}$, is variable (Table 3) and the coefficients c_1 and c_2 come from the total scattering equations above.

4.1.2 Apparent optical properties (AOPs)

The optical model is forced with the downwelling short wave radiation just above the sea surface, based on remotely-sensed cloud fraction observations and calculations of top-of-the-atmosphere clear sky irradiance and solar angle. The calculation of downwelling radiation and surface albedo (a function of solar elevation and cloud cover) is detailed in the hydrodynamic scientific description (`https://research.csiro.au/cem/software/ems/ems-documentation/`, Sec 9.1.1).

The downwelling irradiance just above the water interface is split into wavebands using the weighting for clear sky irradiance (Fig. 10). Snell's law is used to calculate the azimuth angle of the mean light path through the water, θ_{sw}, as calculated from the atmospheric azimuth angle, θ_{air}, and the refraction of light at the air/water interface (Kirk, 1994):

$$\frac{\sin\theta_{air}}{\sin\theta_{sw}} = 1.33 \tag{16}$$

Calculation of in-water light field. Given the IOPs determined above, the exact solution for AOPs would require a radiative transfer model (Mobley, 1994), which is too computationally-expensive for a complex ecosystem model such as developed here. Instead, the in-water light field is solved for using empirical approximations of the relationship between IOPs and AOPs (Kirk, 1991; Mobley, 1994).

The vertical attenuation coefficient at wavelength λ when considering absorption and scattering, K_λ, is given by:

$$K_\lambda = \frac{a_{T,\lambda}}{\cos\theta_{sw}} \sqrt{1 + (g_i \cos\theta_{sw} - g_{ii}) \frac{b_{T,\lambda}}{a_{T,\lambda}}} \tag{17}$$

The term outside the square root quantifies the effect of absorption, where $a_{T,\lambda}$ is the total absorption. The term within the square root of Eq. 17 represents scattering as an extended pathlength through the water column, where g_i and g_{ii} are empirical constants and take values of 0.402 and 0.180 respectively. The values of g_i and g_{ii} depend on the average cosine of scattering. For filtered water with scattering only due to water molecules, the values of g_i and g_{ii} are quite different to natural waters. But for waters ranging from coastal to open ocean, the average cosine of scattering varies by only a small amount (0.86 - 0.95, Kirk (1991)), and thus uncertainties in g_i and g_{ii} do not strongly affect K_λ.

The downwelling irradiance at wavelength λ at the bottom of a layer h thick, $E_{d,\lambda,bot}$, is given by:

$$E_{d,bot,\lambda} = E_{d,top,\lambda} e^{-K_\lambda h} \tag{18}$$

where $E_{d,top,\lambda}$ is the downwelling irradiance at wavelength λ at the top of the layer and K_λ is the vertical attenuation coefficient at wavelength λ, a result of both absorption and scattering processes.

Assuming a constant attenuation rate within the layer, the average downwelling irradiance at wavelength λ, $E_{d,\lambda}$, is given by:

$$E_{d,\lambda} = \frac{1}{h} \int_{bot}^{top} E_{d,z,\lambda} e^{-K_\lambda z} dz = \frac{E_{d,top,\lambda} - E_{d,bot,\lambda}}{K_\lambda h} \tag{19}$$

We can now calculate the scalar irradiance, E_o, for the calculation of absorbing components, from downwelling irradiance, E_d. The light absorbed within a layer must balance the difference in downwelling irradiance from the top and bottom of the layer (since scattering in this model only increases the pathlength of light), thus:

$$E_{o,\lambda} a_{T,\lambda} h = E_{d,top,\lambda} - E_{d,bot,\lambda} = E_{d,\lambda} K_\lambda h \tag{20}$$

Cancelling h, the scalar irradiance as a function of downwelling irradiance is given by:

$$E_{o,\lambda} = \frac{E_{d,\lambda} K_\lambda}{a_{T,\lambda}} \tag{21}$$

This correction conserves photons within the layer, although it is only as a good as the original approximation of the impact of scattering and azimuth angle on vertical attenuation (Eq. 17).

Vertical attenuation of heat. The vertical attenuation of heat is given by:

$$K_{heat} = -\int \frac{1}{E_{d,z,\lambda}} \frac{\partial E_{d,z,\lambda}}{\partial z} d\lambda \tag{22}$$

and the local heating by:

$$\frac{\partial T}{\partial t} = -\frac{1}{\rho c_p} \int \frac{\partial E_{d,\lambda}}{\partial z} d\lambda \tag{23}$$

where T is temperature, ρ is the density of water, and $c_p = 4.1876$ J m^{-3} K^{-1} is the specific heat of water. This calculation does not feed back to the hydrodynamic model.

4.2 Epibenthic optical model

The spectrally-resolved light field at the base of the water column is attenuated, from top to bottom, by macroalgae, seagrass (*Zostera* then shallow and then deep forms of *Halophila*), followed by the zooxanthellae in corals. The downwelling irradiance at wavelength λ after passing through each macroalgae and seagrass species is given by, $E_{below,\lambda}$:

$$E_{below,\lambda} = E_{d,above,\lambda} e^{-A_\lambda \Omega_X X} \tag{24}$$

where $E_{above,\lambda}$ for macroalgae is $E_{d,bot,\lambda}$, the downwelling irradiance of the bottom water column layer, A_λ is the leaf-specific absorptance, Ω is the nitrogen specific leaf area, and X is the leaf nitrogen biomass.

The light absorbed by corals is assumed to be entirely due to zooxanthellae, and is given by:

$$E_{below,\lambda} = E_{above,\lambda} e^{-n\alpha_\lambda} \tag{25}$$

where $n = CS/m_{N,CS}$ is the areal density of zooxanthellae cells and α_λ is the absorption cross-section of a cell a result of the absorption of multiple pigment types.

The optical model for microphytobenthic algae, and the bottom reflectance due to sediment and bottom types, is described in Sec. 7.1.

4.3 Sediment optical model

The optical model in the sediment only concerns the benthic microalgae growing in the porewaters of the top sediment layer. The calculation of light absorption by benthic microalgae assumes they are the only attenuating component in a layer that lies on top layer of sediment, with a perfectly absorbing layer below and no scattering by any other components in the layer. Thus no light penetrates through to the second sediment layer where benthic microalgae also reside. Thus the downwelling irradiance at wavelength λ at the bottom of a layer, $E_{d,\lambda,bot}$, is given by:

$$E_{d,bot,\lambda} = E_{d,top,\lambda} e^{-n\alpha_\lambda h} \tag{26}$$

where $E_{d,top,\lambda}$ is the downwelling irradiance at wavelength λ at the top of the layer and α_λ is the absorption cross-section of the cell at wavelength λ, and n is the concentration of cells in the layer. The layer thickness used here, h, is the thickness of the top sediment layer, so as to convert the concentration of cells in that layer, n, into the areal concentration of cells in the biofilm, nh.

Given no scattering in the cell, and that the vertical attenuation coefficient is independent of azimuth angle, the scalar irradiance that the benthic microalgae are exposed to in the surface biofilm is given by:

$$E_{o,\lambda} = \left(E_{d,top,\lambda} - E_{d,bot,\lambda}\right) / \left(n \alpha_\lambda h\right) \tag{27}$$

The photons captured by each cell, and the microalgae process, follow the same equations as for the water column (Sec. 5.1.3).

5 Pelagic processes

5.1 Microalgae

The model contains four functional groups of suspended microalgae: small and large phytoplankton, microphytobenthos and *Trichodesmium*. The growth from internal reserves for each of the functional groups is identical and explained below. The differences in the ecological interactions of the four functional groups are summarised in Table 4. *Trichodesmium*, a nitrogen fixers, also contains additional processes described below.

	small phyto.	large phyto.	benthic phyto.	*Trichodesmium*
Radius (μm)	1	4	10	5
[a]Maximum growth rate (d^{-1})	1.6	1.4	0.839	0.2
Sink rate (m d^{-1})				variable
Surface sediment growth	×	×	√	×
Nitrogen fixation	×	×	×	√
Water column mort.	√	√	×	√
Sediment mort.	√	√	√	√

Table 4. Traits of suspended microalgae.[a] At $T_{ref} = 20°C$.

5.1.1 Microalgal growth

The growth of microalgae has been modelled in many ways, from simple exponential growth and logistic growth curves, to single and multiple-nutrient based curves, through to equations that contain a state variable for the physiological state of the cell (variously described as stores, quotas, reserves etc.) and to consider the complex processing of photons in the microalgae photosystem.

It is now common for complex biogeochemical models to contain state variables for the physiological state variables of each of potentially limiting nutrients (Baretta-Bekker et al., 1997; Vichi et al., 2007) and include adaptation to photosystems (Geider et al., 1998). In the context of many different microalgae models, the model that is described here has taken another path again. As articulated above, we chose to base nutrient uptake and light absorption on using geometric constraints. This meant that any

Variable	Symbol	Units
Scalar irradiance	E_o	W m^{-2}
Dissolved inorganic nitrogen (DIN)	N	mg N m^{-3}
Dissolved inorganic phosphorus (DIP)	P	mg P m^{-3}
Dissolved inorganic carbon (DIC)	DIC	mg C m^{-3}
Dissolved oxygen	$[O_2]$	mg O m^{-3}
Reserves of nitrogen	R_N	mg N cell^{-1}
Reserves of phosphorus	R_P	mg P cell^{-1}
Reserves of carbon	R_C	mg C cell^{-1}
Maximum reserves of nitrogen	$R_N^{\max}$	mg N cell^{-1}
Maximum reserves of phosphorus	$R_P^{\max}$	mg P cell^{-1}
Maximum reserves of carbon	$R_C^{\max}$	mg C cell^{-1}
Normalised reserves of nitrogen	$R_N^* \equiv R_N/R_N^{\max}$	-
Normalised reserves of phosphorus	$R_P^* \equiv R_P/R_P^{\max}$	-
Normalised reserves of carbon	$R_C^* \equiv R_C/R_C^{\max}$	-
Intracellular Chl *a* concentration	c_i	mg m^{-3}
Structural phytoplankton biomass	B	mg N m^{-3}
Absorption cross-section	α	m^2 cell^{-1}
Diffusion shape factor	ψ	m cell^{-1}
Wavelength	λ	nm
Maximum Chl *a* synthesis rate	$k_{\mathrm{Chl}}^{\max}$	mg Chl m^{-3} d^{-1}
Photon absorption-weighted opaqueness	$\overline{\Theta}$	-
Non-dimensional absorption	$\rho_\lambda = \gamma_\lambda c_i r$	-

Table 5. State and derived variables for the microalgae growth model. DIN is given by the sum of nitrate and ammonia concentrations, $[NO_3]$+$[NH_4]$.

growth model needed to be formulated around the maximum rate of supply of each of the limiting nutrients (and light) (see Fig 2 of Baird et al. (2006)).

In the microalgae model (most fully described in Baird et al. (2001)), the uptake of nutrients and light absorption increases the reserves of nutrients and light, as quantified by a reserve, R, which has units of mass per cell. In the equations we often use a normalised reserve, R^*, which is a quantity between zero and one (Tab. 5). The reserves are in turn consumed to generate structural material. Thus the total content of nitrogen in the microalgae is equal to the sum of the structural material and the reserves.

The model considers the diffusion-limited supply of dissolved inorganic nutrients (N and P) and the absorption of light, delivering N, P and fixed C to the internal reserves of the cell (Fig. 11). Nitrogen and phosphorus are taken directly into the

reserves, but carbon is first fixed through photosynthesis (Kirk, 1994):

$$106\mathrm{CO_2} + 212\mathrm{H_2O} \overset{1060\ \mathrm{photons}}{\longrightarrow} 106\mathrm{CH_2O} + 106\mathrm{H_2O} + 106\mathrm{O_2} \tag{28}$$

The internal reserves of C, N, and P are consumed to form structural material at the Redfield ratio (Redfield et al., 1963):

$$\begin{aligned} &106\mathrm{CH_2O} + 16\mathrm{NH_4^+} + \mathrm{PO_4^{3-}} + 16\mathrm{H_2O} \\ &\qquad \longrightarrow \quad (\mathrm{CH_2O})_{106}(\mathrm{NH_3})_{16}\mathrm{H_3PO_4} + 13\mathrm{H^+} \end{aligned} \tag{29}$$

where we have represented nitrogen as ammonia (NH_4) in Eq. 29. When the nitrogen source to the cell is nitrate, NO_3, it is assumed to lose its oxygen at the cell wall (Sec. 9.1). The growth rate of microalgae is given by the maximum growth rate, μ^{max}, multiplied by the normalised reserves, R^*, of each of N, P and C:

$$\mu = \mu^{max} R_N^* R_P^* R_C^* \tag{30}$$

The mass of the reserves (and therefore the total C:N:P:Chl *a* ratio) of the cell depends on the interaction of the supply and consumption rates (Fig. 11). When consumption exceeds supply, and the supply rates are non-Redfield, the normalised internal reserves of the non-limiting nutrients approach 1 while the limiting nutrient becomes depleted. Thus the model behaves like a 'Law of the Minimum' growth model, except during fast changes in nutrient supply rates.

The molar ratio of a cell, the addition of structural material and reserves, is given by:

$$\mathrm{C:N:P} = 106(1 + R_C^*) : 16(1 + R_N^*) : 1 + R_P^* \tag{31}$$

5.1.2 Nutrient uptake

The diffusion-limited nutrient uptake to a single phytoplankton cell, J, is given by:

$$J = \psi D \left(C_b - C_w\right) \tag{32}$$

where ψ is the diffusion shape factor ($= 4\pi r$ for a sphere), D is the molecular diffusivity of the nutrient, C_b is the average extracellular nutrient concentration, and C_w is the concentration at the wall of the cell. The diffusion shape factor is determined by equating the divergence of the gradient of the concentration field to zero ($\nabla^2 C = 0$).

A semi-empirical correction to Eq. 32, to account for fluid motion around the cell, and the calculation of non-spherical diffusion shape factors, has been applied in earlier work (Baird and Emsley, 1999). For the purposes of biogeochemical modelling these uncertain corrections for small scale turbulence and non-spherical shape are not quantitatively important, and have not been pursued here.

Numerous studies have considered diffusion-limited transport to the cell surface at low nutrient concentrations saturating to a physiologically-limited nutrient uptake from the cell wall (Hill and Whittingham, 1955; Pasciak and Gavis, 1975; Mann

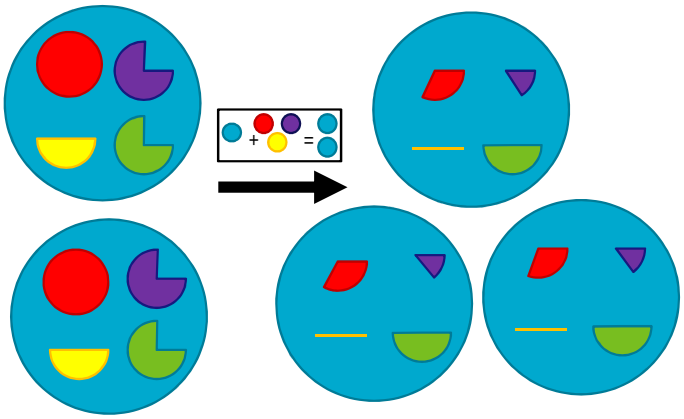

Figure 11. Schematic of the process of microalgae growth from internal reserves. Blue circle - structural material; Red pie - nitrogen reserves; Purple pie - phosphorus reserves; Yellow pie - carbon reserves; Green pie - pigment content. Here a circular pie has a value of 1, representing the normalised reserve (a value between 0 and 1). The box shows that to generate structural material for an additional cell requires the equivalent of 100 % internal reserves of carbon, nitrogen and phosphorus of one cell. This figure shows the discrete growth of 2 cells to 3, requiring both the generation of new structural material from reserves and the reserves being diluted as a result of the number of cells in which they are divided increasing from 2 to 3. Thus the internal reserves for nitrogen after the population increases from 2 to 3 is given by: two from the initial 2 cells, minus one for building structural material of the new cell, shared across the 3 offspring, to give 1/3. The same logic applies to carbon and phosphorus reserves, with phosphorus reserves being reduced to 1/6, and carbon reserves being exhausted. In contrast, pigment is not required for structural material so the only reduction is through dilution; the 3/4 content of 2 cells is shared among 3 cells to equal 1/2 in the 3 cells. This schematic shows one limitation of a population-style model whereby reserves are 'shared' across the population (as opposed to individual based modelling, Beckmann and Hense (2004)). A proof of the conservation of mass for this scheme, including under mixing of populations of suspended microalgae, is given in Baird et al. (2004). The model equations also include terms affecting internal reserves through nutrient uptake, light absorption, respiration and mortality that are not shown in this simple schematic.

and Lazier, 2006) at higher concentrations. The physiological limitation is typically considered using a Michaelis-Menten type equation. Here we simply consider the diffusion-limited uptake to be saturated by the filling-up of reserves, $(1 - R^*)$. Thus, nutrient uptake is given by:

$$J = \psi D C_b \left(1 - R^*\right) \tag{33}$$

where R^* is the normalised reserve of the nutrient being considered. As shown later when considering preferential ammonia uptake, under extreme limitation relative to other nutrients, R^* approaches 0, and uptake approaches the diffusion limitation.

5.1.3 Light capture and chlorophyll synthesis

Light absorption by microalgae cells has already been considered above Eq. 6. The same absorption cross-section, α, is used to calculate the capture of photons:

$$\frac{\partial R_C^*}{\partial t} = (1 - R_C^*) \frac{(10^9 hc)^{-1}}{A_V} \int \alpha_\lambda E_{o,\lambda} \lambda \, d\lambda \tag{34}$$

where $(1 - R_C^*)$ accounts for the reduced capture of photons as the reserves becomes saturated, and $\frac{(10^9 hc)^{-1}}{A_V}$ converts from energy to photons. The absorption cross-section is a function of intracellular pigment concentration, which is a dynamic variable determined below. While a drop-off of photosynthesis occurs as the carbon reserves become replete, this formulation does not consider photoinhibition due to photooxidation, although it has been considered elsewhere for zooxanthallae (Baird et al., 2018).

The dynamic C:Chl component determines the rate of synthesis of pigment based on the incremental benefit of adding pigment to the rate of photosynthesis. This calculation includes both the reduced benefit when carbon reserves are replete, $(1 - R_C^*)$, and the reduced benefit due to self-shading, χ. The factor χ is calculated for the derivative of the absorption cross-section per unit projected area (see Eq. 6), α/PA, with non-dimensional group $\rho = \gamma c_i r$. For a sphere of radius r (Baird et al., 2013):

$$\frac{1}{PA} \frac{\partial \alpha}{\partial \rho} = \frac{1 - e^{-2\rho}(2\rho^2 + 2\rho + 1)}{\rho^3} = \chi \tag{35}$$

where χ represents the area-specific incremental rate of change of absorption with ρ. The rate of chlorophyll synthesis is given by:

$$\frac{\partial c_i}{\partial t} = k_{\mathrm{Chl}}^{\max} (1 - R_C^*) \overline{\chi} \quad \text{if C : Chl} > \theta_{min} \tag{36}$$

where $k_{\mathrm{Chl}}^{\max}$ is the maximum rate of synthesis and θ_{min} is the minimum C:Chl ratio. Below θ_{min}, pigment synthesis is zero. Both self-shading, and the rate of photosynthesis itself, are based on photon absorption rather than energy absorption (Table 6), as experimentally shown in Nielsen and Sakshaug (1993).

For each phytoplankton type the model considers multiple pigments with distinct absorption spectra. The model needs to represent all photo-absorbing pigments as the C:Chl model calculates the pigment concentration based on that required to maximise photosynthesis. If only Chl *a* was represented, the model would predict a Chl *a* concentration that was accounting for the absorption of Chl *a* and the auxiliary pigments, thus over-predicting the Chl *a* concentration when compared to observations. Thus the Chl-a predicted by the model is like a HPLC-determined Chl-a concentration, and not the sum of the photosynthetic pigments.

5.1.4 Carbon fixation / respiration

When photons are captured (photosynthesis) there is an increase in reserves of carbon, $k_I(1-R_C^*)$ (Eq. 48), and an accompanying uptake of dissolved inorganic carbon, $\frac{106}{1060}12k_I(1-R_C^*)$ (Eq. 44), and release of oxygen, $\frac{106}{1060}32k_I(1-R_C^*)$ (Eq. 45), per cell to the water column (Table 6).

Additionally, there is a basal respiration, representing a constant cost of cell maintenance. The loss of internal reserves, $\mu_B^{\max} m_{B,C}\phi R_C^*$, results in a gain of water column dissolved inorganic carbon per cell, $\frac{106}{1060}\frac{12}{14}\mu_B^{\max}\phi R_C^*$, as well as a loss in water column dissolved oxygen per cell, $\frac{106}{1060}\frac{32}{14}\mu_B^{\max}\phi R_C^*$ (Table 6). The loss in water column dissolved oxygen per cell represents an instantaneous respiration of the fixed carbon of the reserves. Basal respiration decreases internal reserves, and therefore growth rate, but does not directly lead to cell mortality at zero carbon reserves. Implicit in this scheme is that the basal cost is higher when the cell has more carbon reserves, R_C^*.

A linear mortality term, resulting in the loss of structural material and carbon reserves, is considered later.

5.1.5 Application of single cell rates to a population

As mentioned above, the nutrient uptake and light absorption rates are calculated on a per cell basis. This has allowed geometric considerations to be explicitly used, and contrasts with most biogeochemical models that formulate planktonic rates based on population interactions. However, the state variables for microalgae (and zooplankton) are for the population. Therefore, rates per cell need to be multiplied by the number of cells to obtain population rates. In the case of microalgae, the number of cells n is given by $B/m_{B,N}$. It should be noted that firstly this assumes all cells in the population are identical, and that the state variable for the population, B, is quantifying only the nitrogen (or oxygen, carbon and phosphorus) associated with the structural material. It should also be noted that all cells in a population have the same quantity in their reserves.

5.1.6 Conservation of mass of microalgae model

The conservation of mass during transport, growth and mortality is proven in Baird et al. (2004). Briefly, for microalgal growth, total concentration of nitrogen in microalgae cells is given by $B + BR_N^*$. For conservation of mass, the time derivatives must equate to zero:

$$\frac{\partial B}{\partial t} + \frac{\partial (R_N B/R_N^{max})}{\partial t} = 0. \tag{37}$$

using the product rule to differentiate the second term on the LHS:

$$\frac{\partial B}{\partial t} + \frac{\partial B}{\partial t}\frac{R_N}{R_N^{max}} + \frac{B}{R_N^{max}}\frac{\partial R_N}{\partial t} = 0 \tag{38}$$

Where:

$$\frac{\partial B}{\partial t} = +\mu_B^{max} R_C^* R_N^* R_P^* B \tag{39}$$

$$\frac{\partial B}{\partial t}\frac{R_N}{R_N^{max}} = +\mu_B^{max} R_C^* R_N^* R_P^* B \frac{R_N}{R_N^{max}} \tag{40}$$

$$
\begin{aligned}
\frac{\partial N}{\partial t} &= -\psi D_N N(1-R_N^*)\,(B/m_{B,N}) && (42)\\
\frac{\partial P}{\partial t} &= -\psi D_P P(1-R_P^*)\,(B/m_{B,N}) && (43)\\
\frac{\partial DIC}{\partial t} &= -\left(\frac{106}{1060}12k_I(1-R_C^*) - \frac{106}{16}\frac{12}{14}\mu_B^{\max}\phi R_C^*\right)(B/m_{B,N}) && (44)\\
\frac{\partial [\mathrm{O_2}]}{\partial t} &= \left(\frac{106}{1060}32k_I(1-R_C^*) - \frac{106}{16}\frac{32}{14}\mu_B^{\max}\phi R_C^*\right)(B/m_{B,N}) && (45)\\
\frac{\partial R_N}{\partial t} &= \psi D_N N(1-R_N^*) - \mu_B^{\max}\,(m_{B,N}+R_N)\,R_P^* R_N^* R_C^* && (46)\\
\frac{\partial R_P}{\partial t} &= \psi D_P P(1-R_P^*) - \mu_B^{\max}\,(m_{B,P}+R_P)\,R_P^* R_N^* R_C^* && (47)\\
\frac{\partial R_C}{\partial t} &= k_I(1-R_C^*) - \mu_B^{\max}\,(m_{B,C}+R_C)\,R_P^* R_N^* R_C^* - \mu_B^{\max}\phi m_{B,C} R_C^* && (48)\\
\frac{\partial B}{\partial t} &= \mu_B^{\max} R_P^* R_N^* R_C^* B && (49)\\
\frac{\partial c_i}{\partial t} &= k_{\mathrm{Chl}}^{\max}(1-R_C^*)\overline{\chi} - \mu_P^{\max} R_P^* R_N^* R_C^* c_i && (50)\\
\psi &= 4\pi r && (51)\\
k_I &= \frac{(10^9 hc)^{-1}}{A_V}\int \alpha_\lambda E_{o,\lambda}\lambda\, d\lambda && (52)\\
\alpha_\lambda &= \pi r^2\left(1 - \frac{2(1-(1+2\rho_\lambda)e^{-2\rho_\lambda})}{4\rho_\lambda^2}\right) && (53)\\
\overline{\chi} &= \int \chi_\lambda E_{o,\lambda}\lambda\; d\lambda \;\Big/ \int E_{o,\lambda}\lambda\; d\lambda && (54)\\
\chi_\lambda &= \frac{1}{\pi r^2}\frac{\partial \alpha_\lambda}{\partial \rho_\lambda} = \frac{1-e^{-2\rho_\lambda}(2\rho_\lambda^2+2\rho_\lambda+1)}{\rho_\lambda^3} && (55)\\
\rho_\lambda &= \gamma c_i r && (56)
\end{aligned}
$$

Table 6. Microalgae growth model equations. The term $B/m_{B,N}$ is the concentration of cells. The equation for organic matter formation gives the stoichiometric constants; 12 g C mol C^{-1}; 32 g O mol O_2^{-1}. The equations are for scalar irradiance specified as an energy flux.

$$
\frac{B}{R_N^{max}}\frac{\partial R_N}{\partial t} = -B(1+R_N^*)\mu_B^{max} R_C^* R_N^* R_P^* \frac{R_N}{R_N^{max}} \qquad (41)
$$

Thus demonstrating conservation of mass when $m_{B,N} = R_N^{max}$, as used here.

The state variables, equations and parameter values are listed in Tables 5, 6 and 7 respectively. The equations in Table 6 described nitrogen uptake from the DIN pool, where the partitioning between nitrate and ammonia due to preferential ammonia uptake is described in Sec. 9.1. Earlier published versions of the microalgae model are described with multiple nutrient limitation (Baird et al., 2001), with variable C:N ratios (Wild-Allen et al., 2010) and variable C:Chl ratios (Baird et al., 2013).

	Symbol	Value
Constants		
[d]Molecular diffusivity of NO_3	D_N	$f(T,S)$ m^2 s^{-1}
[d]Molecular diffusivity of PO_4	D_P	$f(T,S)$ m^2 s^{-1}
Speed of light	c	2.998×10^8 m s^{-1}
Planck constant	h	6.626×10^{-34} J s^{-1}
Avogadro constant	A_V	6.02×10^{23} mol^{-1}
[a]Pigment-specific absorption coefficient	$\gamma_{\mathrm{pig},\lambda}$	$f(\mathrm{pig},\lambda)$ m^{-1} $\left(\mathrm{mg\ m^{-3}}\right)^{-1}$
[d]Minimum C:Chl ratio	θ_{min}	20.0 wt/wt
Allometric relationships		
[b]Carbon content	$m_{B,C}$	$12010 \times 9.14 \times 10^3 V$ mg C cell^{-1}
[c]Maximum intracellular Chl *a* concentration	$c_i^{\max}$	$2.09 \times 10^7 V^{-0.310}$ mg Chl m^{-3}
Nitrogen content of phytoplankton	$m_{B,N}$	$\frac{14}{12}\frac{16}{106} m_{B,C}$ mg N cell^{-1}

Table 7. Constants and parameter values used in the microalgae model. V is cell volume in μm^3. [a] Figs. 5 6 & 7,[b]Straile (1997),[c] Finkel (2001), Sathyendranath et al. (2009) using HPLC-determination which isolate Chl-a; [d] Li and Gregory (1974).

Further, demonstration of the conservation of mass during transport is given in Baird et al. (2004). Here the microalgae model is presented with variable C:Chl ratios (with an additional auxiliary pigment), and both nitrogen and phosphorus limitation, and a preference for ammonia uptake when compared to nitrate.

5.2 Nitrogen-fixing *Trichodesmium*

The growth of *Trichodesmium* follows the microalgae growth and C:Chl model above, with the following additional processes of nitrogen fixation and physiological-dependent buoyancy adjustment, as described in Robson et al. (2013). Additional parameter values for *Trichodesmium* are given in Table 8.

5.2.1 Nitrogen fixation

Nitrogen fixation occurs when the DIN concentration falls below a critical concentration, DIN_{crit}, typically 0.3 to 1.6 μmol L^{-1} (i.e. 4 to 20 mg N m^{-3}, Robson et al. (2013)), at which point *Trichodesmium* produce nitrogenase to allow fixation of N_2. It is assumed that nitrogenase becomes available whenever ambient DIN falls below the value of DIN_{crit} and carbon and phosphorus are available to support nitrogen uptake. The rate of change of internal reserves of nitrogen, R_N, due to nitrogen fixation if $DIN < DIN_{crit}$ is given by:

$$N_{fix} = \frac{\partial R_N}{\partial t}|_{N_{fix}} = \max\left(4\pi r D_{\mathrm{NO_3}} DIN_{crit} R_P^* R_C^* (1 - R_N^*) - 4\pi r D_{\mathrm{NO_3}} \left[\mathrm{NO_3} + \mathrm{NH_4}\right](1 - R_N^*), 0\right) \quad (57)$$

	Symbol	Value
Maximum growth rate	μ^{max}	0.2 d^{-1}
[b]Ratio of xanthophyll to Chl *a*	f_{xan}	0.5
Linear mortality	m_L	0.10 d^{-1}
Quadratic mortality	m_Q	0.10 d^{-1} (mg N m^{-3})$^{-1}$
Cell radius	r	5 μm
Colony radius	r_{col}	5 μm
Max. cell density	ρ_{max}	1050 kg m^{-3}
Min. cell density	ρ_{min}	900 kg m^{-3}
Critical threshold for N fixation	DIN_{crit}	10 mg N m^{-3}
Fraction of energy used for nitrogenase	$f_{nitrogenase}$	0.07
Fraction of energy used for N fixation	f_{Nfix}	0.33
Nitrogen gas in equilibrium with atm.	[N_2]	2 $\times 10^4$ mg N m^{-3}

Table 8. Parameter values used in the *Trichodesmium* model (Robson et al., 2013). [b] The major accessory pigments in *Trichodesmium* are the red-ish phycourobilin and phycoerythrobilin (Subramaniam et al., 1999). For simplicity in this model their absorption cross-section is approximated by photosynthetic xanthophyll, which has an absorption peak approximately 10 nm less than the phycourobilin.

where N_{fix} is the rate of nitrogen fixation per cell and r is the radius of the individual cell. Using this formulation, *Trichodesmium* is able to maintain its nitrogen uptake rate at that achieved through diffusion limited uptake at DIN_{crit} even when DIN drops below DIN_{crit}, provided phosphorus and carbon reserves, R_P^* and R_C^* respectively, are available.

The energetic cost of nitrogen fixation is represented as a fixed proportion of carbon fixation, f_{Nfix}, equivalent to a reduction in quantum efficiency, and as a proportion, $f_{nitrogenase}$, of the nitrogen fixed:

$$\frac{\partial R_C}{\partial t} = -(1 - f_{Nfix})(1 - f_{nitrogenase})k_I \tag{58}$$

where k_I is the rate of photon absorption per cell obtain from the microalgal growth model (Table 6).

5.2.2 Buoyancy adjustment

The rate of change of *Trichodesmium* biomass, B, as a result of density difference between the cell and the water, is approximated by Stokes' Law:

$$\frac{\partial B}{\partial t} = -\frac{2}{9}\frac{g r_{col}^2}{\mu}(\rho - \rho_w)\frac{\partial B}{\partial z} \tag{59}$$

where z is the distance in the vertical (+ve up), μ is the dynamic viscosity of water, g is acceleration due to gravity, r_{col} is the equivalent spherical radius of the sinking mass representing a colony radius, ρ_w is the density of water, and ρ is the cell density is given by:

$$\rho = \rho_{min} + R_C^* \left(\rho_{max} - \rho_{min}\right) \tag{60}$$

where R_C^* is the normalised carbon reserves of the cell (see above), and ρ_{min} and ρ_{max} are the densities of the cell when there is no carbon reserves and full carbon reserves respectively. Thus, when light reserves are depleted, the cell is more buoyant, facilitating the retention of *Trichodesmium* in the surface waters.

5.3 Water column inorganic chemistry

5.3.1 Carbon chemistry

The major pools of dissolved inorganic carbon species in the ocean are HCO_3^-, CO_3^-, and dissolved CO_2, which influence the speciation of H^+, and OH^- ions, and therefore pH. The interaction of these ions reaches an equilibrium in seawater within a few tens of seconds (Zeebe and Wolf-Gladrow, 2001). In the biogeochemical model here, where calculation timesteps are of order tens of minutes, it is reasonable to assume that the carbon chemistry system is at equilibrium.

The Ocean-Carbon Cycle Model Intercomparison Project (OCMIP) has developed numerical methods to quantify air-sea carbon fluxes and carbon dioxide system equilibria (Najjar and Orr, 1999). Here we use a modified version of the OCMIP-2 Fortran code developed for MOM4 (GFDL Modular Ocean Model version 4, (Griffies et al., 2004)). The OCMIP procedures quantify the state of the carbon dioxide (CO_2) system using two prognostic variables, the concentration of dissolved inorganic carbon, DIC, and total alkalinity, A_T. The value of these prognostic variables, along with salinity and temperature, are used to calculate the pH and partial pressure of carbon dioxide, $p\mathrm{CO}_2$, in the surface waters using a set of governing chemical equations which are solved using a Newton-Raphson method (Najjar and Orr, 1999).

One alteration from the global implementation of the OCMIP scheme is to increase the search space for the iterative scheme from $\pm$0.5 pH units (appropriate for global models) to $\pm$2.5. With this change, the OCMIP scheme converges over a broad range of DIC and A_T values (Munhoven, 2013).

For more details see Mongin and Baird (2014); Mongin et al. (2016b).

5.3.2 Nitrification

Nitrification is the oxidation of ammonia with oxygen, to form nitrite followed by the rapid oxidation of these nitrites into nitrates. This is represented in a one step processes, with the rate of nitrification given by:

$$\frac{\partial[\mathrm{NH_4}]}{\partial t} = -\tau_{nit,wc}[\mathrm{NH_4}]\frac{[\mathrm{O_2}]}{K_{nit,\mathrm{O}} + [\mathrm{O_2}]} \tag{67}$$

where the equations and parameter values are defined in Tables 10 and 11.

Variable	Symbol	Units
Ammonia concentration	$[\mathrm{NH_4}]$	mg N $\mathrm{m^{-3}}$
Water column Dissolved Inorganic Carbon (DIC)	DIC	mg C $\mathrm{m^{-3}}$
Water column Dissolved Inorganic Phosphorus (DIP)	P	mg P $\mathrm{m^{-3}}$
Water column Particulate Inorganic Phosphorus (PIP)	PIP	mg P $\mathrm{m^{-3}}$
Water column Non-Algal Particulates (NAP)	NAP	kg $\mathrm{m^{-3}}$
Water column dissolved oxygen concentration	$[\mathrm{O_2}]$	mg O $\mathrm{m^{-3}}$

Table 9. State and derived variables for the water column inorganic chemistry model.

$$\mathrm{NH_4^+ + 2O_2 \longrightarrow NO_3^- + H_2O + 2H^+} \tag{61}$$

$$\frac{\partial[\mathrm{NH_4}]}{\partial t} = -\tau_{nit,wc}[\mathrm{NH_4}]\frac{[\mathrm{O_2}]}{K_{nit,\mathrm{O}}+[\mathrm{O_2}]} \tag{62}$$

$$\frac{\partial[\mathrm{O_2}]}{\partial t} = -2\tau_{nit,wc}[\mathrm{NH_4}]\frac{[\mathrm{O_2}]}{K_{nit,\mathrm{O}}+[\mathrm{O_2}]} \tag{63}$$

$$\frac{\partial[\mathrm{NO_3}]}{\partial t} = \tau_{nit,wc}[\mathrm{NH_4}]\frac{[\mathrm{O_2}]}{K_{nit,\mathrm{O}}+[\mathrm{O_2}]} \tag{64}$$

$$\frac{\partial P}{\partial t} = \tau_{Pabs}\left(\frac{PIP}{k_{Pads,wc}NAP} - \frac{[\mathrm{O_2}]P}{K_{\mathrm{O_2,abs}}+[\mathrm{O_2}]}\right) \tag{65}$$

$$\frac{\partial PIP}{\partial t} = -\tau_{Pabs}\left(\frac{PIP}{k_{Pads,wc}NAP} - \frac{[\mathrm{O_2}]P}{K_{\mathrm{O_2,abs}}+[\mathrm{O_2}]}\right) \tag{66}$$

Table 10. Equations for the water column inorganic chemistry.

Description	Symbol	Units
Maximum rate of nitrification in the water column	$\tau_{nit,wc}$	0.1 $\mathrm{d^{-1}}$
Oxygen half-saturation constant for nitrification	$K_{nit,\mathrm{O}}$	500 mg O $\mathrm{m^{-3}}$
Rate of P adsorbed/desorbed equilibrium	τ_{Pabs}	0.04 $\mathrm{d^{-1}}$
Isothermic const. P adsorption for NAP	$k_{Pads,wc}$	30 kg $\mathrm{NAP^{-1}}$
Oxygen half-saturation for P adsorption	$K_{\mathrm{O_2,abs}}$	2000 mg O $\mathrm{m^{-3}}$

Table 11. Constants and parameter values used in the water column inorganic chemistry.

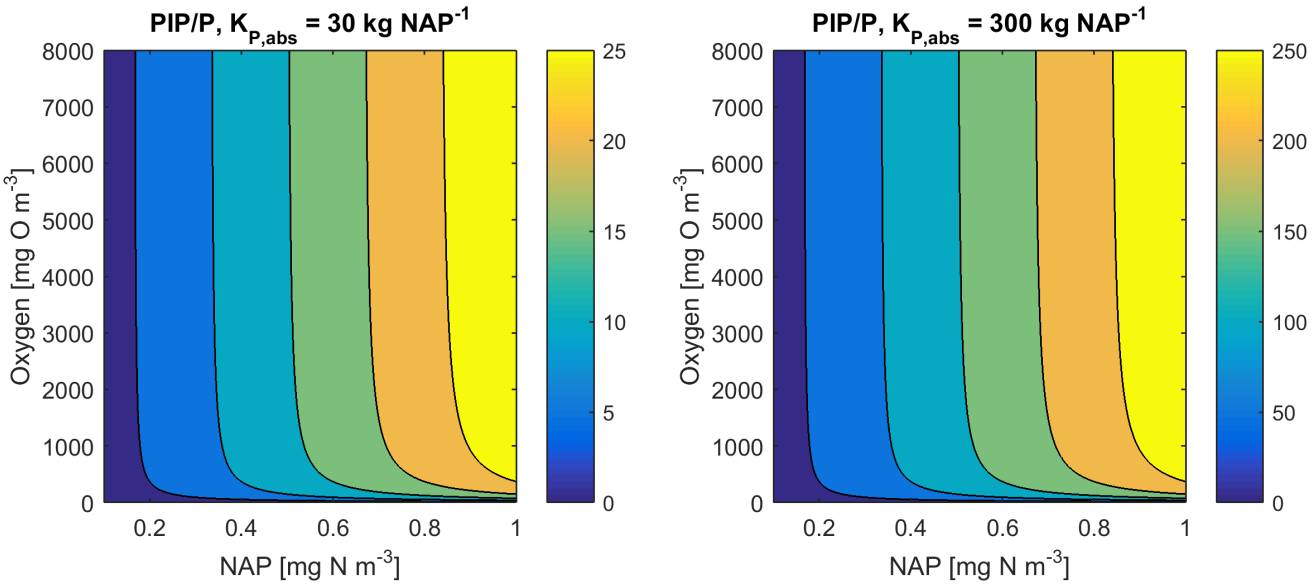

Figure 12. Phosphorus adsorption - desorption equilibria, $K_{\mathrm{O_2,abs}}$ = 74 mg O m^{-3}.

5.3.3 Phosphorus absorption - desorption

The rate of phosphorus desorption from particulates is given by:

$$\frac{\partial P}{\partial t} = \tau_{Pabs}\left(\frac{PIP}{k_{Pads,wc}NAP} - \frac{[\mathrm{O_2}]P}{K_{\mathrm{O_2,abs}} + [\mathrm{O_2}]}\right) = -\frac{\partial PIP}{\partial t} \tag{68}$$

where [O$_2$] is the concentration of oxygen, P is the concentration of dissolved inorganic phosphorus, PIP is the concentration of particulate inorganic phosphorus, NAP is the sum of the non-algal inorganic particulate concentrations, and τ_{Pabs}, $k_{Pads,wc}$ and $K_{\mathrm{O_2,abs}}$ are model parameters described in Table 11.

At steady-state, the PIP concentration is given by:

$$PIP = k_{Pads,wc}P\frac{[\mathrm{O_2}]}{K_{\mathrm{O_2,abs}} + [\mathrm{O_2}]}NAP \tag{69}$$

As an example for rivers flowing into the eReefs configuration, [O$_2$] = 7411 mg m^{-3} (90% saturation at T = 25, S = 0), NAP = 0.231 kg m^{-3}, $k_{Pads,wc}$ = 30 kg NAP^{-1}, $K_{\mathrm{O_2,abs}}$ = 74 mg O m^{-3}, P = 4.2 mg m^{-3}, thus the ratio PIP/DIP = 6.86 (see Fig. 12).

Limited available observations of absorption-desorption include from the Johnstone River (Pailles and Moody, 1992) and the GBR (Monbet et al., 2007).

5.4 Zooplankton herbivory

In the simple food web of the model, herbivory involves small zooplankton consuming small phytoplankton, and large zooplankton consuming large phytoplankton, microphytobenthos and *Trichodesmium*. For simplicity the state variables and equations are only given for small plankton grazing (Tables 12, 14), but the parameters are given for all grazing terms (Table 13).

The rate of zooplankton grazing is determined by the encounter rate of the predator and all its prey up until the point at which it saturates the growth of the zooplankton (Eq. 77), and then it is constant. This is effectively a Hollings Type I grazing response (Gentleman, 2002). Under the condition of multiple prey types, there is no preferential grazing other than that determined by the chance of encounter. The encounter rate is the result of the relative motion of individuals brought about by diffusive (Eq. 79), swimming (Eq. 80), and shear (Eq. 81) determined relative velocities (Eq. 82) (Jackson, 1995; Baird, 2003). One particular advantage of formulating the encounter rate on individuals is that should the number of populations considered in the model change (i.e. an additional phytoplankton class is added), there is no need for empirical coefficients in the model to change. More recent uses of encounter based grazing functions are described in Flynn and Mitra (2016).

Unlike the microalgae, zooplankton does not contain reserves of nutrients and fixed carbon, and therefore has a fixed stoichiometry of the Redfield ratio. As the zooplankton are grazing on the phytoplankton that contain internal reserves of nutrients an addition flux of dissolved inorganic nutrients (gR^*_N for nitrogen) is returned to the water column (for more details see Sec. 5.4.1).

5.4.1 Conservation of mass in zooplankton grazing

It is important to note that the microalgae model presented above represents internal reserves of nutrients, carbon and chlorophyll as a per cell quantity. Using this representation there are no losses of internal quantities with either grazing or mortality. However the implication of their presence is represented in the (gR^*_N) terms (Table 14) that return the reserves to the water column. These terms represent the fast return of a fraction of phytoplankton nitrogen due to processes like "sloppy eating".

An alternative and equivalent formulation would be to consider total concentration of microalgal reserves in the water column, then the change in water column concentration of reserves due to mortality (either grazing or natural mortality) must be considered. This alternate representation will not be undertaken here as the above considered equations are fully consistent, but it is worth noting that the numerical solution of the model within the EMS package represents total water column concentrations of internal reserves, and therefore must include the appropriate loss terms due to mortality.

5.5 Zooplankton carnivory

Large zooplankton consume small zooplankton. This process uses similar encounter rate and consumption rate limitations calculated for zooplankton herbivory (Table 14). As zooplankton contain no internal reserves, the equations are simplified from the herbivory case to those listed in Table 15). Assuming that the efficiency of herbivory, γ, is equal to that of carnivory,

Variable	Symbol	Units
Ammonia concentration	$[NH_4]$	mg N m^{-3}
Water column dissolved Inorganic Carbon (DIC)	DIC	mg C m^{-3}
Water column dissolved Inorganic Phosphorus (DIP)	P	mg P m^{-3}
Water column dissolved oxygen concentration	$[O_2]$	mg O m^{-3}
Reserves of phytoplankton nitrogen	R_N	mg N $cell^{-1}$
Reserves of phytoplankton phosphorus	R_P	mg P $cell^{-1}$
Reserves of phytoplankton carbon	R_C	mmol photon $cell^{-1}$
Maximum reserves of nitrogen	$R_N^{\max}$	mg N $cell^{-1}$
Maximum reserves of phosphorus	$R_P^{\max}$	mg P $cell^{-1}$
Maximum reserves of carbon	$R_C^{\max}$	mmol photon $cell^{-1}$
Normalised reserves of nitrogen	$R_N^* \equiv R_N/R_N^{\max}$	-
Normalised reserves of phosphorus	$R_P^* \equiv R_P/R_P^{\max}$	-
Normalised reserves of carbon	$R_C^* \equiv R_C/R_C^{\max}$	-
Phytoplankton structural biomass	B	mg N m^{-3}
Zooplankton biomass	Z	mg N m^{-3}
Detritus at the Redfield ratio	D_{Red}	mg N m^{-3}
Zooplankton grazing rate	g	mg N m^{-3} s^{-1}
Encounter rate coefficient due to molecular diffusion	ϕ_{diff}	m^3 s^{-1} cell Z^{-1}
Encounter rate coefficient due to relative motion	ϕ_{rel}	m^3 s^{-1} cell Z^{-1}
Encounter rate coefficient due to turbulent shear	ϕ_{shear}	m^3 s^{-1} cell Z^{-1}
Phytoplankton cell mass	$m_{B,N}$	mg N $cell^{-1}$
Zooplankton cell mass	$m_{Z,N}$	mg N $cell^{-1}$

Table 12. State and derived variables for the zooplankton grazing. Zooplankton cell mass, $m_Z = 16000 \times 14.01 \times 10.5 V_Z$ mg N $cell^{-1}$, where V_Z is the volume of zooplankton (Hansen et al., 1997).

Description	Symbol	Small	Large
Maximum growth rate of zooplankton at T_{ref} (d^{-1})	μ_Z	4.0	1.33
Nominal cell radius of zooplankton (μm)	r_Z	5	320
Growth efficiency of zooplankton	E_Z	0.462	0.426
Fraction of growth inefficiency lost to detritus	γ_Z	0.5	0.5
Swimming velocity ($\mu m\ s^{-1}$)	U_Z	200	3000
Constants			
Boltzmann's constant	κ	1.38066×10^{-23}	$J\ K^{-1}$
Viscosity	ν	10^{-6}	$m^2\ s^{-1}$
Dissipation rate of TKE	ϵ	10^{-6}	$m^3\ s^{-1}$
Oxygen half-saturation for aerobic respiration	K_{OA}	256	$mg\ O\ m^{-3}$

Table 13. Constants and parameter values used for zooplankton grazing. Dissipation rate of turbulent kinetic energy (TKE) is considered constant.

and therefore assigned the same parameter, the additional process of carnivory adds no new parameters to the biogeochemical model.

5.6 Zooplankton respiration

In the model there is no change in water column oxygen concentration if organic material is exchanged between pools with the same elemental ratio. Thus, when zooplankton consume phytoplankton no oxygen is consumed due to the consumption of phytoplankton structural material (B_P). However, the excess carbon reserves represent a pool of fixed carbon, which when released from the phytoplankton must consume oxygen. Further, zooplankton mortality and growth inefficiency results in detritial production, which when remineralised consumes oxygen. Additionally, carbon released to the dissolved inorganic pool during inefficiency grazing on phytoplankton structural material also consumes oxygen. Thus zooplankton respiration is implicitly captured in these associated processes.

5.7 Non-grazing plankton mortality

The rate of change of plankton biomass, B, as a result of natural mortality is given by:

$$\frac{\partial B}{\partial t} = -m_L B - m_Q B^2 \tag{91}$$

where m_L is the linear mortality coefficient and m_Q is the quadratic mortality coefficient.

A combination of linear and quadratic mortality rates are used in the model. When the mortality term is the sole loss term, such as zooplankton in the water column or benthic microalgae in the sediments, a quadratic term is employed to represent

$$\frac{\partial[\mathrm{NH_4}]}{\partial t} = g(1-E)(1-\gamma) + gR_N^* \quad (70)$$

$$\frac{\partial P}{\partial t} = g\frac{1}{16}\frac{31}{14}(1-E)(1-\gamma) + \frac{1}{16}\frac{31}{14}gR_P^* \quad (71)$$

$$\frac{\partial DIC}{\partial t} = g\frac{106}{16}\frac{12}{14}(1-E)(1-\gamma) + \frac{106}{16}\frac{12}{14}gR_C^* \quad (72)$$

$$\frac{\partial B}{\partial t} = -g \quad (73)$$

$$\frac{\partial Z}{\partial t} = Eg \quad (74)$$

$$\frac{\partial D_{Red}}{\partial t} = g(1-E)\gamma \quad (75)$$

$$\frac{\partial[\mathrm{O_2}]}{\partial t} = -\frac{\partial DIC}{\partial t}\frac{32}{12}\frac{[\mathrm{O_2}]}{K_{OA}+[\mathrm{O_2}]} \quad (76)$$

$$g = \min\left[\mu_Z^{max} Z/E, \frac{Z}{m_{Z_L}}(\phi_{diff}+\phi_{rel}+\phi_{shear})\,B\right] \quad (77)$$

$$\phi = \phi_{diff}+\phi_{rel}+\phi_{shear} \quad (78)$$

$$\phi_{diff} = (2\kappa T/(3\rho\nu))(1/r_Z+1/r_B)(r_B+r_Z) \quad (79)$$

$$\phi_{rel} = \pi(r_Z+r_B)^2 U_{eff} \quad (80)$$

$$\phi_{shear} = 1.3\sqrt{\epsilon/\nu}(r_Z+r_B)^3 \quad (81)$$

$$U_{eff} = (U_B^2+3U_Z^2)/3U_Z \quad (82)$$

Table 14. Equations for zooplankton grazing. The terms represent a predator Z consuming a phytoplankton B. Notes (1) If the zooplankton diet contains multiple phytoplankton classes, and grazing is prey saturated, then phytoplankton loss must be reduced to account for the saturation by other types of microalgae; (2) $\frac{Z}{m_Z}$ is the number of individual zooplankton; (3) Phytoplankton pigment is lost to water column without being conserved. Chl *a* has chemical formulae $C_{55}H_{72}O_5N_4Mg$, and a molecular weight of 893.49 g mol^{-1}. The uptake (and subsequent remineralisation) of molecules for chlorophyll synthesis could make up a maximum (at C:Chl = 20) of $(660/893)/20$ and $(56/893)/20\times(16/106)\times(14/12))$, or ∼4 and ∼2 per cent of the exchange of C and N between the cell and water column, and will cancel out over the lifetime of a cell. Thus the error in ignoring chlorophyll loss to the water column is small.

$$\frac{\partial[\mathrm{NH_4}]}{\partial t} = g(1-E)(1-\gamma) \quad (83)$$

$$\frac{\partial P}{\partial t} = g\frac{1}{16}\frac{31}{14}(1-E)(1-\gamma) \quad (84)$$

$$\frac{\partial DIC}{\partial t} = g\frac{106}{16}\frac{12}{14}(1-E)(1-\gamma) \quad (85)$$

$$\frac{\partial Z_S}{\partial t} = -g \quad (86)$$

$$\frac{\partial Z_L}{\partial t} = Eg \quad (87)$$

$$\frac{\partial D_{Red}}{\partial t} = g(1-E)\gamma \quad (88)$$

$$\frac{\partial[\mathrm{O_2}]}{\partial t} = -\frac{\partial DIC}{\partial t}\frac{32}{12}\frac{[\mathrm{O_2}]}{K_{OA}+[\mathrm{O_2}]} \quad (89)$$

$$g = \min\left[\mu_{Z_L}^{max} Z_L/E, \frac{Z_L}{m_{Z,N}}\left(\phi_{diff}+\phi_{rel}\phi_{shear}\right)Z_S\right] \quad (90)$$

Table 15. Equations for zooplankton carnivory, represent large zooplankton Z_L consuming small zooplankton Z_S. The parameters values and symbols are given in Table 13 and Table 12

.

Description	water column		sediment	
	linear	quadratic	linear	quadratic
	d^{-1}	d^{-1} (mg N m^{-3})$^{-1}$	d^{-1}	d^{-1} (mg N m^{-3})$^{-1}$
Small phytoplankton	0.1	-	1	-
Large phytoplankton	0.1	-	10	-
Microphytobenthos	-	-	-	0.0001
Trichodesmium	0.1	0.1	-	-

Table 16. Constants and parameter values used for plankton mortality.

increasing predation / viral disease losses in dense populations. For suspended microalgae we have used only a linear term (i.e. $m_Q = 0$). Linear terms have been used to represent a basal respiration rate.

As described in Sec 5.1.6, the mortality terms need to account for the internal properties of lost microalgae.

For definitions of the state variables see Tables 16 & 17.

$$\frac{\partial[\mathrm{NH_4}]}{\partial t} = m_{L,B} B R_N^* \quad (92)$$

$$\frac{\partial DIP}{\partial t} = \frac{1}{16}\frac{31}{14} m_{L,B} B R_P^* \quad (93)$$

$$\frac{\partial DIC}{\partial t} = \frac{106}{16}\frac{12}{14} m_{L,B} B R_C^* \quad (94)$$

$$\frac{\partial[\mathrm{O_2}]}{\partial t} = -\frac{\partial DIC}{\partial t}\frac{32}{12}\frac{[\mathrm{O_2}]}{K_{OA}+[\mathrm{O_2}]} \quad (95)$$

$$\frac{\partial B}{\partial t} = -m_{L,B} B \quad (96)$$

$$\frac{\partial D_{Red}}{\partial t} = m_{L,B} B \quad (97)$$

Table 17. Equations for linear phytoplankton mortality.

$$\frac{\partial Z_S}{\partial t} = -m_{Q,ZS} Z_S^2 \quad (98)$$

$$\frac{\partial Z_L}{\partial t} = -m_{Q,ZL} Z_L^2 \quad (99)$$

$$\frac{\partial D_{Red}}{\partial t} = f_{Z2det}\left(m_{Q,ZS} Z_S^2 + m_{Q,ZL} Z_L^2\right) \quad (100)$$

$$\frac{\partial[\mathrm{NH_4}]}{\partial t} = (1 - f_{Z2det})\left(m_{Q,ZS} Z_S^2 + m_{Q,ZL} Z_L^2\right) \quad (101)$$

Table 18. Equations for the zooplankton mortality. f_{Z2det} is the fraction of zooplankton mortality that is remineralised, and is equal to 0.5 for both small and large zooplankton.

5.8 Air-sea gas exchange

Air-sea gas exchange is calculated using wind speed (we choose a cubic relationship, Wanninkhof and McGillis (1999)), saturation state of the gas (described below) and the Schmidt number of the gas (Wanninkhof, 1992). The transfer coefficient, k, is given by:

$$k = \frac{0.0283}{360000} u_{10}^3 \left(\mathrm{Sc}/660\right)^{-1/2} \tag{102}$$

where 0.0283 cm hr^{-1} is an empirically-determined constant (Wanninkhof and McGillis, 1999), u_{10} is the short-term steady wind at 10 m above the sea surface [m s^{-1}], the Schmidt number, Sc, is the ratio of the diffusivity of momentum and that of the exchanging gas, and is given by a cubic temperature relationship (Wanninkhof, 1992). Finally, a conversion factor of 360000 m s^{-1} (cm hr^{-1})$^{-1}$ is used.

In practice the hydrodynamic model can contain thin surface layers as the surface elevation moves between z-levels. Further, physical processes of advection and diffusion and gas fluxes are done sequentially, allowing concentrations to build up through a single timestep. To avoid unrealistic changes in the concentration of gases in thin surface layers, the shallowest layer thicker than 20 cm receives all the surface fluxes.

5.8.1 Oxygen

The saturation state of oxygen $[\mathrm{O_2}]_{sat}$ is determined as a function of temperature and salinity following Weiss (1970). The change in concentration of oxygen in the surface layer due to a sea-air oxygen flux (positive from sea to air) is given by:

$$\frac{\partial[\mathrm{O_2}]}{\partial t} = k_{\mathrm{O_2}} \left([\mathrm{O_2}]_{sat} - [\mathrm{O_2}]\right)/h \tag{103}$$

where $k_{\mathrm{O_2}}$ is the transfer coefficient for oxygen (Eq. 102), [$\mathrm{O_2}$] is the dissolved oxygen concentration in the surface waters, and h is the thickness of the surface layer of the model into which sea-air flux flows.

5.8.2 Carbon dioxide

The change in surface dissolved inorganic carbon concentration, DIC, resulting from the sea-air flux (+ve from sea to air) of carbon dioxide is given by:

$$\frac{\partial DIC}{\partial t} = k_{\mathrm{CO_2}} \left([\mathrm{CO_2}]_{atm} - [\mathrm{CO_2}]\right)/h \tag{104}$$

where $k_{\mathrm{CO_2}}$ the transfer coefficient for carbon dioxide (Eq. 102), [$\mathrm{CO_2}$] is the dissolved carbon dioxide concentration in the surface waters determined from DIC and A_T using the carbon chemistry equilibria calculations described in Sec 5.3.1, $[\mathrm{CO_2}]_{atm}$ is the partial pressure of carbon dioxide in the atmosphere, and h is the thickness of the surface layer of the model into which sea-air flux flows.

Note the carbon dioxide flux is not determined by the gradient in DIC, but the gradient in [$\mathrm{CO_2}$]. At pH values around 8, [$\mathrm{CO_2}$] makes up only approximately 1/200th of DIC in seawater, significantly reducing the air-sea exchange. Counteracting

this reduced gradient, note that changing DIC results in an approximately 10 fold change in [CO_2] (quantified by the Revelle factor (Zeebe and Wolf-Gladrow, 2001)). Thus, the gas exchange of CO_2 is approximately $1/200 \times 10 = 1/20$ of the oxygen flux for the same proportional perturbation in DIC and oxygen. At a Sc number of 524 (25°C seawater) and a wind speed of 12 m s^{-1}, 1 m of water equilibrates with CO_2 in the atmosphere with an e-folding timescale of approximately 1 day.

6 Epibenthic processes

In the model, benthic communities are quantified as a biomass per unit area, or areal biomass. At low biomass, the community is composed of a few specimens spread over a small fraction of the bottom, with no interaction between the nutrient and energy acquisition of individuals. Thus, at low biomass the areal fluxes are a linear function of the biomass.

As biomass increases, the individuals begin to cover a significant fraction of the bottom. For nutrient and light fluxes that are constant per unit area, such as downwelling irradiance and sediment releases, the flux per unit biomass decreases with increasing biomass. Some processes, such as photosynthesis in a thick seagrass meadow or nutrient uptake by a coral reef, become independent of biomass (Atkinson, 1992) as the bottom becomes completely covered. To capture the non-linear effect of biomass on benthic processes, we use an effective projected area fraction, A_{eff}.

To restate, at low biomass, the area on the bottom covered by the benthic community is a linear function of biomass. As the total leaf area approaches and exceeds the projected area, the projected area for the calculation of water-community exchange approaches 1, and becomes independent of biomass. This is represented using:

$$A_{eff} = 1 - \exp(-\Omega_B \ B) \tag{105}$$

where A_{eff} is the effective projected area fraction of the benthic community (m^2 m^{-2}), B is the biomass of the benthic community (g N m^{-2}), and Ω_B is the nitrogen-specific leaf area coefficient (m^2 g N^{-1}). For further explanation of Ω_B see Baird et al. (2016a).

The parameter Ω_B is critical: it provides a means of converting between biomass and fractions of the bottom covered, and is used in calculating the absorption cross-section of the leaf and the nutrient uptake of corals and macroalgae. That Ω_B has a simple physical explanation, and can be determined from commonly undertaken morphological measurement (see below), gives us confidence in its use throughout the model.

6.1 Macroalgae

The macroalgae model considers the diffusion-limited supply of dissolved inorganic nutrients (N and P) and the absorption of light, delivering N, P and fixed C respectively. Unlike the microalgae model, no internal reserves are considered, implying that the macroalgae has a fixed stoichiometry that can be specified as:

$$550\mathrm{CO_2} + 30\mathrm{NO_3^-} + \mathrm{PO_4^{3-}} + 792\mathrm{H_2O} \overset{5500 \text{ photons}}{\longrightarrow} (\mathrm{CH_2O})_{550}(\mathrm{NH_3})_{30}\mathrm{H_3PO_4} + 716\mathrm{O_2} \tag{106}$$

where the stoichiometry is based on Atkinson and Smith (1983) (see also Baird and Middleton (2004); Hadley et al. (2015a, b)). Note that when ammonia is taken up instead of nitrate there is a slightly different O_2 balance (Sec. 9.1). In the next section will consider the maximum nutrient uptake and light absorption, and then bring them together to determine the realised growth rate.

Variable	Symbol	Units
Downwelling irradiance	E_d	W m^{-2}
Macroalgae biomass	MA	g N m^{-2}
Water column detritus, C:N:P = 550:30:1	D_{Atk}	g N m^{-3}
Effective projected area of macroalgae	A_{eff}	m^2 m^{-2}
Leaf-specific absorptance	$A_{L,\lambda}$	-
Bottom stress	τ	N m^{-2}
Wavelength	λ	nm
Bottom water layer thickness	h_{wc}	m

Table 19. State and derived variables for the macroalgae model. For simplicity in the equations all dissolved constituents are given in grams, although elsewhere they are shown in milligrams.

6.1.1 Nutrient uptake

Nutrient uptake by macroalgae is a function of nutrient concentration, water motion (Hurd, 2000) and internal physiology. The maximum flux of nutrients is specified as a mass transfer limit per projected area of macroalgae and is given by (Falter et al., 2004; Zhang et al., 2011):

$$S_{\mathrm{x}} = 2850 \left(\frac{2\tau}{\rho}\right)^{0.38} {\mathrm{Sc_x}}^{-0.6}, \mathrm{Sc_x} = \frac{\nu}{D_{\mathrm{x}}} \tag{107}$$

where S_{x} is the mass transfer rate coefficient of element x = N, P, τ is the shear stress on the bottom, ρ is the density of water and $\mathrm{Sc_x}$ is the Schmidt number. The Schmidt number is the ratio of the diffusivity of momentum, ν, and mass, D_{x} (Tab. 7), and varies with temperature, salinity and nutrient species. The rate constant S can be thought of as the height of water cleared of mass per unit of time by the water-macroalgae exchange.

6.1.2 Light capture

The calculation of light capture by macroalgae involves estimating the fraction of light that is incident upon the leaves, and the fraction that is absorbed. The rate of photon capture is given by:

$$k_I = \frac{\left(10^9 hc\right)^{-1}}{A_V} \int E_{d,\lambda} \left(1 - \exp\left(-A_{L,\lambda} \Omega_{MA} MA\right)\right) \lambda d\lambda \tag{108}$$

where h, c and A_V are fundamental constants, 10^9 nm m^{-1} accounts for the typical representation of wavelength, λ in nm, and $A_{L,\lambda}$ is the spectrally-resolved leaf-specific absorptance. As shown in Eq. 105, the term $1 - \exp\left(-\Omega_{MA} MA\right)$ gives the effective projected area fraction of the community. In the case of light absorption of macroalgae, the exponent is multiplied by the leaf-specific absorptance, $A_{L,\lambda}$, to account for the transparency of the leaves. At low macroalgae biomass, absorption

at wavelength λ is equal to $E_{d,\lambda}A_{L,\lambda}\Omega_{MA}MA$, increasing linearly with biomass as all leaves at low biomass are exposed to full light (i.e. there is no self-shading). At high biomass, the absorption by the community asymptotes to $E_{d,\lambda}$, at which point increasing biomass does not increase the absorption as all light is already absorbed.

For more details on the calculation of Ω_{MA} see Baird et al. (2016a).

6.1.3 Growth

The growth rate combines nutrient, light and maximum organic matter synthesis rates following:

$$\mu_{MA} = \min\left[\mu_{MA}^{max}, \frac{30}{5500}14\frac{k_I}{MA}, \frac{S_N A_{eff} N}{MA}, \frac{30}{1}\frac{14}{31}\frac{S_P A_{eff} P}{MA}\right] \tag{109}$$

and the production of macroalgae is given by $\mu_{MA}MA$. We have used the commonly applied multiple minimum function (von Liebig, 1840), although it is noted that others use the multiple of limitation terms (Fasham, 1993). The microalgae model described above uses dynamical reserves to determine the growth rate. The growth approximated using dynamical reserves closer approximates a multiple minimum function than a multiple of minimum terms, so it was deemed more appropriate to use a multiple minimum function for macroalgae and seagrass for which internal reserves were not resolved.

As per seagrass, that the maximum growth rates sits within the minimum operator. This allows the growth of macroalgae to the independent of temperature at low light, but still have an exponential dependence at maximum growth rates (Baird et al., 2003).

6.1.4 Mortality

Mortality is defined as a simple linear function of biomass:

$$\frac{\partial MA}{\partial t} = -\zeta_{MA}MA \tag{121}$$

A quadratic formulation is not necessary as both the nutrient and light capture rates become independent of biomass as $MA \gg 1/\Omega_{MA}$. Thus the steady-state biomass of macroalgae under nutrient limitation is given by:

$$(MA)_{SS} = \frac{S_N A_{eff} N}{\zeta} \tag{122}$$

and for light-limited growth by:

$$(MA)_{SS} = \frac{k_I}{\zeta} \tag{123}$$

The full macroalgae equations, parameters and symbols are listed in Tables 19, 20 and 21.

$$\frac{\partial N}{\partial t} = -\mu_{MA} MA / h_{wc} \tag{110}$$

$$\frac{\partial P}{\partial t} = -\frac{1}{30}\frac{31}{14}\mu_{MA} MA / h_{wc} \tag{111}$$

$$\frac{\partial DIC}{\partial t} = -\frac{550}{30}\frac{12}{14}\mu_{MA} MA / h_{wc} \tag{112}$$

$$\frac{\partial [\mathrm{O_2}]}{\partial t} = \frac{716}{30}\frac{32}{14}\left(\mu_{MA} MA\right) / h_{wc} \tag{113}$$

$$\frac{\partial MA}{\partial t} = \mu_{MA} MA - \zeta_{MA} MA \tag{114}$$

$$\frac{\partial D_{Atk}}{\partial t} = \zeta_{MA} MA / h_{wc} \tag{115}$$

$$\mu_{MA} = \min\left[\mu_{MA}^{max}, \frac{30}{5500} 14 \frac{k_I}{MA}, \frac{S_N A_{eff} N}{MA}, \frac{30}{1}\frac{14}{31}\frac{S_P A_{eff} P}{MA}\right] \tag{116}$$

$$S_{\mathrm{x}} = 2850\left(\frac{2\tau}{\rho}\right)^{0.38} \mathrm{Sc}^{-0.6}, Sc = \frac{\nu}{D_{\mathrm{x}}} \tag{117}$$

$$k_I = \frac{\left(10^9 hc\right)^{-1}}{A_V} \int E_{d,\lambda}\left(1 - \exp\left(-A_{L,\lambda}\Omega_{MA} MA\right)\right)\lambda d\lambda \tag{118}$$

$$A_{eff} = 1 - \exp(-\Omega_{MA}\ MA) \tag{119}$$

$$550\mathrm{CO_2} + 30\mathrm{NO_3^-} + \mathrm{PO_4^{3-}} + 792\mathrm{H_2O} \xrightarrow{5500\ \mathrm{photons}} (\mathrm{CH_2O})_{550}(\mathrm{NH_3})_{30}\mathrm{H_3PO_4} + 716\mathrm{O_2} + 391\mathrm{H^+} \tag{120}$$

Table 20. Equations for the macroalgae model. Other constants and parameters are defined in Table 21. 14 g N mol N^{-1}; 12 g C mol C^{-1}; 31 g P mol P^{-1}; 32 g O mol $\mathrm{O_2}^{-1}$. Uptake shown here is for nitrate, see Sec. 9.1 for ammonia uptake.

	Symbol	Value	Units
Parameters			
Maximum growth rate of macroalgae	μ_{MA}^{max}	1.0	d^{-1}
Nitrogen-specific area of macroalgae	Ω_{MA}	1.0	$(\mathrm{g\ N\ m^{-2}})^{-1}$
[a]Leaf-specific absorptance	$A_{L,\lambda}$	~ 0.7	-
Mortality rate	ζ_{MA_A}	0.01	d^{-1}

Table 21. Constants and parameter values used to model macroalgae. [a]Spectrally-resolved values

Variable	Symbol	Units
Downwelling irradiance	E_d	W m^{-2}
Porewater DIN concentration	N_s	g N m^{-3}
Porewater DIP concentration	P_s	g P m^{-3}
Water column DIC concentration	DIC	g C m^{-3}
Water column oxygen concentration	$[O_2]$	g O m^{-3}
Above-ground seagrass biomass	SG_A	g N m^{-2}
Below-ground seagrass biomass	SG_B	g N m^{-2}
Detritus at 550:30:1 in sediment	$D_{Atk,sed}$	g N m^{-3}
Effective projected area of seagrass	A_{eff}	m^2 m^{-2}
Bottom stress	τ	N m^{-2}
Thickness of sediment layer l	$h_{s,l}$	m
Bottom water layer thickness	h_{wc}	m
Wavelength	λ	nm
Translocation rate	Υ	g N m^{-2} s^{-1}
Porosity	ϕ	-

Table 22. State and derived variables for the seagrass model. For simplicity in the equations all dissolved constituents are given in grams, although elsewhere they are shown in milligrams. The bottom water column thickness varies is spatially-variable, depending on bathymetry.

6.2 Seagrass

Seagrasses are quantified per m^2 with a constant stoichiometry (C:N:P = 550:30:1) for both above-ground, SG_A, and below-ground, SG_B, biomass, and can translocate organic matter at this constant stoichiometry between the two stores of biomass. Growth occurs only in the above-ground biomass, but losses (grazing, decay etc.) occur in both. Multiple seagrass varieties are represented. The varieties are modelled using the same equations for growth, respiration and mortality, but with different parameter values.

$$\frac{\partial N_w}{\partial t} = -\left(\mu_{SG} - \frac{\mu_{SG}^{max}\overline{N_s}}{K_{SG,N}+\overline{N_s}}\right)/h_{wc} \tag{124}$$

$$\frac{\partial P_w}{\partial t} = -\left(\frac{1}{30}\frac{31}{14}\mu_{SG} - \frac{\mu_{SG}^{max}\overline{P_s}}{K_{SG,P}+\overline{P_s}}\right)/h_{wc} \tag{125}$$

$$\frac{\partial N_{s,l}}{\partial t} = -f_{N,l}/\left(h_{s,l}\phi_l\right) \tag{126}$$

$$\frac{\partial P_{s,l}}{\partial t} = -\frac{1}{30}\frac{31}{14}f_{P,l}/\left(h_{s,l}\phi_l\right) \tag{127}$$

$$\frac{\partial DIC}{\partial t} = -\frac{550}{30}\frac{12}{14}\left(\mu_{SG_A}SG_A\right)/h_{wc} \tag{128}$$

$$\frac{\partial [\mathrm{O_2}]}{\partial t} = \frac{716}{30}\frac{32}{14}\left(\mu_{SG_A}SG_A\right)/h_{wc} \tag{129}$$

$$\frac{\partial SG_A}{\partial t} = \mu_{SG_A}SG_A - \left(\zeta_{SG_A}+\zeta_{SG,\tau}\right)\left(SG_A - \frac{f_{seed}}{\Omega_{SG}}\left(1-f_{below}\right)\right) - \Upsilon \tag{130}$$

$$\frac{\partial SG_B}{\partial t} = -\left(\zeta_{SG_B}+\zeta_{SG,\tau}\right)\left(SG_B - \frac{f_{seed}}{\Omega_{SG}}f_{below}\right) + \Upsilon \tag{131}$$

$$\frac{\partial D_{Atk,sed}}{\partial t} = \left(\left(\zeta_{SG_A}+\zeta_{SG,\tau}\right)\left(SG_A - \frac{f_{seed}}{\Omega_{SG}}\left(1-f_{below}\right)\right)\right)/\left(h_{sed}\phi\right) + \left(\left(\zeta_{SG_B}+\zeta_{SG,\tau}\right)\left(SG_B - \frac{f_{seed}}{\Omega_{SG}}f_{below}\right)\right)/\left(h_{sed}\phi\right) \tag{132}$$

$$\mu_{SG_A} = \min\left[\frac{\mu_{SG}^{max}\overline{N_s}}{K_{SG,N}+\overline{N_s}} + S_N A_{eff} N, \frac{\mu_{SG}^{max}\overline{P_s}}{K_{SG,P}+\overline{P_s}} + S_P A_{eff} P, \frac{30}{5500}14\frac{\max(0, k_I - k_{resp})}{SG_A}\right] \tag{133}$$

$$\overline{N_s} = \frac{\sum_{l=1}^{L} N_{s,l}h_{s,l}\phi_l}{\sum_{l=1}^{L} h_{s,l}\phi_l} \tag{134}$$

$$\overline{P_s} = \frac{\sum_{l=1}^{L} P_{s,l}h_{s,l}\phi_l}{\sum_{l=1}^{L} h_{s,l}\phi_l} \tag{135}$$

$$f_{N,l} = \frac{N_{s,l}h_{s,l}\phi_l}{\sum_{l=1}^{L} N_{s,l}h_{s,l}\phi_l}\mu_{SG}SG_A \tag{136}$$

$$f_{P,l} = \frac{P_{s,l}h_{s,l}\phi_l}{\sum_{l=1}^{L} P_{s,l}h_{s,l}\phi_l}\mu_{SG}SG_A \tag{137}$$

$$k_I = \frac{\left(10^9 hc\right)^{-1}}{A_V}\int E_{d,\lambda}\left(1-\exp\left(-A_{L,\lambda}\Omega_{SG}SG_A\sin\beta_{blade}\right)\right)\lambda d\lambda \tag{138}$$

$$k_{resp} = 2\left(E_{comp}A_L\Omega_{SG}\sin\beta_{blade} - \frac{5500}{30}\frac{1}{14}\zeta_{SG_A}\right)SG_A \tag{139}$$

$$\Upsilon = \left(f_{below} - \frac{SG_B}{SG_B+SG_A}\right)\left(SG_A+SG_B\right)\tau_{tran} \tag{140}$$

$$550\mathrm{CO_2} + 30\mathrm{NO_3^-} + \mathrm{PO_4^{3-}} + 792\mathrm{H_2O} \xrightarrow{5500\ \text{photons}} (\mathrm{CH_2O})_{550}(\mathrm{NH_3})_{30}\mathrm{H_3PO_4} + 716\mathrm{O_2} + 391\mathrm{H^+} \tag{141}$$

Table 23. Equations for the seagrass model. Other constants and parameters are defined in Table 24. The equation for organic matter formation gives the stoichiometric constants; 14 g N mol N^{-1};12 g C mol C^{-1}; 31 g P mol P^{-1}; 32 g O mol O_2^{-1}.

	Symbol	*Zostera capricorni*	*Halophila ovalis*	*Halophila decipens*	Units
Parameters					
[a]Maximum growth rate of seagrass	μ_{SG}^{max}	0.4	0.4	0.4	d^{-1}
[b]Nitrogen-specific area of seagrass	Ω_{SG}	1.5	1.9	1.9	$(g\ N\ m^{-2})^{-1}$
[c]Leaf-specific absorptance	$A_{L,\lambda}$	~ 0.7	~ 0.7	~ 0.7	-
[d]Fraction biomass below ground	f_{below}	0.75	0.25	0.5	-
[e]Translocation rate	τ_{tran}	0.033	0.033	0.033	d^{-1}
[f]Half-saturation P uptake	$K_{SG,P}$	96	96	96	$mg\ P\ m^{-3}$
[g]Half-saturation N uptake	$K_{SG,N}$	420	420	420	$mg\ N\ m^{-3}$
[h]Compensation scalar PAR irradiance	E_{comp}	4.5	2.0	1.5	$mol\ photon\ m^{-2}\ d^{-1}$
[h]Leaf loss rate	ζ_{SG_A}	0.04	0.08	0.06	d^{-1}
[h]Root loss rate	ζ_{SG_B}	0.004	0.004	0.004	d^{-1}
Seed biomass as a fraction of 63 % cover	f_{seed}	0.01	0.01	0.01	-
[i]Seagrass root depth	z_{root}	0.15	0.08	0.05	m
Sine of nadir canopy bending angle	$\sin\beta_{blade}$	0.5	1.0	1.0	-
Mortality critical shear stress	$\tau_{SG,shear}$	1.0	1.0	1.0	$N\ m^{-2}$
Mortality shear stress time-scale	$\tau_{SG,time}$	0.5	0.5	0.5	d
Max. shear stress loss rate	$\zeta_{SG,\tau}^{\max}$	2	2	2	d^{-1}

Table 24. Constants and parameter values used to model seagrass. [a] $\times 2$ for nighttime $\times 2$ for roots; [b] Zostera - calculated from leaf characteristics in (Kemp et al., 1987; Hansen et al., 2000), *Halophia ovalis* - calculated from leaf dimensions in Vermaat et al. (1995) - Ω_{SG} can also be determined from specific leaf area such as determined in Cambridge and Lambers (1998) for 9 Australian seagrass species; [c] Spectrally-resolved values in Baird et al. (2016a); [d] Duarte and Chiscano (1999); [e] loosely based on Kaldy et al. (2013); [f] *Thalassia testudinum* Gras et al. (2003); [g] *Thalassia testudinum* (Lee and Dunton, 1999); [h] Chartrand et al. (2012); Longstaff (2003); Chartrand et al. (2017); [i] Roberts (1993).

Here we present just the equations for the seagrass submodel. A description of the seagrass processes of growth, translocation between roots and leaves, and mortality has been published in Baird et al. (2016a), along with a comparison to observations from Gladstone Harbour on the northeast Australian coast.

6.3 Coral polyps

The coral polyp parameterisation consists of a microalgae growth model to represent zooxanthellae growth based on Baird et al. (2013), and the parameterisation of coral - zooxanthellae interaction based on the host - symbiont model of Gustafsson et al. (2013), a new photoadaptation, photoinhibition and reaction centre dynamics models. The extra detail on the zooxanthellae photosystem is required due to its important role in thermal-stress driven coral bleaching (Yonge, 1930; Suggett et al., 2008).

6.3.1 Coral host, symbiont and the environment

The state variables for the coral polyp model (Table 25) include the biomass of coral tissue, CH (g N m^{-2}), and the structure material of the zooxanthellae cells, CS (mg N m^{-2}). The structure material of the zooxanthellae, CS, in addition to nitrogen, contains carbon and phosphorus at the Redfield ratio. The zooxanthellae cells also contain reserves of nitrogen, R_N (mg N m^{-2}), phosphorus, R_P (mg P m^{-2}), and carbon, R_C (mg C m^{-2}).

The zooxanthellae light absorption capability is resolved by considering the time-varying concentrations of pigments chlorophyll a, Chl, diadinoxanthin, X_p, and diatoxanthin X_h, for which the state variable represents the areal concentration. A further three pigments, chlorophyll c_2, peridinin, and β-carotene are considered in the absorption calculations, but their concentrations are in fixed ratios to chlorophyll a. Exchanges between the coral community and the overlying water can alter the water column concentrations of dissolved inorganic carbon, DIC, nitrogen, N, and phosphorus, P, as well as particulate phytoplankton, B, zooplankton, Z, and detritus, D, where multiple nitrogen, plankton and detritus types are resolved (Table 25).

The coral host is able to assimilate particulate organic nitrogen either through translocation from the zooxanthellae cells or through the capture of water column organic detritus and/or plankton. The zooxanthellae varies its intracellular pigment content depending on potential light limitation of growth, and the incremental benefit of adding pigment, allowing for the package effect (Baird et al., 2013). The coral tissue is assumed to have a Redfield C:N:P stoichiometry (Redfield et al., 1963), as shown by Muller-Parker et al. (1994). The zooxanthellae are modelled with variable C:N:P ratios (Muller-Parker et al., 1994), based on a structure material at the Redfield ratio, but with variable internal reserves. The fluxes of C, N and P with the overlying water column (nutrient uptake and detritial / mucus release) can therefore vary from the Redfield ratio.

An explanation of the individual processes follows, with tables in the Appendix listing all the model state variables (Table 25), derived variables (Table 26), equations (Tables 27, 28, 29 and 30), and parameters values (Tables 31 and 32).

Here we present just the equations for the coral submodel. The description of the coral processes has been published in Baird et al. (2018), along with a comparison to observations from the Great Barrier Reef on the northeast Australian coast. The effect of coral calcification on water column properties is described below.

Variable	Symbol	Units
Dissolved inorganic nitrogen (DIN)	N	mg N m^{-3}
Dissolved inorganic phosphorus (DIP)	P	mg P m^{-3}
Zooxanthellae biomass	CS	mg N m^{-2}
Reserves of nitrogen	R_N	mg N $cell^{-1}$
Reserves of phosphorus	R_P	mg P $cell^{-1}$
Reserves of carbon	R_C	mg C $cell^{-1}$
Coral biomass	CH	g N m^{-2}
Suspended phytoplankton biomass	B	mg N m^{-3}
Suspended zoooplankton biomass	Z	mg N m^{-3}
Suspended detritus at 106:16:1	D_{Red}	mg N m^{-3}
Macroalgae biomass	MA	mg N m^{-3}
Temperature	T	°C
Absolute salinity	S_A	kg m^{-3}
zooxanthellae chlorophyll *a* concentration	Chl	mg m^{-2}
zooxanthellae diadinoxanthin concentration	X_p	mg m^{-2}
zooxanthellae diatoxanthin concentration	X_h	mg m^{-2}
Oxidised reaction centre concentration	Q_{ox}	mg m^{-2}
Reduced reaction centre concentration	Q_{red}	mg m^{-2}
Inhibited reaction centre concentration	Q_{in}	mg m^{-2}
Reactive oxygen species concentration	[ROS]	mg m^{-2}
Chemical oxygen demand	COD	mg O_2 m^{-3}

Table 25. Model state variables for the coral polyp model. Note that water column variables are 3 dimensional, benthic variables are 2 dimensional, and unnormalised reserves are per cell.

6.3.2 Coral calcification

The rate of coral calcification is a function of the water column aragonite saturation, Ω_a, and the normalised reserves of fixed carbon in the symbiont, R_C^*. The rates of change of DIC and total alkalinity, A_T, in the bottom water column layer of thickness h_{wc} due to calcification becomes:

$$\frac{\partial DIC}{\partial t} = -12gA_{eff}/h_{wc} \tag{186}$$

$$\frac{\partial A_T}{\partial t} = -2gA_{eff}/h_{wc} \tag{187}$$

Variable	Symbol	Units
Downwelling irradiance	E_d	W m^{-2}
Maximum reserves of nitrogen	$R_N^{\max}$	mg N cell^{-1}
Maximum reserves of phosphorus	$R_P^{\max}$	mg P cell^{-1}
Maximum reserves of carbon	$R_C^{\max}$	mg C cell^{-1}
Normalised reserves of nitrogen	$R_N^* \equiv R_N / R_N^{\max}$	-
Normalised reserves of phosphorus	$R_P^* \equiv R_P / R_P^{\max}$	-
Normalised reserves of carbon	$R_C^* \equiv R_C / R_C^{\max}$	-
Intracellular chlorophyll *a* concentration	c_i	mg m^{-3}
Intracellular diadinoxanthin concentration	x_p	mg m^{-3}
Intracellular diatoxanthin concentration	x_h	mg m^{-3}
Total reaction centre concentration	Q_{T}	mg m^{-2}
Total active reaction centre concentration	Q_{a}	mg m^{-2}
Concentration of zooxanthellae cells	n	cell m^{-2}
Thickness of the bottom water column layer	h_{wc}	m
Effective projected area fraction	A_{eff}	m^2 m^{-2}
Area density of zooxanthellae cells	n_{CS}	cell m^{-2}
Absorption cross-section	α	m^2 cell^{-1}
Rate of photon absorption	k_I	mol photon cell^{-1} s^{-1}
Photon-weighted average opaqueness	$\overline{\chi}$	-
Maximum Chl. synthesis rate	$k_{\mathrm{Chl}}^{\max}$	mg Chl m^{-3} d^{-1}
Density of water	ρ	kg m^{-3}
Bottom stress	τ	N m^{-2}
Schmidt number	Sc	-
Mass transfer rate coefficient for particles	S_{part}	m d^{-1}
Heterotrophic feeding rate	G	g N m^{-2} d^{-1}
Wavelength	λ	nm
Translocation fraction	f_{tran}	-
Active fraction of oxidised reaction centres	$a_{Q_{ox}}^*$	-

Table 26. Derived variables for the coral polyp model.

$$\frac{\partial N}{\partial t} = -S_N N(1-R_N^*)A_{eff} \quad (142)$$

$$\frac{\partial P}{\partial t} = -S_P P(1-R_P^*)A_{eff} \quad (143)$$

$$\frac{\partial DIC}{\partial t} = -\left(\frac{106}{1060}12k_I\frac{Q_{\rm ox}}{Q_{\rm T}}a^*_{Q_{ox}}(1-R_C^*) - \frac{106}{16}\frac{12}{14}\mu_{CS}^{\max}\phi R_C^*\right)(CS/m_{B,N}) \quad (144)$$

$$\frac{\partial [{\rm O_2}]}{\partial t} = \left(\frac{106}{1060}32k_I\frac{Q_{\rm ox}}{Q_{\rm T}}a^*_{Q_{ox}}(1-R_C^*) - \frac{106}{16}\frac{32}{14}\mu_{CS}^{\max}\phi R_C^*\right)(CS/m_{B,N}) \quad (145)$$

$$\frac{\partial R_N}{\partial t} = S_N N(1-R_N^*)/(CS/m_{B,N}) - \mu_{CS}^{\max}R_P^*R_N^*R_C^*(m_{B,N}+R_N) \quad (146)$$

$$\frac{\partial R_P}{\partial t} = S_P P(1-R_P^*)/(CS/m_{B,N}) - \mu_{CS}^{\max}R_P^*R_N^*R_C^*(m_{B,P}+R_P) \quad (147)$$

$$\frac{\partial R_C}{\partial t} = k_I\left(\frac{Q_{\rm ox}}{Q_{\rm T}}\right)a^*_{Q_{ox}}(1-R_C^*) - \mu_{CS}^{\max}R_P^*R_N^*R_C^*(m_{B,C}+R_C)$$
$$-\mu_{CS}^{\max}\phi m_{B,C}R_C^* \quad (148)$$

$$\frac{\partial CS}{\partial t} = \mu_{CS}^{\max}R_P^*R_N^*R_C^*CS - \zeta_{CS}CS \quad (149)$$

$$\frac{\partial c_i}{\partial t} = (k_{\rm Chl}^{\max}(1-R_C^*)(1-Q_{in}/Q_T)\overline{\chi} - \mu_P^{\max}R_P^*R_N^*R_C^*c_i)(CS/m_{B,N}) \quad (150)$$

$$\frac{\partial X_p}{\partial t} = \Theta_{xan2chl}(k_{\rm Chl}^{\max}(1-R_C^*)(1-Q_{in}/Q_T)\overline{\chi}) \quad (151)$$
$$-8(Q_{in}/Q_t-0.5)^3\tau_{xan}\Phi(X_p+X_h) \quad (152)$$

$$\frac{\partial X_h}{\partial t} = 8(Q_{in}/Q_{\rm T}-0.5)^3\tau_{xan}\Phi(X_p+X_h) \quad (153)$$

$$\frac{\partial CS}{\partial t} = (1-f_{tran})\mu_{CS}CS - \zeta_{CS}CS + f_{remin}\frac{\zeta_{CH}}{A_{eff}}CH^2 \quad (154)$$

$$k_I = \frac{(10^9hc)^{-1}}{A_V}\int \alpha_\lambda E_{d,\lambda}\lambda\, d\lambda \quad (155)$$

$$S_{\rm x} = 2850\left(\frac{2\tau}{\rho}\right)^{0.38}{\rm Sc_x}^{-0.6}, {\rm Sc_x} = \frac{\nu}{D_{\rm x}} \quad (156)$$

$$\Phi = 1-4\left(\frac{X_p}{X_p+X_h}-0.5\right)^2 \text{ or } \Phi = 1 \quad (157)$$

Table 27. Equations for the interactions of coral host, symbiont and environment excluding bleaching loss terms that appear in Table 30. The term $CS/m_{B,N}$ is the concentration of zoothanxellae cells. The equation for organic matter formation gives the stoichiometric constants; 12 g C mol C^{-1}; 32 g O mol O_2^{-1}.

$$\frac{\partial CH}{\partial t} = G' - \frac{\zeta_{CH}}{A_{eff}} CH^2 \tag{158}$$

$$\frac{\partial B}{\partial t} = -S_{part} A_{eff} B \frac{G'}{G} / h_{wc} \tag{159}$$

$$\frac{\partial Z}{\partial t} = -S_{part} A_{eff} Z \frac{G'}{G} / h_{wc} \tag{160}$$

$$\frac{\partial D_{Red}}{\partial t} = \left(-S_{part} A_{eff} D_{Red} \frac{G'}{G} + (1 - f_{remin}) \frac{\zeta_{CH}}{A_{eff}} CH^2 \right) / h_{wc} \tag{161}$$

$$f_{tran} = \frac{\pi r_{CS}^2 n_{CS}}{2 CH \Omega_{CH}} \tag{162}$$

$$G = S_{part} A_{eff} \left(B + Z + D_{Red} \right) \tag{163}$$

$$G' = \min \left[\min \left[\mu_{CH}^{max} CH - f_{tran} \mu_{CS} CS - \zeta_{CS} CS, 0 \right], G \right] \tag{164}$$

$$A_{eff} = 1 - \exp(-\Omega_{CH} CH) \tag{165}$$

Table 28. Equations for the coral polyp model. The term $CS/m_{B,N}$ is the concentration of zoothanxellae cells. The equation for organic matter formation gives the stoichiometric constants; 12 g C mol C^{-1}; 32 g O mol O_2^{-1}. Other constants and parameters are defined in Table 32.

$$\frac{\partial Q_{\mathrm{ox}}}{\partial t} = -k_I n \, m_{\mathrm{RCII}} \left(\frac{Q_{\mathrm{ox}}}{Q_{\mathrm{T}}} \right) \left(1 - a_{Q_{ox}}^* \left(1 - R_C^* \right) \right) + f_2(T) R_N^* R_P^* R_C^* Q_{\mathrm{in}} \tag{166}$$

$$\frac{\partial Q_{\mathrm{red}}}{\partial t} = k_I n \, m_{\mathrm{RCII}} \left(\frac{Q_{\mathrm{ox}}}{Q_{\mathrm{T}}} \right) \left(1 - a_{Q_{ox}}^* \left(1 - R_C^* \right) \right) - k_I n m_{RCII} \frac{Q_{\mathrm{red}}}{Q_T} \tag{167}$$

$$\frac{\partial Q_{\mathrm{in}}}{\partial t} = -268 \; m_{RCII} Q_{\mathrm{in}} + k_I n m_{RCII} \frac{Q_{\mathrm{red}}}{Q_T} \tag{168}$$

$$\frac{\partial [\mathrm{ROS}]}{\partial t} = -f(T) R_N^* R_P^* R_C^* [\mathrm{ROS}] + 32 \frac{1}{10} k_I n \, m_{\mathrm{RCII}} \left(\frac{Q_{\mathrm{in}}}{Q_{\mathrm{T}}} \right) \tag{169}$$

Table 29. Equations for symbiont reaction centre dynamics. Bleaching loss terms appear in Table 30.

$$\frac{\partial[\mathrm{NH_4}]}{\partial t} = \min\left[\gamma, \max\left[0, \frac{[\mathrm{ROS}]-[\mathrm{ROS}_{threshold}]}{m_O}\right]\right] CSR_N^*/h_{wc} \quad (170)$$

$$\frac{\partial P}{\partial t} = \frac{1}{16}\frac{31}{14}\min\left[\gamma, \max\left[0, \frac{[\mathrm{ROS}]-[\mathrm{ROS}_{threshold}]}{m_O}\right]\right] CSR_P^*/h_{wc} \quad (171)$$

$$\frac{\partial DIC}{\partial t} = \frac{106}{16}\frac{12}{14}\min\left[\gamma, \max\left[0, \frac{[\mathrm{ROS}]-[\mathrm{ROS}_{threshold}]}{m_O}\right]\right] CSR_C^*/h_{wc} \quad (172)$$

$$\frac{\partial[\mathrm{O_2}]}{\partial t} = -\frac{\partial DIC}{\partial t}\frac{32}{12}\frac{[\mathrm{O_2}]^2}{K_{OA}^2+[\mathrm{O_2}]^2} \quad (173)$$

$$\frac{\partial[\mathrm{COD}]}{\partial t} = \frac{\partial DIC}{\partial t}\frac{32}{12}\left(1-\frac{[\mathrm{O_2}]^2}{K_{OA}^2+[\mathrm{O_2}]^2}\right) \quad (174)$$

$$\frac{\partial CS}{\partial t} = -\min\left[\gamma, \max\left[0, \frac{[\mathrm{ROS}]-[\mathrm{ROS}_{threshold}]}{m_O}\right]\right] CS \quad (175)$$

$$\frac{\partial R_N}{\partial t} = -\min\left[\gamma, \max\left[0, \frac{[\mathrm{ROS}]-[\mathrm{ROS}_{threshold}]}{m_O}\right]\right] R_N \quad (176)$$

$$\frac{\partial R_P}{\partial t} = -\min\left[\gamma, \max\left[0, \frac{[\mathrm{ROS}]-[\mathrm{ROS}_{threshold}]}{m_O}\right]\right] R_P \quad (177)$$

$$\frac{\partial R_C}{\partial t} = -\min\left[\gamma, \max\left[0, \frac{[\mathrm{ROS}]-[\mathrm{ROS}_{threshold}]}{m_O}\right]\right] R_C \quad (178)$$

$$\frac{\partial Chl}{\partial t} = -\min\left[\gamma, \max\left[0, \frac{[\mathrm{ROS}]-[\mathrm{ROS}_{threshold}]}{m_O}\right]\right] Chl \quad (179)$$

$$\frac{\partial X_p}{\partial t} = -\min\left[\gamma, \max\left[0, \frac{[\mathrm{ROS}]-[\mathrm{ROS}_{threshold}]}{m_O}\right]\right] X_p \quad (180)$$

$$\frac{\partial X_h}{\partial t} = -\min\left[\gamma, \max\left[0, \frac{[\mathrm{ROS}]-[\mathrm{ROS}_{threshold}]}{m_O}\right]\right] X_h \quad (181)$$

$$\frac{\partial Q_{\mathrm{ox}}}{\partial t} = -\min\left[\gamma, \max\left[0, \frac{[\mathrm{ROS}]-[\mathrm{ROS}_{threshold}]}{m_O}\right]\right] Q_{\mathrm{ox}} \quad (182)$$

$$\frac{\partial Q_{\mathrm{red}}}{\partial t} = -\min\left[\gamma, \max\left[0, \frac{[\mathrm{ROS}]-[\mathrm{ROS}_{threshold}]}{m_O}\right]\right] Q_{\mathrm{red}} \quad (183)$$

$$\frac{\partial Q_{\mathrm{in}}}{\partial t} = -\min\left[\gamma, \max\left[0, \frac{[\mathrm{ROS}]-[\mathrm{ROS}_{threshold}]}{m_O}\right]\right] Q_{\mathrm{in}} \quad (184)$$

$$\frac{\partial D_{Red}}{\partial t} = \min\left[\gamma, \max\left[0, \frac{[\mathrm{ROS}]-[\mathrm{ROS}_{threshold}]}{m_O}\right]\right] CS/h_{wc} \quad (185)$$

Table 30. Equations describing the expulsion of zooxanthellae, and the resulting release of inorganic and organic molecules into the bottom water column layer.

	Symbol	Value
Constants		
Molecular diffusivity of NO_3	D	$f(T, S_A) \sim 17.5 \times 10^{-10}$ m^2 s^{-1}
Speed of light	c	2.998×10^8 m s^{-1}
Planck constant	h	6.626×10^{-34} J s^{-1}
Avogadro constant	A_V	6.02×10^{23} mol^{-1}
[a]Pigment-specific absorption coefficients	γ_λ	$f(\text{pig}, \lambda)$ m^{-1} $\left(\text{mg m}^{-3}\right)^{-1}$
Kinematic viscosity of water	ν	$f(T, S_A) \sim 1.05 \times 10^{-6}$ m^2 s^{-1}
Parameters		
[b]Nitrogen content of zooxanthellae cells	m_N	5.77×10^{-12} mol N cell^{-1}
[c]Carbon content of zooxanthellae cells	m_C	(106/16) m_N mol C cell^{-1}
[d]Maximum intracellular Chl concentration	$c_i^{\max}$	3.15×10^6 mg Chl m^{-3}
Radius of zooxanthellae cells	r_{CS}	5 μm
Maximum growth rate of coral	μ_{CH}^{max}	0.05 d^{-1}
[e]Rate coefficient of particle capture	S_{part}	3.0 m d^{-1}
Maximum growth rate of zooxanthellae	μ_{CS}^{max}	0.4 d^{-1}
Quadratic mortality coefficient of polyps	ζ_{CH}	0.01 d^{-1} (g N m^{-2})$^{-1}$
Linear mortality of zooxanthellae	ζ_{CS}	0.04 d^{-1}
[g]Remineralised fraction of coral mortality	f_{remin}	0.5
Nitrogen-specific host area coefficient of polyps	Ω_{CH}	2.0 m^2 g N^{-1}
Fractional (of μ_{CS}^{max}) respiration rate	ϕ	0.1

Table 31. Constants and parameter values used to model coral polyps. V is zooxanthellae cell volume in μm^3. [a]Baird et al. (2016a),[c]Redfield et al. (1963) and Kirk (1994),[d]Finkel (2001),[e]Ribes and Atkinson (2007); Wyatt et al. (2010),[f,g]Gustafsson et al. (2013, 2014).

	Symbol	Value
Parameters		
Maximum growth rate of zooxanthellae	μ_{CS}^{max}	1 d^{-1}
Rate coefficient of xanthophyll switching	τ_{xan}	1/600 s^{-1}
[a]Atomic ratio of Chl a to RCII in *Symbiodinium*	A_{RCII}	500 mol Chl mol $RCII^{-1}$
[a]Stoichiometric ratio of RCII units to photons	m_{RCII}	0.1 mol RCII mol $photon^{-1}$
Maximum rate of zooxanthellae expulsion	γ	1 d^{-1}
Oxygen half-saturation for aerobic respiration	K_{OA}	500 mg O m^{-3}
Molar mass of Chl a	M_{Chla}	893.49 g mol^{-1}
[b]Ratio of Chl a to xanthophyll	$\Theta_{chla2xan}$	0.2448 mg Chl mg X^{-1}
[b]Ratio of Chl a to Chl c	$\Theta_{chla2chlc}$	0.1273 mg Chl-a mg Chl-c^{-1}
[b]Ratio of Chl a to peridinin	$\Theta_{chla2per}$	0.4733 mg Chl mg^{-1}
[b]Ratio of Chl a to β-carotene	$\Theta_{chla2caro}$	0.0446 mg Chl mg^{-1}
[c]Lower limit of ROS bleaching	$[\mathrm{ROS}_{threshold}]$	5×10^{-4} mg O $cell^{-1}$

Table 32. Constants and parameter values used in the coral bleaching model. [a]In Suggett et al. (2009). [b] ratio of constant terms in multivariate analysis in Hochberg et al. (2006). [c]Fitted parameter based on the existence of non-bleaching threshold (Suggett et al., 2009), and a comparison of observed bleaching and model output in the $\sim$1 km model.

$$g = k_{day}(\Omega_a - 1)(R_C^*)^2 + k_{night}(\Omega_a - 1) \tag{188}$$

where g is the rate of net calcification, k_{day} and k_{night} are defined in Table 31 with habitat-specific values (Anthony et al., 2011; Mongin and Baird, 2014). The fluxes are scaled by the effective projected area of the community, A_{eff}. The power of 2 for R_C^* ensures that generally light replete symbionts provide the host with sufficient energy for calcification.

6.3.3 Dissolution of shelf carbonate sands

In addition to the dissolution of carbonate sands on a growing coral reef, which is captured in the net dissolution quantified above, the marine carbonates on the continental shelf dissolve (Eyre et al., 2018). Like above, the dissolution of marine carbonates is approximated as a source of DIC and alkalinity but does not affect the properties (mass, porosity etc.) of the underlying sediments.

We assume carbonate dissolution from the sediment bed is proportional to the fraction of the total surface sediment is composed of either sand or mud carbonates. Other components, whose fraction do not release DIC and alkalinity, including carbonate gravel and non-carbonate mineralogies. Thus the change in DIC and A_T in the bottom water column layer is given

Calcification	$Ca^{2+} + 2HCO_3^- $	$\longrightarrow$	$CaCO_3 + CO_2 + H_2O$	(192)
	$\frac{\partial A_T}{\partial t}$	$=$	$-2gA_{eff}/h_{wc}$	(193)
	$\frac{\partial DIC}{\partial t}$	$=$	$-12gA_{eff}/h_{wc}$	(194)
	g	$=$	$k_{day}(\Omega_a - 1)(R_C^*)^2 + k_{night}(\Omega_a - 1)$	(195)
	Ω_a	$=$	$\frac{[CO_3^{2-}][Ca^{2+}]}{K_{sp}}$	(196)
Dissolution	$CaCO_3 + CO_2 + H_2O$	$\longrightarrow$	$Ca^{2+} + 2HCO_3^-$	(197)
	$\frac{\partial A_T}{\partial t}$	$=$	$2d_{CaCO_3}\left(\frac{Mud_{CaCO_3} + Sand_{CaCO_3}}{M}\right)/h_{wc}$	(198)
	$\frac{\partial DIC}{\partial t}$	$=$	$12d_{CaCO_3}\left(\frac{Mud_{CaCO_3} + Sand_{CaCO_3}}{M}\right)/h_{wc}$	(199)
	d_{CaCO_3}	$=$	$-11.51\Omega_a + 33.683$	(200)

Table 33. Equations for coral polyp calcification and dissolution. The concentration of carbonate ions, $[CO_3^{2-}]$, is determined from equilibrium carbon chemistry as a function of A_T, DIC, temperature and salinity, and the concentration of calcium ions, $[Ca^{2+}]$, is a mean oceanic value. 12 g C mol C^{-1}. Other constants and parameters are defined in Table 31.

by:

$$\frac{\partial DIC}{\partial t} = -12d_{CaCO_3}\left(\frac{Mud_{CaCO_3} + Sand_{CaCO_3}}{M}\right)/h_{wc} \tag{189}$$

$$\frac{\partial A_T}{\partial t} = -2d_{CaCO_3}\left(\frac{Mud_{CaCO_3} + Sand_{CaCO_3}}{M}\right)/h_{wc} \tag{190}$$

where M is the total mass of surface layer inorganic sediments (see Sec. 7), d_{CaCO_3} is the dissolution rate of $CaCO_3$, and is the reverse reaction to calcification and h_{wc} is the thickness of the water column layer. The dissolution rate, d_{CaCO_3} [mmol m^{-2} d^{-1}] is assumed to be a function of Ω_a (Eyre et al., 2018):

$$d_{CaCO_3} = -11.51\Omega_a + 33.683 \tag{191}$$

Name	Nom. size μm	Sinking vel. m d^{-1}	Organic	Origin	Phosphorus adsorption	Colour
Gravel $CaCO_3$	10^4	60,480	N	I	N	W
Gravel non-$CaCO_3$	10^4	60,480	N	I	N	B
Sand $CaCO_3$	10^2	172.8	N	I	N	W
Sand non-$CaCO_3$	10^2	172.8	N	I	N	B
Mud $CaCO_3$	30	17.2	N	I	Y	W
Mud non-$CaCO_3$	30	17.2	N	I	Y	B
FineSed	30	17.2	N	C	Y	B
Dust	1	1	N	C	Y	B
D_{Atk}	-	10	Y	OM	N	B
D_{Red}	-	10	Y	OM	N	B
D_C,D_N,D_P	-	100	Y	OM	N	B

Table 34. Characteristics of the particulate classes. Y - Yes, N - No, I - initial condition, C - catchment, OM - remineralistion from organic matter, B - brown, W - white (Condie et al., 2009; Margvelashvili, 2009).

7 Sediment processes

7.1 Brief summary of processes in the sediments

The EMS model contains a multi-layered sediment compartment with time and space-varying vertical layers, and the same horizontal grid as the water column and epibenthic models. All state variables that exist in the water column layers have an equivalent in the sediment layers. The dissolved tracers are given as a concentration in the porewater, while the particulate tracers are given as a concentration per unit volume (see Sec. 10.3.2).

The sediment model contains inorganic particles of different sizes (Dust, Mud, Sand and Gravel) and different mineralogies (carbonate and non-carbonate) (Tab. 34). The sediment model includes the processes of particulate advection and mixing in the water column, resuspension sinking and settling, as well as sediment overturning and bioturbation (Margvelashvili, 2009). These processes, along with initial conditions, determine the mass of each inorganic particulate type in the sediments.

The critical shear stress for resuspension, and the sinking rates, are generally larger for large particles, while and mineralogy only affects the optical properties. The size-class Dust comes only in a non-carbonate mineralogy, and the Mud-carbonate class contains a category of FineSed-mineral that has the same physical and optical properties as Mud-mineral, except that it is initialised with a zero value and only enters the domain from rivers.

The organic matter classes are discussed in the Sec. 8.1. The inorganic and organic particulate classes are summarised in Table 34, and undergo resuspension, sinking, settling, sediment overturning and bioturbation in a manner similar to the inorganic particulates.

Variable	Symbol	Units
Ammonia concentration	$[NH_4]$	mg N m^{-3}
Sediment Dissolved Inorganic Carbon (DIC)	DIC	mg C m^{-3}
Sediment Dissolved Inorganic Phosphorus (DIP)	P	mg P m^{-3}
Sediment Particulate Inorganic Phosphorus (PIP)	PIP	mg P m^{-3}
Sediment Immobolised Particulate Inorganic Phosphorus (PIPI)	$PIPI$	mg P m^{-3}
Sediment Non-Algal Particulates (NAP)	NAP	kg m^{-3}
Sediment dissolved oxygen concentration	$[O_2]$	mg O m^{-3}

Table 35. State and derived variables for the sediment inorganic chemistry model.

Description	Symbol	Units
Maximum rate of nitrification in the water column	$\tau_{nit,wc}$	0.1 d^{-1}
Maximum rate of nitrification in the sediment	$\tau_{nit,sed}$	20 d^{-1}
Oxygen half-saturation constant for nitrification	$K_{O_2,nit}$	500 mg O m^{-3}
Maximum rate of denitrification	τ_{denit}	0.8 d^{-1}
Oxygen half-saturation constant for de-nitrification	$K_{O_2,denit}$	10000 mg O m^{-3}
Rate of P adsorbed/desorbed equilibrium	τ_{Pabs}	0.04 d^{-1}
Isothermic const. P adsorption for NAP	$k_{Pads,wc}$	300 kg NAP^{-1}
Oxygen half-saturation for P adsorption	$K_{O_2,\mathrm{abs}}$	2000 mg O m^{-3}
Rate of P immobilisation	τ_{Pimm}	0.0012 d^{-1}

Table 36. Constants and parameter values used in the sediment inorganic chemistry.

7.2 Sediment chemistry

7.2.1 Sediment nitrification - denitrification

Nitrification in the sediment is similar to the water-column, but with a sigmoid rather than hyperbolic relationship at low oxygen, for numerical reasons (Eq. 206). Denitrification occurs only in the sediment.

7.2.2 Sediment phosphorus absorption - desorption

Sediment phosphorus absorption - desorption is similar to water column (Eq. 208).

There is an additional pool of immobilised particulate inorganic phosphorus, $PIPI$, which accumulates in the model over time as PIP becomes immobilised, and represents permanent sequestration (Eq. 209).

$$\text{Nitrification} : \mathrm{NH_4^+ + 2O_2} \longrightarrow \mathrm{NO_3^- + H_2O + 2H^+} \tag{201}$$

$$\text{De-nitrification} : \mathrm{NO_3^- + \frac{1}{2}O_2} \longrightarrow \mathrm{\frac{1}{2}N_{2(g)} + 2O_2} \tag{202}$$

$$\tag{203}$$

$$\frac{\partial[\mathrm{NH_4}]}{\partial t} = -\tau_{nit,wc}[\mathrm{NH_4}]\frac{[\mathrm{O_2}]^2}{K^2_{\mathrm{O_2},nit}+[\mathrm{O_2}]^2} \tag{204}$$

$$\frac{\partial[\mathrm{O_2}]}{\partial t} = -2\frac{32}{14}\tau_{nit,wc}[\mathrm{NH_4}]\frac{[\mathrm{O_2}]^2}{K^2_{\mathrm{O_2},nit}+[\mathrm{O_2}]^2} + 2\frac{32}{14}\tau_{denit}[\mathrm{NO_3}]\frac{K_{\mathrm{O_2},denit}}{K_{\mathrm{O_2},denit}+[\mathrm{O_2}]} \tag{205}$$

$$\frac{\partial[\mathrm{NO_3}]}{\partial t} = \tau_{nit,wc}[\mathrm{NH_4}]\frac{[\mathrm{O_2}]^2}{K^2_{\mathrm{O_2},nit}+[\mathrm{O_2}]^2} - \tau_{denit}[\mathrm{NO_3}]\frac{K_{\mathrm{O_2},denit}}{K_{\mathrm{O_2},denit}+[\mathrm{O_2}]} \tag{206}$$

$$\frac{\partial P}{\partial t} = \left(\tau_{Pabs}\left(\frac{PIP}{k_{Pads,sed}NAP} - \frac{[\mathrm{O_2}]P}{K_{\mathrm{O_2,abs}}+[\mathrm{O_2}]}\right)\right)/\phi \tag{207}$$

$$\frac{\partial PIP}{\partial t} = -\tau_{Pabs}\left(\frac{PIP}{k_{Pads,wc}NAP} - \frac{[\mathrm{O_2}]P}{K_{\mathrm{O_2,abs}}+[\mathrm{O_2}]}\right) - \tau_{Pimm}PIP \tag{208}$$

$$\frac{\partial PIPI}{\partial t} = \tau_{Pimm}PIP \tag{209}$$

Table 37. Equations for the sediment inorganic chemistry.

8 Common water / epibenthic / sediment processes

8.1 Detritus remineralisation

The non-living components of C, N, and P cycles include the particulate labile and refractory pools, and a dissolved pool (Fig. 4). The labile detritus has a pool at the Redfield ratio, D_{Red}, and at the Atkinson ratio, D_{Atk}, resulting from dead organic matter at these ratios. The labile detritus from both pools then breaks down into refractory detritus and dissolved organic matter. The refractory detritus and dissolved organic matter pools are quantified by individual elements (C, N, P), in order to account for the mixed source of labile detritus. Finally, a component of the breakdown of each of these pools is returned to dissolved inorganic components. The variables, parameters and equations can be found in Tables 38, 40 & 39 respectively.

As the refractory and dissolved components are separated into C, N and P components, this introduces the possibility to have P components break down quicker than C and N. This is specified as the breakdown rate of P relative to N, Φ_{RD_P} and Φ_{DOM_P} respectively for refractory and dissolved detritus respectively.

Variable	Symbol	Units
Ammonia concentration	$[\mathrm{NH_4}]$	mg N $\mathrm{m^{-3}}$
Dissolved Inorganic Carbon (DIC)	DIC	mg C $\mathrm{m^{-3}}$
Dissolved Inorganic Phosphorus (DIP)	P	mg P $\mathrm{m^{-3}}$
Dissolved oxygen concentration	$[\mathrm{O_2}]$	mg O $\mathrm{m^{-3}}$
Labile detritus at Redfield ratio	D_{Red}	mg N $\mathrm{m^{-3}}$
Labile detritus at Atkinson ratio	D_{Atk}	mg N $\mathrm{m^{-3}}$
Refractory Detritus C	D_C	mg C $\mathrm{m^{-3}}$
Refractory Detritus N	D_N	mg N $\mathrm{m^{-3}}$
Refractory Detritus P	D_P	mg P $\mathrm{m^{-3}}$
Dissolved Organic C	O_C	mg C $\mathrm{m^{-3}}$
Dissolved Organic N	O_N	mg N $\mathrm{m^{-3}}$
Dissolved Organic P	O_P	mg P $\mathrm{m^{-3}}$
Chemical Oxygen Demand (COD)	COD	mg O $\mathrm{m^{-3}}$

Table 38. State and derived variables for the detritus remineralisation model in both the sediment and water column.

8.1.1 Anaerobic and anoxic respiration

The processes of remineralisation, phytoplankton mortality and zooplankton grazing return carbon dioxide to the water column. In oxic conditions, these processes consume oxygen in a ratio of $DIC : \frac{32}{12}[\mathrm{O_2}]$. At low oxygen concentrations, the oxygen consumed is reduced:

$$\frac{\partial[\mathrm{O_2}]}{\partial t} = -\frac{\partial DIC}{\partial t}\frac{32}{12}\frac{[\mathrm{O_2}]^2}{K_{OA}^2 + [\mathrm{O_2}]^2} \tag{223}$$

where K_{OA} = 256 mg O $\mathrm{m^{-3}}$ is the half-saturation constant for anoxic respiration (Boudreau, 1996). A sigmoid saturation term is used because it is more numerically stable as the oxygen concentration approaches 0. The anoxic component of remineralisation results in an increased chemical oxygen demand (COD):

$$\frac{\partial COD}{\partial t} = \frac{\partial DIC}{\partial t}\frac{32}{12}\left(1 - \frac{[\mathrm{O_2}]^2}{K_{OA}^2 + [\mathrm{O_2}]^2}\right) \tag{224}$$

COD is a dissolved tracer, with the same units as oxygen.

When oxygen and COD co-exist they react to reduce both, following:

$$\frac{\partial[\mathrm{O_2}]}{\partial t} = -\tau_{COD}\min[COD, 8000]\frac{[\mathrm{O_2}]}{8000} \tag{225}$$

$$\frac{\partial COD}{\partial t} = -\tau_{COD}\min[COD, 8000]\frac{[\mathrm{O_2}]}{8000} \tag{226}$$

$$\frac{\partial D_{Red}}{\partial t} = -r_{Red} D_{Red} \tag{210}$$

$$\frac{\partial D_{Atk}}{\partial t} = -r_{Atk} D_{Atk} \tag{211}$$

$$\frac{\partial D_C}{\partial t} = \frac{106}{16}\frac{12}{14}\zeta_{Red} r_{Red} D_{Red} + \frac{550}{30}\frac{12}{14}\zeta_{Atk} r_{Atk} D_{Atk} - r_R D_C \tag{212}$$

$$\frac{\partial D_N}{\partial t} = \zeta_{Red} r_{Red} D_{Red} + \zeta_{Atk} r_{Atk} D_{Atk} - r_R D_N \tag{213}$$

$$\frac{\partial D_P}{\partial t} = \frac{1}{16}\frac{31}{14}\zeta_{Red} r_{Red} D_{Red} + \frac{1}{30}\frac{31}{14}\zeta_{Atk} r_{Atk} D_{Atk} - \Phi_{RD_P} r_R D_P \tag{214}$$

$$\frac{\partial O_C}{\partial t} = \frac{106}{16}\frac{12}{14}\vartheta_{Red} r_{Red} D_{Red} + \frac{550}{30}\frac{12}{14}\vartheta_{Atk} r_{Atk} D_{Atk} + \vartheta_{Ref} r_R D_C - r_O O_C \tag{215}$$

$$\frac{\partial O_N}{\partial t} = \vartheta_{Red} r_{Red} D_{Red} + \vartheta_{Atk} r_{Atk} D_{Atk} + \vartheta_{Ref} r_R D_N - r_O O_N \tag{216}$$

$$\frac{\partial O_P}{\partial t} = \frac{1}{16}\frac{31}{14}\vartheta_{Red} r_{Red} D_{Red} + \frac{1}{30}\frac{31}{14}\vartheta_{Atk} r_{Atk} D_{Atk} + \vartheta_{Ref}\Phi_{RD_P} r_R D_P - \Phi_{DOM_P} r_O O_P \tag{217}$$

$$\frac{\partial [\mathrm{NH_4}]}{\partial t} = r_{Red} D_{Red}(1 - \zeta_{Red} - \vartheta_{Red}) + r_{Atk} D_{Atk}(1 - \zeta_{Atk} - \vartheta_{Atk}) + r_R D_N (1 - \vartheta_{Ref}) + r_O O_N \tag{218}$$

$$\frac{\partial DIC}{\partial t} = \frac{106}{16}\frac{12}{14} r_{Red} D_{Red}(1 - \zeta_{Red} - \vartheta_{Red}) + \frac{550}{30}\frac{12}{14} r_{Atk} D_{Atk}(1 - \zeta_{Atk} - \vartheta_{Atk}) + r_R D_C (1 - \vartheta_{Ref}) + r_O O_C \tag{219}$$

$$\frac{\partial P}{\partial t} = \frac{1}{16}\frac{31}{14} r_{Red} D_{Red}(1 - \zeta_{Red} - \vartheta_{Red}) + \frac{1}{30}\frac{31}{14} r_{Atk} D_{Atk}(1 - \zeta_{Atk} - \vartheta_{Atk}) + \Phi_{RD_P} r_R D_P (1 - \vartheta_{Ref}) + \Phi_{DOM_P} r_O O_P \tag{220}$$

$$\frac{\partial [\mathrm{O_2}]}{\partial t} = -\frac{32}{12}\frac{\partial DIC}{\partial t}\frac{[\mathrm{O_2}]^2}{K_{OA}^2 + [\mathrm{O_2}]^2} \tag{221}$$

$$\frac{\partial [COD]}{\partial t} = \frac{32}{12}\frac{\partial DIC}{\partial t}\left(1 - \frac{[\mathrm{O_2}]^2}{K_{OA}^2 + [\mathrm{O_2}]^2}\right) \tag{222}$$

Table 39. Equations for detritus remineralisation in the water column and sediment.

Description	Symbol	Red	Atk	Refractory	Dissolved
Detritus breakdown rate (d^{-1})	$r_{Red,Atk,R,O}$	0.04	0.01	0.001	0.0001
Fraction of detritus to refractory	$\zeta_{Red,Atk}$	0.19	0.19	-	-
Fraction of detritus to DOM	$\vartheta_{Red,Atk,R}$	0.1	0.1	0.05	
Breakdown rate of P relative to N	$\Phi_{R,O}$	N/A	N/A	2	2

Table 40. Constants and parameter values used in the water column detritus remineralisation model. Red = Redfield ratio (C:N:P = 106:16:1); Atk = Atkinson ratio (C:N:P = 550:30:1); Ref = Refractory. See L∅nborg et al. (2017).

	Labile Det., D_{Red}	Refractory Det., D	Dissolved Organic, O
Redfield	25	-	-
Carbon	-	27	767
Nitrogen	-	4.75	135
Phosphorus	-	0.66	18.7

Table 41. Steady-state detrital and dissolved organic C, N and P concentrations for primary production equal to 2 mg N m^{-1}

where 8000 mg O m^{-3} is approximately the saturation concentration of oxygen in seawater, and τ_{COD} is the timescale of this reduction. The term $\min[COD, 8000]$ is required because COD represents the end stage of anoxic reduction and can become large for long simulations. Even with this limitation, if $\tau_{COD} = 1$ hr^{-1}, the processes in Eqs. 225 and 226 proceed faster than most of the other porewater processes.

9 Common ecological parameterisations

Most of the ecological processes contain a temperature-dependence and, for those uptaking dissolved inorganic nitrogen, preferential ammonia uptake. To simplify the description of the above processes, these common parameterisations are described separately in this section. An additional processes common to all variables, and across multiples zones, is the diffusive sediment / water exchange.

9.1 Preferential uptake of ammonia

The model contains two forms of dissolved inorganic nitrogen (DIN), dissolved ammonia (NH_4) and dissolved nitrate (NO_3):

$$N = [\mathrm{NH_4}] + [\mathrm{NO_3}] \tag{227}$$

where N is the concentration of DIN, $[\mathrm{NH_4}]$ is the concentration of dissolved ammonia and $[\mathrm{NO_3}]$ is the concentration of nitrate. In the model, the ammonia component of the DIN pool is assumed to be taken up first by all primary producers,

followed by the nitrate, with the caveat that the uptake of ammonia cannot exceed the diffusion limit for ammonia. The underlying principle of this assumption is that photosynthetic organisms can entirely preference ammonia, but that the uptake of ammonia is still limited by diffusion to the organism's surface.

As the nitrogen uptake formulation varies for the different autotrophs, the formulation of the preference of ammonia also varies. The diffusion coefficient of ammonia and nitrate are only 3 % different, so for simplicity we have used the nitrate diffusion coefficient for both.

Thus, for microalgae (Eq. 42) and *Trichodesmium* (Eq. 57), that both contain internal reserves of nitrogen, the partitioning of nitrogen uptake is given by:

$$\frac{\partial N}{\partial t} = -\psi D_N N(1-R_N^*)\left(B/m_{B,N}\right) \tag{228}$$

$$\frac{\partial [\mathrm{NH_4}]}{\partial t} = -\min\left[\psi D_N N(1-R_N^*), \psi D_N [\mathrm{NH_4}]\right]\left(B/m_{B,N}\right) \tag{229}$$

$$\frac{\partial [\mathrm{NO_3}]}{\partial t} = -\left(\psi D_N N(1-R_N^*) - \min\left[\psi D_N N(1-R_N^*), \psi D_N [\mathrm{NH_4}]\right]\right)\left(B/m_{B,N}\right) \tag{230}$$

For macroalgae (Eq. 110) and seagrass leaves (Eq. 124), which also have diffusion limits to uptake, but are not represented with internal reserves of nitrogen, the terms are:

$$\frac{\partial N}{\partial t} = -\mu_{MA} MA \tag{231}$$

$$\frac{\partial [\mathrm{NH_4}]}{\partial t} = -\min\left[SA_{eff}[\mathrm{NH_4}], \mu_{MA} MA\right] \tag{232}$$

$$\frac{\partial [\mathrm{NO_3}]}{\partial t} = -\left(\mu_{MA} MA - \min\left[SA_{eff}[\mathrm{NH_4}], \mu_{MA} MA\right]\right) \tag{233}$$

Zooxanthellae is a combination of the two cases above, because in the model they contain reserves like microalgae, but the uptake rate is across a 2D surface like macroalage.

In the case of nutrient uptake by seagrass roots (Eq. 126), which has a saturating nitrogen uptake functional form, the terms are:

$$\frac{\partial N_s}{\partial t} = -\mu_{SG} SG \tag{234}$$

$$\frac{\partial [\mathrm{NH_4}]_s}{\partial t} = -\min\left[\mu_{SG} SG, \frac{\mu_{SG}^{max} [\mathrm{NH_4}]_s SG}{K_N + [\mathrm{NH_4}]_s}\right] \tag{235}$$

$$\frac{\partial [\mathrm{NO_3}]_s}{\partial t} = -\left(\mu_{SG} SG - \min\left[\mu_{SG} SG, \frac{\mu_{SG}^{max} [\mathrm{NH_4}]_s SG}{K_N + [\mathrm{NH_4}]_s}\right]\right) \tag{236}$$

where K_N is a function of the ratio of above ground to below ground biomass described in Baird et al. (2016a).

One feature worth noting is that the above formulation for preferential ammonia uptake requires no additional parameters, which is different to other classically applied formulations (Fasham et al., 1990) that require a new parameter, potentially for each autotroph. This simple use of the geometric constraint has an important role in reducing model complexity.

9.2 Oxygen release during nitrate uptake

For all autotrophs, the uptake of a nitrate ion results in the retention of the one nitrogen atom in their reserves or structural material, and the release of the three oxygen atoms into the water column or porewaters.

$$\frac{\partial[\mathrm{O}]}{\partial t} = -\frac{48}{14}\frac{\partial[\mathrm{NO_3}]}{\partial t} \tag{237}$$

The oxygen that is part of the structural material is assumed to have been taken up through photosynthesis.

For simplicity, in the equations for autotroph driven changes in dissolved oxygen above, we have assumed that DIN uptake is ammonia. Thus after partitioning on nitrogen uptake, the term Eq. 237 needs to be added to change in oxygen in microalgae (Eq. 42), *Trichodesmium* (Eq. 57) and other autotrophs.

9.3 Temperature dependence of ecological rates

Physiological rate parameters (maximum growth rates, mortality rates, remineralisation rates) have a temperature dependence that is determined from:

$$r_T = r_{Tref} Q_{10}^{(T-T_{ref})/10} \tag{238}$$

where r_T is the physiological rate parameter (e.g. μ, ζ etc.) at temperature T, T_{ref} is the reference temperature (nominally 20°C for GBR), r_T the physiological rate parameter at temperature T_{ref}, Q_{10} is the Q10 temperature coefficient and represents the rate of change of a biological rate as a result of increasing temperature by 10°C.

Note that while physiological rates may be temperature-dependent, the ecological processes they are included in may not. For example, for extremely light-limited growth, all autotrophs capture light at a rate independent of temperature. With the reserves of nutrients replete, the steady-state realised growth rate, μ, becomes the rate of photon capture, k. This can be shown algebracially: $\mu = \mu^{max} R_C^* = k(1 - R^*)$, where R^* is the reserves of carbon. Rearranging, $R^* = k/(\mu^{max} + k)$. At $k << \mu^{max}$, $R^* = k/\mu^{max}$, thus $\mu = \mu^{max} k/\mu^{max} = k$. This corresponds with observations of no temperature dependence of photosynthesis at low light levels (Kirk, 1994).

Similar arguments show that extremely nutrient limited autorophs will have the same temperature dependence to that of the diffusion coefficient. Thus, the autotroph growth model has a temperature-dependence that adjust appropriately to the physiological condition of the autotroph, and is a combination of constant, exponential, and polynomial expressions.

Physiological rates in the model that are not temperature dependent are: mass transfer rate constant for particulate grazing by corals, S_{Part}; net coral calcification g; maximum chlorophyll synthesis, k_{Chl}^{max};and rate of translocation between leaves and roots in seagrass, τ_{tran}.

9.4 Diffusive exchange of dissolved tracers across sediment-water interface

Due to the thin surface sediment layer, and the potentially large epibenthic drawndown of porewater dissolved tracers, the exchange of dissolved tracers between the bottom water column layer and the top sediment layer is solved in the same numerical

operation as the ecological tracers (other transport processes occurring between ecological timesteps). The flux, J, is given by:

$$J = k(C_s - C) \tag{239}$$

where C and C_s are the concentration in water column and sediment respectively, $k = 4.6 \times 10^{-7}$ m s^{-1} is the transfer coefficient. In the model parameterisation, $k = D/h$ where $D = 3 \times 10^{-9}$ m^2 s^{-1} is the diffusion coefficient and $h = 0.0065$ mm is the thickness of the diffusive layer.

While in reality k would vary with water column and sediment hydrodynamics as influenced by community type etc, these complexities has not been considered. In addition to the diffusive flux between the sediment and water column, particulate deposition entrains water column water into the sediments, and particulate resuspension releases porewaters into the water column. Sediment model details can be found at: `https://research.csiro.au/cem/software/ems/ems-documentation/`.

10 Numerical integration

10.1 Splitting of physical and ecological integrations

The numerical solution of the time-dependent advection-diffusion-reaction equations for each of the ecological tracers is implemented through sequential solving of the partial differential equations (PDEs) for advection and diffusion, and the ordinary differential equations (ODEs) for reactions. This technique, called operator splitting, is common in geophysical science (Hundsdorfer and Verwer, 2003; Butenschön et al., 2012).

Under the sequential operator splitting technique used, first the advection-diffusion processes are solved for the period of the time-step (15 min - 1 hour, Table 42). The value of the tracers at the end of this PDE integration, and the initial time, are then used as initial conditions for the ODE integration. After the ODE integration has run for the same time period, the values of the tracers are updated, and time is considered to have moved forward just one time-step. The integration continues to operate sequentially for the whole model simulation. The errors due to operator splitting can be significant (Butenschön et al., 2012), although tests in relatively coarse (4 km) models show that reducing the time-step from 60 min to 30 min does not substantially change the model solution. For higher resolution models shorter time scales are required to resolve finer scale motion, and its interaction with ecological processes.

The PDE solvers are described in the physical model description available at:
`www.emg.cmar.csiro.au/www/en/emg/software/EMS/hydrodynamics.html`.

The code allows 4-5th and 7-8th order adaptive ODE solvers following Dormand and Prince (1980), as well as the Euler method and adaptive first and second order solvers. The preferred scheme is the adaptive 4th-5th order (similar to ode45 in MATLAB), and implement in numerous biogeochemical models (Yool, 1997). This requires 7 function evaluations for the first step and 6 for each step after. A tolerance of 1×10^{-5} is required for the integration step to be accepted.

The solution of the ecological equations are independent for each vertical column, and depend only on the layers above through which the light has propagated. For an n_{wc}-layer water column and n_{sed}-layer sediment, the integrator sequentially

solves the top $n_{wc} - 1$ water column layers; the nth water column layer, epibenthic and top sediment layer together; and then the $n_{sed} - 1$ to bottom sediment layers.

Description	Values
Timestep of hydrodynamic model	90 s
[a]Timestep of ODE ecological model	3600 s
Timestep of optical and carbon chemistry models	3600 s
Optical model resolution in PAR	$\sim$ 20 nm
ODE integrator	Adaptive 4th-5th order (Dormand and Prince, 1980)
ODE tolerance	10^{-5}
Maximum number of ODE steps in ecology	2000
Maximum number of iterations in carbon chemistry	100
Accuracy of carbon chemistry calculations	$[H^+] = 10^{-12}$ mol

Table 42. Integration details. Optical wavelengths (nm): 290 310 330 350 370 390 410 430 440 450 470 490 510 530 550 570 590 610 630 650 670 690 710 800.[a] Since the integrator is 4-5th order, the ecological derivatives are evaluated at least every approximately $3600/5 = 900$ s, and more regularly for stiff equations. The ODE tolerance is a fraction of the value of the state variable.

10.2 Optical integration

The inherent and apparent optical properties are calculated between the physical and ecological integrations. The light climate used for each ecological timestep is that calculated at the start time of the ecological integration. The spectral resolution of 25 wavebands has been chosen to resolve the absorption peaks associated with Chl *a*, and to span the optical wavelengths. As IOPs can be calculated at any wavelength given the model state, IOPs and AOPs at observed wavelengths are recalculated after the integration.

Additionally, the wavelengths integrated have been chosen such that the lower end of one waveband and the top end of another fall on 400 and 700 nm respectively, allowing precise calculation of photosynthetically available radiation (PAR).

10.3 Additional integration details

10.3.1 Approximation of stoichiometric coefficients

In this model description we have chosen to explicitly include atomic mass as integer values, so that the conversion are more readable in the equations than if they had all been rendered as mathematical symbols. Nonetheless these values are more precisely given in the numerical code (Table 43).

It is worth remembering that the atomic masses are approximations assuming the ratio of isotopes found in the Periodic Table (Atkins, 1994), based on the natural isotopic abundance of the Earth. So, for example, ^{14}N and ^{15}N have atomic masses

of 14.00307 and 15.00011 respectively, with ^{14}N making up 99.64 % of the abundance on Earth. Thus the value 14.01 comes from $14.00307 \times 99.64 + 15.00011 \times 0.36 = 14.0067$. The isotopic discrimination in the food web of 3 ppt per trophic level would increase the mean atomic mass by $(15.00011 - 14.00307) \times 0.003 = 0.003$ per trophic level. Perhaps more importantly, if the model had state variables for ^{14}N and ^{15}N, then the equations would change to contain coefficients of 14 for the ^{14}N isotope equations, and 15 for the ^{15}N isotope equations, that would be applied in the numerical code using 14.00 and 15.00 respectively.

Element	Value in symbolic equations	Value in code
Nitrogen, N	14	14.01
Carbon, C	12	12.01
Oxygen, O_2	32	32.00
Phosphorus, P	31	30.97

Table 43. Atomic mass of the C, N, P and O_2, both in the model description where two significant figures are used for brevity, and in the numerical code, where precision is more important.

10.3.2 Mass conservation in water column and sediment porewaters

The model checks the conservation of Total C, TC, Total N, TN, Total P, TP, and oxygen, [O_2], within each grid cell at each time step using the following conservation laws. To establish mass conservation, the sum of the change in mass (of N, P, C and O) with time and the mass of sinks / sources (such as sea-air fluxes, denitrification) must equate to zero.

The total mass and conservation equations are same for the water column and porewaters, with the caveats that (1) air-sea fluxes only affect surface layers of the water, (2) denitrification only occurs in the sediment, and (3) the porosity, ϕ, of the water column is 1. In the sediment, the concentration of particulates is given in per unit volume of space, while the concentration of dissolved tracers is given in per unit volume of porewater. The concentration of dissolved tracer, X, per unit space is given by ϕX.

Thus the total carbon in a unit volume of space, and its conservation, are given by:

$$TC = \phi\left(DIC + O_C\right) + \left(\frac{550}{30}\frac{12}{14}D_{Atk} + D_C + \frac{106}{16}\frac{12}{14}\left(D_{red} + \sum B(1 + R_C^*) + \sum Z\right)\right) \tag{240}$$

$$\frac{\partial TC}{\partial t} + \underbrace{k_{\mathrm{CO_2}}\left(\left[\mathrm{CO_2}\right] - \left[\mathrm{CO_2}\right]_{atm}\right)/h}_{\mathrm{sea-air\ flux}} = 0 \tag{241}$$

The total nitrogen in a unit volume of space, and its conservation, are given by:

$$TN = \phi\left(\left[\mathrm{NO_3}\right] + \left[\mathrm{NH_4}\right] + O_N\right) + \left(D_{Atk} + D_{red} + D_N + \sum B(1 + R_N^*) + \sum Z\right) \tag{242}$$

$$\frac{\partial TN}{\partial t} + (\text{denitrification} - \text{nitrogen fixation})/\phi - \text{dust input}/h = 0 \tag{243}$$

The total phosphorus in a unit volume of space, and its conservation, are given by:

$$TP = \phi(DIP + O_P) + PIP + PIPI + \frac{1}{30}\frac{31}{14}D_{Atk} + D_P + \frac{1}{16}\frac{31}{14}\left(D_{red} + \sum B(1+R_P^*) + \sum Z\right) \tag{244}$$

$$\frac{\partial TP}{\partial t} - \text{dust input}/h = 0 \tag{245}$$

The concept of oxygen conservation in the model is more subtle than that of C, N and P due to the mass of oxygen in the water molecules themselves not being considered. When photosynthesis occurs, C is transferred from the dissolved phase to reserves within the cell. With both dissolved and particulate pools considered, mass conservation of C is straightforward. In contrast to C, during photosynthesis oxygen is drawn from the water molecules (i.e. H_2O), whose mass is not being considered, and released into the water column. Conversely, when organic matter is broken down oxygen is consumed from the water column and released as H_2O.

In order to obtain a mass conservation for oxygen, the concept of Biological Oxygen Demand (BOD) is used. Often BOD represents the biological demand for oxygen in say a 5 day incubation, BOD_5. Here, for the purposes of mass conservation checks, we use BOD_∞, the oxygen demand over an infinite time for breakdown. This represents the total oxygen removed from the water molecules for organic matter creation.

Anaerobic respiration reduces BOD_∞ without reducing O_2, but instead creating reduced-oxygen species. This is accounted for in the oxygen balance by the prognostic tracer Chemical Oxygen Demand (COD). In other biogeochemical modelling studies this is represented by a negative oxygen concentration.

Thus at any time point the biogeochemical model will conserve the oxygen concentration minus BOD_∞ minus COD, plus or minus any sources and sinks such as sea-air fluxes. The total oxygen minus BOD_∞ minus COD in a unit volume of water, and its conservation, is given by:

$$[\mathrm{O_2}] + \frac{48}{14}[\mathrm{NO_3}] - BOD_\infty - COD =$$

$$\phi\left([\mathrm{O_2}] + \frac{48}{14}[\mathrm{NO_3}] - COD + \frac{32}{12}O_C\right) - \left(\frac{550}{30}\frac{32}{14}D_{Atk} + \frac{32}{12}D_C + \frac{106}{16}\frac{32}{14}\left(D_{red} + \sum B_N(1+R_C^*)\right)\right) \tag{246}$$

$$\frac{\partial([\mathrm{O_2}] + \frac{48}{14}[\mathrm{NO_3}] - BOD_\infty - COD)}{\partial t} + \mathcal{R} - \overbrace{\frac{k_{\mathrm{O_2}}([\mathrm{O_2}]_{sat} - [\mathrm{O_2}])}{h}}^{sea-air\ flux} \underbrace{-2\frac{106}{16}\frac{32}{14}\tau_{nit,wc}[\mathrm{NH_4}]\frac{[\mathrm{O_2}]}{K_{nit,\mathrm{O}} + [\mathrm{O_2}]}}_{nitrification} = 0 \tag{247}$$

where $\mathcal{R}$ is respiration of organic matter.

In addition to dissolved oxygen, BOD and COD, nitrate (NO_3) appears in the oxygen mass balance. This is necessary because the N associated with nitrate uptake is not taken into the autotrophs, but rather released into the water column or porewater. Other entities that contain oxygen in the ocean include the water molecule (H_2O) and the phosphorus ion (PO_4). In the case of water, this oxygen reservoir is considered very large, with the small flux associated with its change balanced by BOD. In the case of PO_4, this is a small reservoir. As oxygen remains bound to P through the entire processes of uptake into reserves and incorporated into structural material and then release, it is not necessary to include it in the oxygen balance for the purposes of ensuring consistency. Nonetheless, strictly the water column and porewater oxygen reservoirs could include a term $+\frac{64}{31}[PO_4]$, and the BOD would have similar quantities for reserves and structural material.

10.3.3 Mass conservation in the epibenthic

Mass conservation in the epibenthos requires consideration of fluxes between the water column, porewaters and the epibenthic organisms (macroalgae, seagrass and coral hosts and symbionts).

The total carbon in the epibenthos, and its conservation, is given by:

$$TC = \frac{550}{30}\frac{12}{14}(MA + SG_A + SG_B) + \frac{106}{16}\frac{12}{14}(CS(1+R_C^*) + CH) \tag{248}$$

$$\left.\frac{\partial TC}{\partial t}\right|_{epi} + h_{wc}\left.\frac{\partial TC}{\partial t}\right|_{wc} + h_{sed}\left.\frac{\partial TC}{\partial t}\right|_{sed} + \underbrace{12(gA_{eff} - d_{\mathrm{CaCO_3}})}_{coral\ calcification\ -\ dissolution} = 0 \tag{249}$$

where h_{wc} and h_{sed} are the thickness of the bottom water column and top sediment layers, R_C^* is the normalised internal reserves of carbon in zooxanthallae, $12g$ is the rate coral calcification per unit area of coral, A_{eff} is the area of the bottom covered by coral per m^{-2}, and the diffusion terms between porewaters and the water column cancel, so do not appear in the equations. Note the units of mass of CS needs to be in g N, and some configurations may have multiple seagrass and macroalgae species.

Similarly for nitrogen, phosphorus and oxygen in the epibenthos:

$$TN = MA + SG_A + SG_B + CS(1+R_N^*) + CH \tag{250}$$

$$\left.\frac{\partial TN}{\partial t}\right|_{epi} + h_{wc}\left.\frac{\partial TN}{\partial t}\right|_{wc} + h_{sed}\left.\frac{\partial TN}{\partial t}\right|_{sed} = 0 \tag{251}$$

$$TP = \frac{1}{30}\frac{31}{14}(MA + SG_A + SG_B) + \frac{1}{16}\frac{31}{14}(CS(1+R_P^*) + CH) \tag{252}$$

$$\left.\frac{\partial TP}{\partial t}\right|_{epi} + h_{wc}\left.\frac{\partial TP}{\partial t}\right|_{wc} + h_{sed}\left.\frac{\partial TP}{\partial t}\right|_{sed} = 0 \tag{253}$$

$$BOD_\infty = \frac{550}{30}\frac{32}{14}\left(MA + SG_A + SG_B\right) + \frac{106}{16}\frac{32}{14}\left(CS\left(1 + R_C^*\right) + CH\right) \tag{254}$$

$$-\frac{\partial BOD_\infty}{\partial t}\bigg|_{epi} + h_{wc}\frac{\partial([\mathrm{O_2}] - BOD_\infty)}{\partial t}\bigg|_{wc} + h_{sed}\frac{\partial([\mathrm{O_2}] - BOD_\infty)}{\partial t}\bigg|_{sed} = 0 \tag{255}$$

where there is no dissolved oxygen in the epibenthos.

10.3.4 Wetting and drying

When a water column becomes dry (the sea level drops below the seabed depth) ecological processes are turned off.

10.3.5 Unconditional stability

In addition to the above standard numerical techniques, a number of innovations are used to ensure model solutions are reached. Should an integration step fail in a grid cell, no increment of the state variables occurs, and the model continues with a warning flag registered (as `Ecology Error`). Generally the problem does not reoccur due to the transport of tracers alleviating the stiff point in phase space of the model.

11 Model evaluation

The EMS BGC model has been deployed in a range of environments around Australia, and with each deployment skill assessment has been undertaken (for a history of these applications see Sec. 14). More recently, the EMS BGC has been thoroughly assessed against remotely-sensed and in situ observations on the Great Barrier Reef, as part of the eReefs project (Schiller et al., 2014). The assessment of version B1p0 of the eReefs marine model configuration of the EMS included a 497 page report documenting a range of model configurations (4 km, 1 km and relocatable fine resolution versions) (Herzfeld et al., 2016). The optical and carbon chemistry outputs were assessed in Baird et al. (2016b) and Mongin et al. (2016b) respectively.

A more recent assessment of the biogeochemical model (vB2p0) compared simulations against a range of in situ observations that included 24 water quality moorings, 2 nutrient sampling programs (with a total of 18 stations) and time-series of taxon-specific plankton abundance. In addition to providing a range of skill metrics, the assessment included analysis of seasonal plankton dynamics (Skerratt et al., 2019).

The techniques and observations used in Skerratt et al. (2019) have been compared to the version described in this paper (vB3p0) (see Supplementary Material). This includes observations of Chl a, dissolved inorganic carbon, nitrogen, phosphorus and ammonia, dissolved organic nitrogen and phosphorus, alkalinity, pH, aragonite saturation, mass of suspended sediments and turbidity and Secchi depth.

In the following section we provide highlights of this assessment, with a focus on water chlorophyll dynamics.

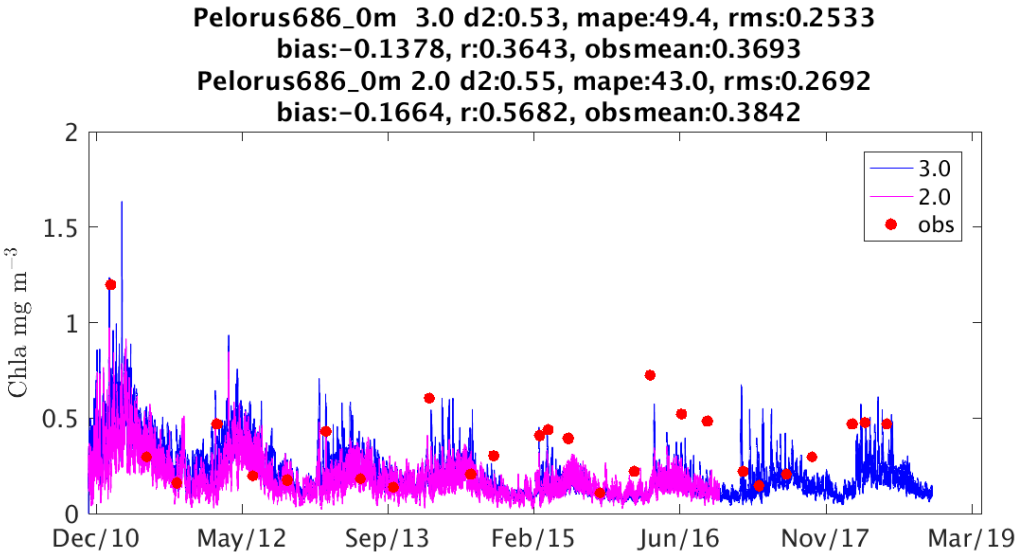

Figure 13. Observed surface chlorophyll concentration (red dots) at Pelorus Island Marine Monitoring Program site (146°29' E, 18°33' S) with a comparison to configurations vB2p0 (pink line) and vB3p0 (blue line). Statistics listed include the Willmott d2 metric (Willmott et al., 1985), mean absolute percent error (mape) and root mean square (rms) error.

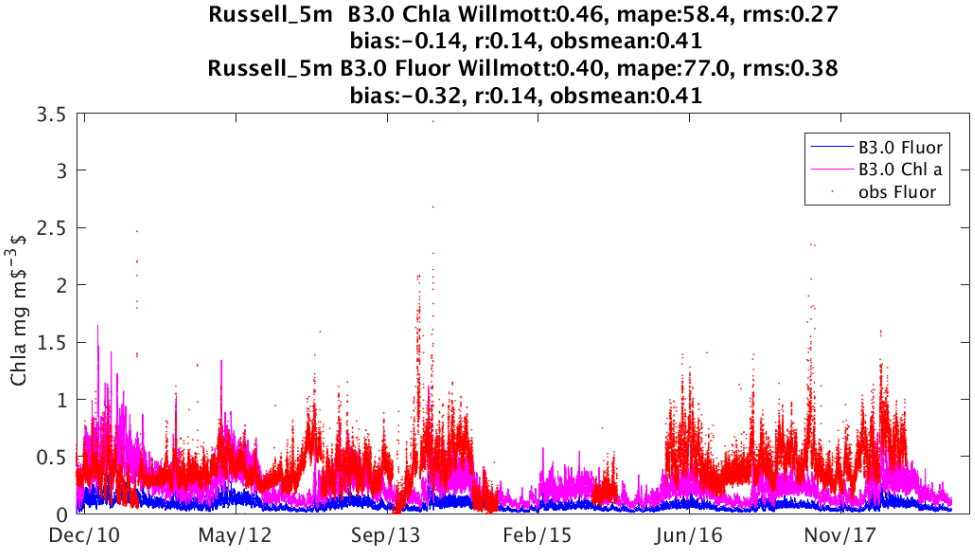

Figure 14. Observed chlorophyll fluorescence (red dots) at 5 m depth at Russell Island Marine Monitoring Program site (146°5' E, 17°14' S) with a comparison to configuration vB3p0 (pink line). The blue line is a trial product simulated fluorescence. For more information see Fig. 13.

11.1 Chlorophyll dynamics in a Great Barrier Reef (GBR) configuration

The most accurate measurements of water column chlorophyll concentrations in the GBR are obtained using high-performance liquid chromatography (HPLC) and chlorophyll extractions from water column samples. Inspection of time-series at Pelorus Island (Fig. 13) shows large variability in both the observations and the simulations, driven by inter-annual trends with 2011-2013 experiencing much greater river loads than 2014-2016, intra-annual trends driven by greater loads of nutrients during the wet season (Jan - May) than the remainder of the year, as well as monthly variability related to tidal movements and predator-prey oscillations. Even given this variability, comparison of the instantaneous state of the extracted chlorophyll concentrations against vB3p0 was able to achieve an rms of 0.25 mg m^{-3}, and a bias of -0.14 mg m^{-3}.

Near the water sample sites, moored flourometers provide a greater temporal resolution of chlorophyll dynamics (Fig. 14). The observed time-series show high daily variability, which is also seen in the vB3p0 simulations. The florescent signal is generally considered to be less accurate than the chlorophyll extractions, with jumps seen between deployments. Nonetheless at this site the skill scores at Russell Island (Fig. 14) were similar to that of chlorophyll extractions at Pelorus Island.

The above model comparisons were undertaken at 14 sites along the GBR inshore waters. The summary of the bias and d2 metrics for extracted chlorophyll is given in Fig. 15. In general there was a small negative bias in simulated chlorophyll, which was reduced in v3p0. There were only small differences between the model formulation of v2p0 and v3p0, with the greatest difference being a reduced denitrification rate that slight increased the chlorophyll concentrations.

The outputs of all hindcasts in the eReefs project can be downloaded from:

`http://dapds00.nci.org.au/thredds/catalogs/fx3/catalog.html`

12 Code availability

The model web page is:

`https://research.csiro.au/cem/software/ems/`

The webpage links to an extensive User Guide for the entire EMS package, which contains any information that is generic across the hydrodynamic, sediment, transport and ecological models, such as input/output formats. A smaller Biogeochemical User Guide documents details relevant only to the biogeochemical and optical models (such as how to specify wavelengths for the optical model), and a Biogeochemical Developer's Guide describes how to add additional processes to the code.

~~The entire~~ A permanent link to the Environmental Modelling Suite (EMS) C code ~~is available on GitHub~~used in this paper is (CSIRO, 2019):

`https://~~github~~doi.~~com~~org/~~csiro-coasts~~10.25919/~~EMS/~~5e701c5c2d9c9.`

The ~~paper describes the BGC library within EMS~~code available is also available on GitHub at `https://github.com/csiro-coa` which continues to be developed. The version is labelled as vB3p0 is to distinguish it from earlier versions of the ecological

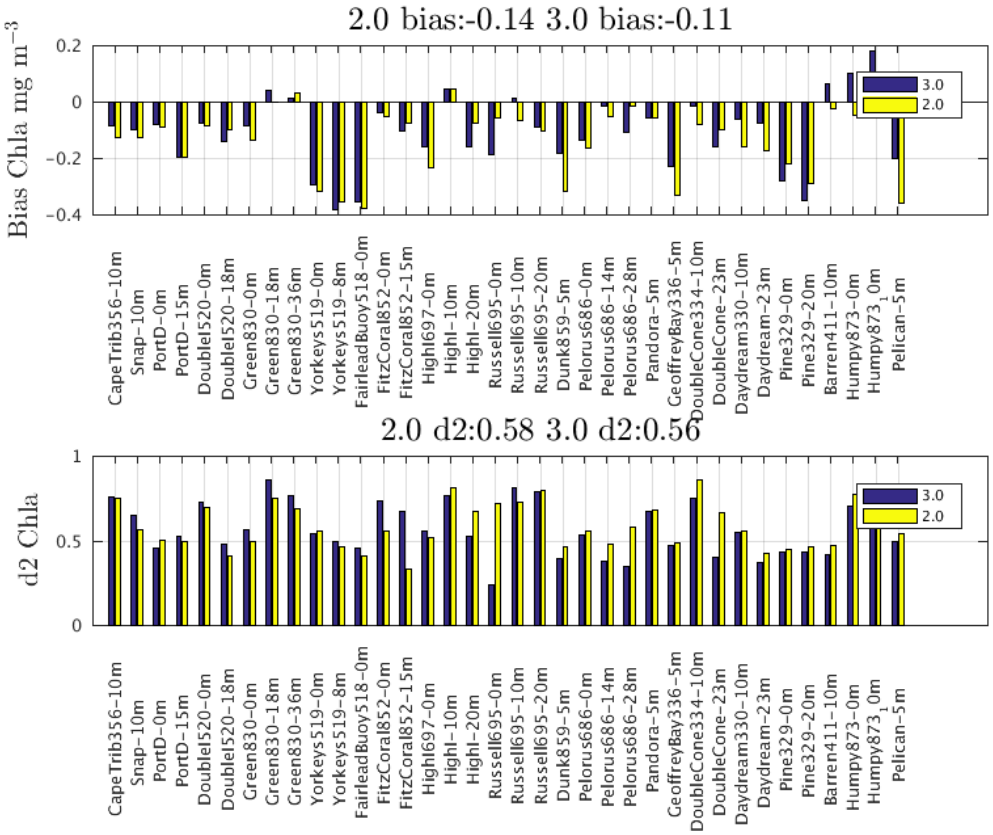

Figure 15. Skill metrics for the comparison of chlorophyll extracts at the Long Term Monitoring sites against observations for model version 3p0 and 2p0. For more information see Fig. 13 and for site locations p161-165 of the Supplementary Material.

library used in the eReefs project and others. At the `GitHub` site, vB3p0 is referred to as ecology v1.1.1, is contained within EMS release v1.1 in the `GitHub` archive, and can be accessed at:

`https://github.com/csiro-coasts/EMS/releases/tag/v1.1.1`

12.1 ~~Code architecture~~

~~This paper is a scientific description of the EMS ecological library (`/EMS/model/lib/ecology`). The ecological library consists primarily of a set of routines describing individual processes . The model chooses which processes it will include based on a configure file, an example of which appears below. The model equations are primarily derivatives of the ecological state variables, and have been split in this paper into separate processes (such as a phytoplankton growth), thus aligning with the code (such as `phytoplankton_spectral_grow_wc.c`). This object-based approach allows individual processes to be included / excluded~~ The list of processes that this paper describes are given in a configuration file ~~without re-writing the~~

model code. in App. A. The library contains other processes that have been retained for backward comparability, or for other applications (i.e. mussel farms).

Within a process file, the routine containing the ecological derivatives is <process_name>_calc, and within that routine the ecological derivatives are stored within the array y1. Each element in the array y1 stores the derivatives of a state variable.The index to the array for each state variable is determined within each process initialisation routine, <process_name>_init, and stored in the processes ' workspace ws. In the case of nitrate, for example, the derivative held in y1 will be the sum of the derivatives calculated in multiple processes (such as each autotrophic growth process, nitrification, denitrification, and each grazing and mortality process).The array of derivatives is then used by the model's adaptive integrator to update the model state, as held in the array y. method in which in differential equations described in this scientific description are incorporated into the model code are described in App. B.

Some components of the ecological model are updated only once every time step without the derivatives being calculated. These include the optical and carbon chemistry model state variables. In these cases, the state variables, which are stored in the array y, are updated directly and this is done in either the routine <process_name>_precalc or <process_name>_postcalc.

The list of processes that this paper describes are for version B3p0, which is invoked with a configuration file listing the processes in each of the domains water, sediment and epibenthic: or alternatively with a call in the configuration file: PROCESSFNAME B3p0.

Other processes in the process_library can be validly called, but their scientific description is not given in this paper. The header in the source code for each process file gives detail about it use within the code, such as any arguments that it requires (for example seagrass_spectral_grow_epi requires the seagrass type as an argument).

13 Relocatable Coast and Ocean Model (RECOM)

A web based interface, RECOM, has been developed to automate the process of downscaling the EMS model using an existing hindcast as boundary conditions (https://research.csiro.au/ereefs/models/models-about/recom/, including the RECOM User Manual). For the purposes of learning how to apply the EMS software available, RECOM provides the user with the ability to generate a complete test case of a domain situated along the northeast Australian coastline. Once a RECOM simulation has been generated using the web interface, the entire simulation including source code, forcing and initial condition files, model configuration files and the model output can be downloaded. This allows the user to repeat the model simulation on their own computing system, and modify code, forcing, and output frequency as required. The technical details of RECOM are detailed in Baird et al. (2018), and in the RECOM User Manual.

14 Discussion

The EMS BGC model development has been a function of the historical applications of the model across a rage of ecosystems, so it is worth giving a brief history of the model development.

14.1 History of the development of the EMS biogeochemical model

The EMS biogeochemical model was first developed as a nitrogen-based model for determining the assimilative capacity for sewerage discharged ~~in to~~ into Port Philip Bay~~(Fig. 3)~~, the embayment of the city of Melbourne (Harris et al., 1996). This study saw a focus on sediment processes such as denitrication, and demonstrated the ability of bay-wide denitrification to prevent change in the ecological state of the bay exposed to sewerage treatment plant loads (Murray and Parslow, 1997; Murray and Parlsow, 1999). The basic structure of the model, and in particular the split of pelagic, epibenthic and sediment zones were in place for this project. This zonation generated the ability to resolve processes in shallow water systems, and in particular to consider benthic flora in detail.

The next major study involved simulating a range of estuarine morphologies (salt wedge, tidal, lagoon, residence times) and forcings (river flow seasonality, nutrient inputs etc.) that were representative of Australia's 1000+ estuaries (Baird et al., 2003). At this point carbon and phosphorus were included in the model, and the process of including physical limits to ecological processes begun (e.g. diffusion limitation of nutrient uptake and encounter rate limitation of grazing).

Following studies in the phosphorus-limited Gippsland Lakes and macro-tidal Ord River system led to the refinement of the phosphorus absorption / desorption processes. Further studies of the biogeochemical - sediment interactions in the sub-tropical Fitzroy River (Robson et al., 2006) and investigation of the impacts of a tropical cyclone (Condie et al., 2009), saw a stronger link to remote observations. At this time the use of offline transport schemes were also implemented (such as the Moreton Bay model), allowing for ~~faster model integration by~~ an order of magnitude faster model integration (Gillibrand and Herzfeld, 2016).

The next major change in the BGC model involved implementing variable C:N:P ratios of microalgae through the introduction of reserves of energy, nitrogen and phosphorus (Wild-Allen et al., 2010), allowing for more accurate prediction of the elemental budgets and impacts of natural and anthropogenic forcing of the Derwent River estuary, southeast Tasmania. This study was followed up by a number of studies developing scenarios to inform management strategies of the region (Wild-Allen et al., 2011, 2013; Skerratt et al., 2013; Hadley et al., 2015a, b).

From 2010 onwards, EMS has been applied to consider the impacts of catchment loads on the Great Barrier Reef. The focus on water clarity led to the development of a spectrally-resolved optical model, and the introduction of simulated true colour ~~(Fig. ??).~~ (Baird et al., 2016b). The eReefs project was the first EMS application to consider corals, resulting in the introduction of the host-symbiont coral system and equilibrium carbon chemistry (Mongin and Baird, 2014; Mongin et al., 2016b, a). Additionally, the calculation of model outputs that match remote-sensing observations allowed the model to be run in a data assimilating system, where the observation-model mis-match was based on remote-sensing reflectance (Jones et al., 2016).

The most recent application of the EMS BGC model has been for investigating the environmental impact of aquaculture in Los Lagos, Chile. For the Los Lagos application, new processes for fish farms, dinoflagellates and benthic filter feeders were added, although these additions aren't described in this document. As a demonstration of the ability to add and remove processes, the Los Lagos application was run with the same EMS C executable file as the Great Barrier Reef application - just with the configuration files altered.

14.2 ~~Future developments~~Comparison with other marine biogeochemical models

~~The EMS has~~ As introduced earlier, there are a number of complex marine biogeochemical model. The most similar model in scope and approach to EMS is the ERSEM (European Regional Seas Ecosystem Model) model (Butenschön et al., 2016). Both ERSEM and EMS consider in detail pelagic, benthic and sediment processes, and could generally be described as functional group models. That is, the state variables, and the processes that link them, are chosen to represent groups of organisms that act in similar ways. This allows the complexity of real systems to be reduced to a tractable model. Many functional group style biogeochemical models exist, and were in fact the earliest models developed (Riley, 1947; Fasham, 1993; Sarmiento et al., 1993) . The most significant differences between EMS and ERSEM are (1) EMS concentrates more on benthic flora than ERSEM, while ERSEM considers lower trophic level ecosystem interactions such as fisheries that are not captured in EMS; and (2) while EMS and ERSEM have similar state variables and processes, EMS has a different set of governing equations that are based on geometric constraints of individuals while ERSEM, like most other functional biogeochemical models, has equations based on empirical relationships determined from population interactions.

The last two decades have seen addition modelling approaches emerge: trait-based models that consider changing processes rates as populations vary (Bruggeman and Kooijman, 2007); size-based models that determine rates based on organism size (Baird et al., 2007a); ecosystem-style models that consider a multiple "species" within a functional group, developing large food-webs (Fulton et al., 2014); and models that consider a large number of functional groups that is refined through competition between groups (Follows et al., 2007). These new approaches are applied primarily in pelagic ecosystems, where the generic nature of pelagic interactions encourages over-arching philosophies to model construction, and with considerable success (Dutkiewicz et al., 2015). The awkwardness of the variety of benthic communities (corals, seagrass, kelp etc.), and their prime role in shallow water, has meant that estuarine and coastal models have, like ERSEM and EMS, typically chosen the functional model approach (Madden and Kemp, 1996; Spillman et al., 2007).

14.3 Future developments in EMS

EMS has been developed to address specific scientific questions in Australia's coastal environment. As a result, the set of processes the EMS considers varies from those typically applied by other groups developing marine BGC models. Processes which have not been considered, but often are considered in marine BGC models, include iron and silicate limitation (which are not common on the Australian continental shelf or estuaries), photoinhibition of microalgae, explicit bacterial biomass. Each of these will be considered as the need arises.

A deliberate decision in the development of the EMS BGC model was made to avoid higher trophic level processes, such fish dynamics and reproduction of long-lived species. This decision was made because: (1) including these longer time-scale, often highly non-linear, processes reduces the ability of development to concentrate on BGC processes; and (2) it was recognised that CSIRO has developed a widely-used ecosystem model (Atlantis, `https://research.csiro.au/atlantis/`, Fulton et al. (2014)), and that coupling the EMS with Atlantis takes advantage of complimentary strengths of the two modelling systems.

A recent capacity introduced to EMS is the development of a relocatable capability (RECOM, Sec. 13), allowing model configurations (grid, river and meteorological forcing, ecological processes, boundary conditions) to be automatically generated. This capability will be a good test of the portability of the BGC model, and in particular the use of geometric description of physical limits to ecological processes.

Future enhancements in the EMS BGC model for tropical systems are likely to continue to pursue those components at risk from human impacts, such as dissolution of marine carbonates affecting sediment substrate and herbicide interactions with photosystems. We also expect to continue to refine the optical model, and in particular the relationship between particle size distribution and mass-specific scattering and absorption properties. In temperate systems, current and near-future deployments of ~~the EMS code~~ EMS in Australia will be focussed on coastal system characterisation for aquaculture, carbon sequestration and management decision support for the Blue Economy. Ongoing research includes improved methods for model validation against observations and translation of model outputs into knowledge that informs stakeholder decisions.

14.4 Concluding thoughts

The BGC model in the CSIRO EMS has developed unique parameterisation when compared to other marine biogeochemical models applied elsewhere due in part to a unique set of scientific challenges of the Australian coastline. It has proved to be useful in many applications, most notably the Great Barrier Reef where extensive observational datasets has allowed new process model development and detailed model skill assessment [(Baird et al., 2016b, a; Mongin et al., 2016b; Skerratt et al., 2019) and `eReefs.info`]. This document provides easy access to some of the novel process formulations that have been important in this success, as well as a complete ~~description of the entire modelling system, which can be downloaded from GitHub~~scientific description of version B3p0.

References

Anthony, K. R. N., Kleypas, J. A., and Gattuso, J.-P.: Coral reefs modify their seawater carbon chemistry - implications for impacts of ocean acidification, Glob. Change Biol., 17, 3655–3666, 2011.

Atkins, P. W.: Physical Chemistry, Oxford University Press, Oxford, 5th edn., 1994.

Atkinson, M. J.: Productivity of Eniwetak Atoll reef predicted from mass-transfer relationships, Cont. Shelf Res., 12, 799–807, 1992.

Atkinson, M. J. and Bilger, B. W.: Effects of water velocity on phosphate uptake in coral reef-flat communities, Limnol. Oceanogr., 37, 273–279, 1992.

Atkinson, M. J. and Smith, S. V.: C:N:P ratios of benthic marine plants, Limnol. Oceanogr., 28, 568–574, 1983.

Aumont, O., Ethé, C., Tagliabue, A., Bopp, L., and Gehlen, M.: PISCES-v2: an ocean biogeochemical model for carbon and ecosystem studies, Geoscientific Model Development, 8, 2465–2513, https://doi.org/10.5194/gmd-8-2465-2015, https://www.geosci-model-dev.net/8/2465/2015/, 2015.

Babcock, R. C., Baird, M. E., Pillans, R., Patterson, T., Clementson, L. A., Haywood, M. E., Rochester, W., Morello, E., Kelly, N., Oubelkheir, K., Fry, G., Dunbabin, M., Perkins, S., Forcey, K., Cooper, S., Donovan, A., Kenyon, R., Carlin, G., and Limpus, C.: Towards an integrated study of the Gladstone marine system 278 pp ISBN: 978-1-4863-0539-1, Tech. rep., CSIRO Oceans and Atmosphere Flagship, Brisbane, 2015.

Baird, M. E.: Numerical approximations of the mean absorption cross-section of a variety of randomly oriented microalgal shapes, J. Math. Biol., 47, 325–336, 2003.

Baird, M. E. and Emsley, S. M.: Towards a mechanistic model of plankton population dynamics, J. Plankton Res., 21, 85–126, 1999.

Baird, M. E. and Middleton, J. H.: On relating physical limits to the carbon: nitrogen ratio of unicellular algae and benthic plants, J. Mar. Sys., 49, 169–175, 2004.

Baird, M. E., Emsley, S. M., and McGlade, J. M.: Modelling the interacting effects of nutrient uptake, light capture and temperature on phytoplankton growth, J. Plankton Res., 23, 829–840, 2001.

Baird, M. E., Walker, S. J., Wallace, B. B., Webster, I. T., and Parslow, J. S.: The use of mechanistic descriptions of algal growth and zooplankton grazing in an estuarine eutrophication model, Est., Coastal and Shelf Sci., 56, 685–695, 2003.

Baird, M. E., Oke, P. R., Suthers, I. M., and Middleton, J. H.: A plankton population model with bio-mechanical descriptions of biological processes in an idealised 2-D ocean basin, J. Mar. Sys., 50, 199–222, 2004.

Baird, M. E., Timko, P. G., Suthers, I. M., and Middleton, J. H.: Coupled physical-biological modelling study of the East Australian Current with idealised wind forcing: Part II: Biological dynamical analysis, J. Mar. Sys., 59, 271–291, 2006.

Baird, M. E., Leth, O., and Middleton, J. F.: Biological response to circulation driven by mean summertime winds off central Chile: A numerical model study, J. Geophys. Res., 112, doi:10.1029/2006JC003 655, 2007a.

Baird, M. E., Timko, P. G., and Wu, L.: The effect of packaging of chlorophyll within phytoplankton and light scattering in a coupled physical-biological ocean model., Mar. Fresh. Res., 58, 966–981, 2007b.

Baird, M. E., Ralph, P. J., Rizwi, F., Wild-Allen, K. A., and Steven, A. D. L.: A dynamic model of the cellular carbon to chlorophyll ratio applied to a batch culture and a continental shelf ecosystem, Limnol. Oceanogr., 58, 1215–1226, 2013.

Baird, M. E., Adams, M. P., Babcock, R. C., Oubelkheir, K., Mongin, M., Wild-Allen, K. A., Skerratt, J., Robson, B. J., Petrou, K., Ralph, P. J., O'Brien, K. R., Carter, A. B., Jarvis, J. C., and Rasheed, M. A.: A biophysical representation of seagrass growth for application in a complex shallow-water biogeochemical model, Ecol. Model., 325, 13–27, 2016a.

Baird, M. E., Cherukuru, N., Jones, E., Margvelashvili, N., Mongin, M., Oubelkheir, K., Ralph, P. J., Rizwi, F., Robson, B. J., Schroeder, T., Skerratt, J., Steven, A. D. L., and Wild-Allen, K. A.: Remote-sensing reflectance and true colour produced by a coupled hydrodynamic, optical, sediment, biogeochemical model of the Great Barrier Reef, Australia: comparison with satellite data., Env. Model. Softw., 78, 79–96, 2016b.

Baird, M. E., Mongin, M., Rizwi, F., Bay, L. K., Cantin, N. E., Soja-Woźniak, M., and Skerratt, J.: A mechanistic model of coral bleaching due to temperature-mediated light-driven reactive oxygen build-up in zooxanthellae, Ecol. Model., 386, 20–37, 2018.

Baretta-Bekker, J., Baretta, J., and Ebenhöh, W.: Microbial dynamics in the marine ecosystem model ERSEM II with decoupled carbon assimilation and nutrient uptake, Journal of Sea Research, 38, 195 – 211, 1997.

Beckmann, A. and Hense, I.: Torn between extremes: the ups and downs of phytoplankton, Ocean Dynamics, 54, 581–592, 2004.

Blondeau-Patissier, D., Brando, V. E., Oubelkheir, K., Dekker, A. G., Clementson, L. A., and Daniel, P.: Bio-optical variability of the absorption and scattering properties of the Queensland inshore and reef waters, Australia, J. Geophys. Res. (Oceans), 114, C05 003, 2009.

Bohren, C. F. and Huffman, D. R.: Absorption and scattering of light particles by small particles, John Wiley & Sons, 1983.

Boudreau, B. P.: A method-of-lines code for carbon and nutrient diagenesis in aquatic sediments, Comp. Geosci., 22, 479–496, 1996.

Brando, V. E., Dekker, A. G., Park, Y. J., and Schroeder, T.: Adaptive semianalytical inversion of ocean color radiometry in optically complex waters, Applied Optics, 51, 2808–2833, 2012.

Bruggeman, J. and Kooijman, S. A. L. M.: A biodiversity-inspired approach to aquatic ecosystem modeling, Limnol. Oceanogr., 52, 1533–1544, 2007.

Butenschön, M., Zavatarelli, M., and Vichi, M.: Sensitivity of a marine coupled physical biogeochemical model to time resolution, integration scheme and time splitting method, Ocean Modelling, 52-53, 36 – 53, 2012.

Butenschön, M., Clark, J., Aldridge, J. N., Allen, J. I., Artioli, Y., Blackford, J., Bruggeman, J., Cazenave, P., Ciavatta, S., Kay, S., Lessin, G., van Leeuwen, S., van der Molen, J., de Mora, L., Polimene, L., Sailley, S., Stephens, N., and Torres, R.: ERSEM 15.06: a generic model for marine biogeochemistry and the ecosystem dynamics of the lower trophic levels, Geosci. Model Dev., 9, 1293–1339, 2016.

Cambridge, M. L. and Lambers, H.: Specific leaf area and functional leaf anatomy in Western Australian seagrasses, in: Inherent variations in plant growth: physiological mechanisms and ecological consequences, edited by Lambers, H., Poorter, H., and Vuren, M. M. I. V., pp. 88–99, Backhuys, Leiden, 1998.

Carpenter, E., O'Neil, J., Dawson, R., Capone, D., Siddiqui, P., Roenneberg, T., and Bergman, B.: The tropical diazotrophic phytoplankter *Trichodesmium*: Biological characteristics of two common species., Mar. Ecol. Prog. Ser., 95, 295–304, 1993.

Chartrand, K. M., Ralph, P. J., Petrou, K., and Rasheed, M. A.: Development of a Light-Based Seagrass Management Approach for the Gladstone Western Basin Dredging Program, Tech. rep., DAFF Publication. Fisheries Queensland, Cairns 126 pp., 2012.

Chartrand, K. M., , Bryant, C. V., Sozou, A., Ralph, P. J., and Rasheed, M. A.: Final Report: Deepwater seagrass dynamics: Light requirements, seasonal change and mechanisms of recruitment, Tech. rep., Centre for Tropical Water and Aquatic Ecosystem Research (TropWATER) Publication, James Cook University, Report No 17/16. Cairns, 67 pp., 2017.

Cherukuru, N., Dekker, A. G., Hardman-Mountford, N. J., Clementson, L. A., and Thompson, P. A.: Bio-optical variability in multiple water masses across a tropical shelf: Implications for ocean colour remote sensing models, Est. Coast. Shelf Sci., 219, 223–230, 2019.

Clementson, L. A. and Wojtasiewicz, B.: Dataset on the absorption characteristics of extracted phytoplankton pigments, Data in Brief, https://doi.org/10.1016/j.dib.2019.103875, 2019.

Condie, S. A., Herzfeld, M., Margvelashvili, N., and Andrewartha, J. R.: Modeling the physical and biogeochemical response of a marine shelf system to a tropical cyclone, Geophys. Res. Lett., 36, https://doi.org/doi:10.1029/2009GL039563, 2009.

CSIRO: EMS Release v1.1.1. v1. CSIRO. Software Collection. https://doi.org/10.25919/5e701c5c2d9c9, 2019.

Dietze, H., Matear, R., and Moore, T.: Nutrient supply to anticyclonic meso-scale eddies off western Australia estimated with artificial tracers released in a circulation model, Deep Sea Res. I, 56, 1440–1448, 2009.

Dormand, J. R. and Prince, P. J.: A family of embedded Runge-Kutta formulae, J. Comp. App. Math., 6, 19–26, 1980.

Duarte, C. M. and Chiscano, C. L.: Seagrass biomass and production: a reassessment, Aquat. Bot., 65, 159–174, 1999.

Dutkiewicz, S., Hickman, A. E., Jahn, O., Gregg, W. W., Mouw, C. B., and Follows, M. J.: Capturing optically important constituents and properties in a marine biogeochemical and ecosystem model, Biogeosciences Discussions, 12, 2607–2695, 2015.

Duysens, L. N. M.: The flattening of the absorption spectra of suspensions as compared to that of solutions, Biochim. Biophys. Acta, 19, 1–12, 1956.

Eyre, B. D., Cyronak, T., Drupp, P., Carlo, E. H. D., Sachs, J. P., and Andersson, A. J.: Coral reefs will transition to net dissolving before end of century, Science, 359, 908–911, 2018.

Falter, J. L., Atkinson, M. J., and Merrifield, M. A.: Mass-transfer limitation of nutrient uptake by a wave-dominated reef flat community, Limnol. Oceanogr., 49, 1820–1831, 2004.

Fasham, M. J. R.: Modelling the marine biota, in: The Global Carbon Cycle, edited by Heimann, M., pp. 457–504, Springer-Verlag, New York, 1993.

Fasham, M. J. R., Ducklow, H. W., and McKelvie, S. M.: A nitrogen-based model of plankton dynamics in the oceanic mixed layer, J. Mar. Res., 48, 591–639, 1990.

Fennel, K., Gehlen, M., Brasseur, P., Brown, C. W., Ciavatta, S., Cossarini, G., Crise, A., Edwards, C. A., Ford, D., Friedrichs, M. A. M., Gregoire, M., Jones, E. M., Kim, H.-C., Lamouroux, J., Murtugudde, R., and Perruche, C.: Advancing marine biogeochemical and ecosystem reanalyses and forecasts as tools for monitoring and managing ecosystem health, Front. Mar. Sci., 6, 89, 2019.

Ficek, D., Kaczmarek, S., Stoń-Egiert, J., Woźniak, B., Majchrowski, R., and Dera, J.: Spectra of light absorption by phytoplankton pigments in the Baltic; conclusions to be drawn from a Gaussian analysis of empirical data, Oceanologia, 46, 533–555, 2004.

Finkel, Z. V.: Light absorption and size scaling of light-limited metabolism in marine diatoms, Limnol. Oceanogr., 46, 86–94, 2001.

Flynn, K. J. and Mitra, A.: Why Plankton Modelers Should Reconsider Using Rectangular Hyperbolic (Michaelis-Menten, Monod) Descriptions of Predator-Prey Interactions, Frontiers Mar. Sci., 3, 165, 2016.

Follows, M., Dutkiewicz, S., Grant, S., and Chisholm, S. W.: Emergent biogeography of microbial communities in a model ocean, Science, 315, 1843–1846, 2007.

Fulton, E. A., Smith, A. D. M., Smith, D. C., and Johnson, P.: An integrated approach is needed for ecosystem based fisheries management: Insights from ecosystem-level management strategy evaluation, PLoS One, 9, e84 242, 2014.

Geider, R. J., MacIntyre, H. L., and Kana, T. M.: A dynamic regulatory model of phytoplanktonic acclimation to light, nutrients, and temperature, Limnol. Oceanogr., 43, 679–694, 1998.

Gentleman, W.: A chronology of plankton dynamics *in silico*: how computer models have been used to study marine ecosystems, Hydrobiologica, 480, 69–85, 2002.

Gillibrand, P. A. and Herzfeld, M.: A mass-conserving advection scheme for offline simulation of tracer transport in coastal ocean models, Env. Model. Soft., 101, 1–16, 2016.

Grant, . D. and Madsen, O.: Movable bed roughness in unsteady oscillatory flow, J. Geophys. Res., 87(C1), 469–481, 1982.

Gras, A. F., Koch, M. S., and Madden, C. J.: Phosphorus uptake kinetics of a dominant tropical seagrass *Thalassia testudinum*, Aquat. Bot., 76, 299–315, 2003.

Griffies, S. M., Harrison, M. J., Pacanowski, R. C., and Rosati, A.: A technical guide to MOM4 GFDL Ocean Group TECHNICAL REPORT NO. 5 Version prepared on March 3, 2004, Tech. rep., NOAA/Geophysical Fluid Dynamics Laboratory, 2004.

Gumley, L., Descloitres, J., and Shmaltz, J.: Creating reprojected true color MODIS images: A tutorial, Tech. Rep 1.0.2, 17 pp., Tech. rep., Univ. of Wisconsin, Madison, 2010.

Gustafsson, M. S. M., Baird, M. E., and Ralph, P. J.: The interchangeability of autotrophic and heterotrophic nitrogen sources in Scleractinian coral symbiotic relationships: a numerical study, Ecol. Model., 250, 183–194, 2013.

Gustafsson, M. S. M., Baird, M. E., and Ralph, P. J.: Modelling photoinhibition and bleaching in Scleractinian coral as a function of light, temperature and heterotrophy, Limnol. Oceanogr., 59, 603–622, 2014.

Hadley, S., Wild-Allen, K. A., Johnson, C., and Macleod, C.: Modeling macroalgae growth and nutrient dynamics for integrated multi-trophic aquaculture, J. Appl. Phycol., 27, 901–916, 2015a.

Hadley, S., Wild-Allen, K. A., Johnson, C., and Macleod, C.: Quantification of the impacts of finfish aquaculture and bioremediation capacity of integrated multi-trophic aquaculture using a 3D estuary model, J. Appl. Phycol., 10.1007/s10811-015-0714-2, 2015b.

Hansen, J. W., Udy, J. W., Perry, C. J., Dennison, W. C., and Lomstein, B. A.: Effect of the seagrass *Zostera capricorni* on sediment microbial processes, Mar. Ecol. Prog. Ser., 199, 83–96, 2000.

Hansen, P. J., Bjornsen, P. K., and Hansen, B. W.: Zooplankton grazing and growth: Scaling within the 2-2,000 μm body size range, Limnol. Oceanogr., 42, 687–704, 1997.

Harris, G., Batley, G., Fox, D., Hall, D., Jernakoff, P., Molloy, R., Murray, A., Newell, B., Parslow, J., Skyring, G., and Walker, S.: Port Phillip Bay Environmental Study Final Report, CSIRO, Canberra, Australia, 1996.

Herzfeld, M.: An alternative coordinate system for solving finite difference ocean models, Ocean Modelling, 14, 174 – 196, 2006.

Herzfeld, M., Andrewartha, J., Baird, M., Brinkman, R., Furnas, M., Gillibrand, P., Hemer, M., Joehnk, K., Jones, E., McKinnon, D., Margvelashvili, N., Mongin, M., Oke, P., Rizwi, F., Robson, B., Seaton, S., Skerratt, J., Tonin, H., and Wild-Allen, K.: eReefs Marine Modelling: Final Report, CSIRO, Hobart 497 pp. `http://www.marine.csiro.au/cem/gbr4/eReefs_Marine_Modelling.pdf`, Tech. rep., CSIRO, 2016.

Hill, R. and Whittingham, C. P.: Photosynthesis, Methuen, London, 1955.

Hochberg, E. J., Apprill, A. M., Atkinson, M. J., and Bidigare, R. R.: Bio-optical modeling of photosynthetic pigments in corals, Coral Reefs, 25, 99–109, 2006.

Hundsdorfer, W. and Verwer, J. G.: Numerical solutions of time-dependent advection-diffusion-reaction equations, Springer, 2003.

Hurd, C. L.: Water motion, marine macroalgal physiology, and production, J. Phycol., 36, 453–472, 2000.

Jackson, G. A.: Coagulation of Marine Algae, in: Aquatic Chemistry: Interfacial and Interspecies Processes, edited by Huang, C. P., O'Melia, C. R., and Morgan, J. J., pp. 203–217, American Chemical Society, Washington, DC, 1995.

Jones, E. M., Baird, M. E., Mongin, M., Parslow, J., Skerratt, J., Lovell, J., Margvelashvili, N., Matear, R. J., Wild-Allen, K., Robson, B., Rizwi, F., Oke, P., King, E., Schroeder, T., Steven, A., and Taylor, J.: Use of remote-sensing reflectance to constrain a data assimilating marine biogeochemical model of the Great Barrier Reef, Biogeosciences, 13, 6441–6469, 2016.

Kaldy, J. E., Brown, C. A., and Andersen, C. P.: *In situ* ^{13}C tracer experiments elucidate carbon translocation rates and allocation patterns in eelgrass *Zostera marina*, Mar. Ecol. Prog. Ser., 487, 27–39, 2013.

Kemp, W. M., Murray, L., Borum, J., and Sand-Jensen, K.: Diel growth in eelgrass *Zostera marina*., Mar. Ecol. Prog. Ser., 41, 79–86, 1987.

Kirk, J. T. O.: A theoretical analysis of the contribution of algal cells to the attenuation of light within natural waters. I. General treatment of suspensions of pigmented cells., New Phytol., 75, 11–20, 1975.

Kirk, J. T. O.: Volume scattering function, average cosines, and the underwater light field., Limnol. Oceanogr., 36, 455–467, 1991.

Kirk, J. T. O.: Light and Photosynthesis in Aquatic Ecosystems, Cambridge University Press, Cambridge, 2nd edn., 1994.

Lee, J.-Y., Tett, P., Jones, K., Jones, S., Luyten, P., Smith, C., and Wild-Allen, K.: The PROWQM physical–biological model with benthic–pelagic coupling applied to the northern North Sea, J. Sea Res., 48, 287–331, 2002.

Lee, K.-S. and Dunton, K. H.: Inorganic nitrogen acquisition in the seagrass *Thalassia testudinum* : Development of a whole-plant nitrogen budget, Limnol. Oceanogr., 44, 1204–1215, 1999.

Li, Y. and Gregory, S.: Diffusion of ions in sea water and in deep-sea sediments, Geochim. Cosmochim. Acta, 38, 703–714, 1974.

Litchman, E. and Klausmeier, C. A.: Trait-based community ecology of phytoplankton, Annu. Rev. Ecol. Evol. Syst., 39, 615–639, 2008.

Longstaff, B. J.: Investigations into the light requirements of seagrasses in northeast Australia, Ph.D. thesis, University of Queensland, 2003.

Lønborg, C., Álvarez–Salgado, X. A., Duggan, S., and Carreira, C.: Organic matter bioavailability in tropical coastal waters: The Great Barrier Reef, Limnol. Oceanogr., 63, 1015–1035, 2017.

Madden, C. J. and Kemp, W. M.: Ecosystem model of an estuarine submersed plant community: calibration and simulation of eutrophication responses, Estuaries, 19, 457–474, 1996.

Mann, K. H. and Lazier, J. R. N.: Dynamics of Marine Ecosystems, Blackwell Scientific Publications Inc., Oxford, 3rd edn., 2006.

Margvelashvili, N.: Stretched Eulerian coordinate model of coastal sediment transport, Computer Geosciences, 35, 1167–1176, 2009.

Mobley, C. D.: Light and Water: Radiative Transfer in Natural Waters, Academic Press, 1994.

Monbet, P., Brunskill, G. J., Zagorskis, I., and Pfitzner, J.: Phosphorus speciation in the sediment and mass balance for the central region of the Great Barrier Reef continental shelf (Australia), Geochimica et Cosmochimica Acta, 71, 2762–2779, 2007.

Mongin, M. and Baird, M. E.: The interacting effects of photosynthesis, calcification and water circulation on carbon chemistry variability on a coral reef flat: a modelling study., Ecol. Mod., 284, 19–34, 2014.

Mongin, M., Baird, M. E., Lenton, A., and Hadley, S.: Optimising reef-scale CO_2 removal by seaweed to buffer ocean acidification., Environ. Res. Lett., 11, 034 023, 2016a.

Mongin, M., Baird, M. E., Tilbrook, B., Matear, R. J., Lenton, A., Herzfeld, M., Wild-Allen, K. A., Skerratt, J., Margvelashvili, N., Robson, B. J., Duarte, C. M., Gustafsson, M. S. M., Ralph, P. J., and Steven, A. D. L.: The exposure of the Great Barrier Reef to ocean acidification, Nature Communications, 7, 10 732, 2016b.

Morel, A. and Bricaud, A.: Theoretical results concerning light absorption in a discrete medium, and application to specific absorption of phytoplankton, Deep Sea Res., 28, 1375–1393, 1981.

Muller-Parker, G., Cook, C. B., and D'Elia, C. F.: Elemental composition of the coral *Pocillopora damicornis* exposed to elevated seawater ammonium, Pac. Sci., 48, 234–246, 1994.

Munhoven, G.: Mathematics of the total alkalinity-pH equation pathway - to robust and universal solution algorithms: the SolveSAPHE package v1.0.1, Geosci. Model Dev., 6, 1367–1388, 2013.

Munk, W. H. and Riley, G. A.: Absorption of nutrients by aquatic plants, J. Mar. Res., 11, 215–240, 1952.

Murray, A. and Parlsow, J. S.: Modelling the nutrient impacts in Port Phillip Bay - a semi enclosed marine Australian ecosystem, Mar. Freshwater Res., 50, 469–81, 1999.

Murray, A. and Parslow, J.: Port Phillip Bay Integrated Model: Final Report, Tech. rep., CSIRO, GPO Box 1666, Canberra, ACT 2601 201pp, 1997.

Najjar, R. and Orr, J.: Biotic-HOWTO. Internal OCMIP Report, LSCE/CEA Saclay, Gif-sur-Yvette, France 15., Tech. rep., 1999.

Nielsen, M. V. and Sakshaug, E.: Photobiological studies of *Skeletonema costatum* adapted to spectrally different light regimes, Limnol. Oceanogr., 38, 1576–1581, 1993.

Orr, J. C., Fabry, V. J., Aumont, O., Bopp, L., Doney, S. C., Feely, R. A., Gnanadesikan, A., Gruber, N., Ishida, A., Joos, F., Key, R. M., Lindsay, K., Maier-Reimer, E., Matear, R., Monfray, P., Mouchet, A., Najjar, R. G., Plattner, G.-K., Rodgers, K. B., Sabine, C. L., Sarmiento, J. L., Schlitzer, R., Slater, R. D., Totterdell, I. J., Weirig, M.-F., Yamanaka, Y., and Yool, A.: Anthropogenic ocean acidification over the twenty-first century and its impact on calcifying organisms, Nature, 437, 681–686, 2005.

Pailles, C. and Moody, P. W.: Phosphorus sorption-desorption by some sediments of the Johnstone Rivers catchments, northern Queensland, Aust. J. Mar. Freshwater Res., 43, 1535–1545, 1992.

Pasciak, W. J. and Gavis, J.: Transport limited nutrient uptake rates in *Dictylum brightwellii*, Limnol. Oceanogr., 20, 604–617, 1975.

Redfield, A. C., Ketchum, B. H., and Richards, F. A.: The influence of organisms on the composition of sea-water, in: The sea, edited by Hill, N., pp. 26–77, Wiley, 2nd edn., 1963.

Reynolds, C. S.: The ecology of freshwater phytoplankton, Cambridge University Press, 1984.

Ribes, M. and Atkinson, M. J.: Effects of water velocity on picoplankton uptake by coral reef communities, Coral Reefs, 26, 413–421, 2007.

Riley, G. A.: A theoretical analysis of the zooplankton population of Georges Bank, J. Mar. Res., 6, 104–113, 1947.

Roberts, D. G.: Root-hair structure and development in the seagrass *Halophila ovalis* (R. Br.) Hook. f., Aust. J. Mar. Freshw. Res., 44, 85–100, 1993.

Robson, B., Webster, I., Margvelashvili, N. Y., and Herzfeld, M.: Scenario modelling: simulating the downstream effects of changes in catchment land use., Tech. rep., CRC for Coastal Zone, Estuary and Waterway Management Technical Report 41. 26 p., 2006.

Robson, B. J., Baird, M. E., and Wild-Allen, K. A.: A physiological model for the marine cyanobacteria, *Trichodesmium*, in: MODSIM2013, 20th International Congress on Modelling and Simulation, edited by Piantadosi, J. R. S. A. and Boland, J., pp. 1652–1658, Modelling and Simulation Society of Australia and New Zealand, ISBN: 978-0-9872143-3-1, www.mssanz.org.au/modsim2013/L5/robson.pdf, 2013.

Robson, B. J., Arhonditsis, G., Baird, M., Brebion, J., Edwards, K., Geoffroy, L., Hébert, M.-P., van Dongen-Vogels, V., Jones, E., Kruk, C., Mongin, M., Shimoda, Y., Skerratt, J., Trevathan-Tackett, S., Wild-Allen, K., Kong, X., and Steven, A.: Towards evidence-based parameter values and priors for aquatic ecosystem modelling, Env. Mod. Soft., 100, 74–81, 2018.

Sarmiento, J. L., Slater, R. D., Fasham, M. J. R., Ducklow, H. W., Toggweiler, J. R., and Evans, G. T.: A seasonal three-dimensional ecosystem model of nitrogen cycling in the North Atlantic euphotic zone, Global Biogeochem. Cycles, 7, 417–450, 1993.

Sathyendranath, S., Stuart, V., Nair, A., Oke, K., Nakane, T., Bouman, H., Forget, M.-H., Maass, H., and Platt, T.: Carbon-to-chlorophyll ratio and growth rate of phytoplankton in the sea, Mar. Ecol. Prog. Ser., 383, 73–84, 2009.

Schiller, A., Herzfeld, M., Brinkman, R., and Stuart, G.: Monitoring, predicting and managing one of the seven natural wonders of the world, Bull. Am. Meteor. Soc., pp. 23–30, 2014.

Schroeder, T., Devlin, M. J., Brando, V. E., Dekker, A. G., Brodie, J. E., Clementson, L. A., and McKinna, L.: Inter-annual variability of wet season freshwater plume extent into the Great Barrier Reef lagoon based on satellite coastal ocean colour observations, Mar. Poll. Bull., 65, 210–223, 2012.

Skerratt, J., Wild-Allen, K. A., Rizwi, F., Whitehead, J., and Coughanowr, C.: Use of a high resolution 3D fully coupled hydrodynamic, sediment and biogeochemical model to understand estuarine nutrient dynamics under various water quality scenarios, Ocean Coast. Man., 83, 52–66, 2013.

Skerratt, J., Mongin, M., Wild-Allen, K. A., Baird, M. E., Robson, B. J., Schaffelke, B., Soja-Woźniak, M., Margvelashvili, N., Davies, C. H., Richardson, A. J., and Steven, A. D. L.: Simulated nutrient and plankton dynamics in the Great Barrier Reef (2011-2016), J. Mar. Sys., 192, 51–74, 2019.

Smith, R. C. and Baker, K. S.: Optical properties of the clearest natural waters, Applied Optics, 20, 177–184, 1981.

Soja-Woźniak, M., Baird, M. E., Schroeder, T., Qin, Y., Clementson, L., Baker, B., Boadle, D., Brando, V., and Steven, A.: Particulate backscattering ratio as an indicator of changing particle composition in coastal waters: observations from Great Barrier Reef waters, J. Geophys. Res. (Oceans), •, •, https://doi.org/10.1029/2019JC014998, 2019.

Spillman, C., Imberger, J., Hamilton, D., Hipsey, M., and Romero, J.: Modelling the effects of Po River discharge, internal nutrient cycling and hydrodynamics on biogeochemistry of the Northern Adriatic Sea, J. Mar. Sys., 68, 167 – 200, 2007.

Stock, C. A., Powell, T. M., and Levin, S. A.: Bottom-up and top-down forcing in a simple size-structured plankton dynamics model, J. Mar. Syst., 74, 134–152, 2008.

Straile, D.: Gross growth efficiencies of protozoan and metazoan zooplankton and their dependence on food concentration, predator-prey weight ratio, and taxonomic group, Limnol. Oceanogr., 42, 1375–1385, 1997.

Stramski, D., Babin, M., and Wozniak, S. B.: Variations in the optical properties of terrigenous mineral-rich particulate matter suspended in seawater, Limnol. Oceanogr., 52, 2418–2433, 2007.

Subramaniam, A., Carpenter, E. J., Karentz, D., and Falkowski, P. G.: Bio-optical properties of the marine diazotrophic cyanobacteria *Trichodesmium* spp. I. Absorption and photosynthetic action spectra, Limnol. Oceanogr., 44, 608–617, 1999.

Suggett, D. J., Warner, M. E., Smith, D. J., Davey, P., Hennige, S., and Baker, N. R.: Photosynthesis and production of hydrogen peroxide by *Symbiodinium* (Pyrrhophyta) phylotypes with different thermal tolerances, J. Phycol., 44, 948–956, 2008.

Suggett, D. J., MacIntyre, H. L., Kana, T. M., and Geider, R. J.: Comparing electron transport with gas exchange: parameterising exchange rates between alternative photosynthetic currencies for eukaryotic phytoplankton, Aquat. Microb. Ecol., 56, 147–162, 2009.

Thompson, P. A., Baird, M. E., Ingleton, T., and Doblin, M. A.: Long-term changes in temperate Australian coastal waters and implications for phytoplankton, Mar. Ecol. Prog. Ser., 394, 1–19, 2009.

Vaillancourt, R. D., Brown, C. W., Guillard, R. R. L., and Balch, W. M.: Light backscattering properties of marine phytoplankton: relationship to cell size, chemical composition and taxonomy, J. Plank. Res., 26, 191–212, 2004.

Vermaat, J. E., Agawin, N. S. R., Duarte, C. M., Fortes, M. D., Marba, N., and Uri, J. S.: Meadow maintenance, growth and productivity of a mixed Philippine seagrass bed, Mar. Ecol. Prog. Ser., 124, 215–225, 1995.

Vichi, M., Pinardi, N., and Masina, S.: A generalized model of pelagic biogeochemistry for the global ocean ecosystem: Part I: Theory, J. Mar. Sys., 64, 89–109, 2007.

von Liebig, J.: Chemistry in its Application to Agriculture and Physiology, Taylor and Walton, London, 1840.

Wanninkhof, R.: Relationship between wind speed and gas exchange over the ocean, J. Geophys. Res., 97, 7373–7382, 1992.

Wanninkhof, R. and McGillis, W. R.: A cubic relationship between air-sea CO_2 exchange and wind speed, Geophys. Res. Letts., 26, 1889–1892, 1999.

Weiss, R.: The solubility of nitrogen, oxygen and argon in water and seawater, Deep Sea Res., 17, 721–735, 1970.

Wild-Allen, K., Herzfeld, M., Thompson, P. A., Rosebrock, U., Parslow, J., and Volkman, J. K.: Applied coastal biogeochemical modelling to quantify the environmental impact of fish farm nutrients and inform managers., J. Mar. Sys., 81, 134–147, 2010.

Wild-Allen, K., Skerratt, J., Whitehead, J., Rizwi, F., and Parslow, J.: Mechanisms driving estuarine water quality: a 3D biogeochemical model for informed management, Est. Coast. Shelf Sci., 135, 33–45, 2013.

Wild-Allen, K. A., Thompson, P. A., Volkman, J., and Parslow, J.: Use of a coastal biogeochemical model to select environmental monitoring sites, J. Mar. Sys., 88, 120–127, 2011.

Willmott, C. J., Ackleson, S. G., Davis, R. E., Feddema, J. J., Klink, K. M., Legates, D. R., O'Donnell, J., and Rowe, C. M.: Statistics for the evaluation and comparison of models, J. Geophys. Res., 90, 8995–9005, 1985.

Wojtasiewicz, B. and Stoń-Egiert, J.: Bio-optical characterization of selected cyanobacteria strains present in marine and freshwater ecosystems, Journal of Applied Phycology, 28, 2299–2314, 2016.

Wright, S., Thomas, D., Marchant, H., Higgins, H., Mackey, M., and Mackey, D.: Analysis of Phytoplankton of the Australian Sector of the Southern Ocean:comparisons of Microscopy and Size Frequency Data with Interpretations of Pigment HPLC Data Using the 'CHEMTAX' Matrix Factorisation Program, Mar. Ecol. Prog. Ser., 144, 285–98, 1996.

Wyatt, A. S. J., Lowe, R. J., Humphries, S., and Waite, A. M.: Particulate nutrient fluxes over a fringing coral reef: relevant scales of phytoplankton production and mechanisms of supply, Mar. Ecol. Prog. Ser., 405, 113–130, 2010.

Yonge, C. M.: A Year on the Great Barrier Reef: The Story of Corals and of the Greatest of their Creations, Putham, London, 1930.

Yool, A.: The Dynamics of Open-Ocean Plankton Ecosystem Models, Ph.D. thesis, Dept. of Biological Sciences, University of Warwick Download: `http://www.oikos.warwick.ac.uk/ecosystems /ThesisArchive/yool_thesis.html`, 1997.

Yool, A. and Fasham, M. J. R.: An examination of the "continental shelf pump" in an open ocean general circulation model, Global Biogeochem. Cyc., 15, 831–844, 2001.

Zeebe, R. E. and Wolf-Gladrow, D.: CO_2 in seawater: equilibrium, kinetics isotopes, Elsevier, 2001.

Zhang, Z., Lowe, R., Falter, J., and Ivey, G.: A numerical model of wave- and current-driven nutrient uptake by coral reef communities, Ecol. Mod., 222, 1456–1470, 2011.

Author contributions. All authors contributed to the CSIRO EMS BGC model through either proposing model formulations, writing significant components of the code, or through applying the model. The primary developers were Mark Baird, Karen Wild-Allen, John Parslow, Mathieu Mongin, Barbara Robson and Farhan Rizwi. Baird was the primary writer of the manuscript, and all co-authors contributed comments.

Competing interests. The authors declare no competing interests.

Acknowledgements

Many scientists and projects have contributed resources and knowhow to the development of this model over 20+ years. For this dedication we are very grateful.

Those who have contributed to the numerical code include (CSIRO unless stated):

Mike Herzfeld, Philip Gillibrand, John Andrewartha, Farhan Rizwi, Jenny Skerratt, Mathieu Mongin, Mark Baird, Karen Wild-Allen, John Parlsow, Emlyn Jones, Nugzar Margvelashvili, Pavel Sakov (BOM, who introduced the process structure),

Jason Waring, Stephen Walker, Uwe Rosebrock, Brett Wallace, Ian Webster, Barbara Robson, Scott Hadley (University of Tasmania), Malin Gustafsson (University of Technology Sydney, UTS), Matthew Adams (University of Queensland, UQ).

We also thank Britta Schaffelke for her commitment to observations that are used in model evaluation detailed in the Supplementary Material, and Cedric Robillot for his leadership of the eReefs Project. Finally, we greatly appreciate Dr. Marcello Vichi's in-depth review has much improved the manuscript.

Collaborating scientists include:

Bronte Tilbrook, Andy Steven, Thomas Schroeder, Nagur Cherukuru, Peter Ralph (UTS), Russ Babcock, Kadija Oubelkheir, Bojana Manojlovic (UTS), Stephen Woodcock (UTS), Stuart Phinn (UQ), Chris Roelfsema (UQ), Miles Furnas (AIMS), David McKinnon (AIMS), David Blondeau-Patissier (Charles Darwin University), Michelle Devlin (James Cook University), Eduardo da Silva (JCU), Julie Duchalais, Jerome Brebion, Leonie Geoffroy, Yair Suari, Cloe Viavant, Lesley Clementson (pigment absorption coefficients), Dariusz Stramski (inorganic absorption and scattering coefficients), Erin Kenna, Line Bay (AIMS), Neal Cantin (AIMS), Luke Morris (AIMS), Daniel Harrison (USYD), Karlie MacDonald.

Funding bodies: CSIRO Wealth from Oceans Flagship, Gas Industry Social & Environmental Research Alliance (GISERA), CSIRO Coastal Carbon Cluster, Derwent Estuary Program, INFORM2, eReefs, Great Barrier Reef Foundation, Australian Climate Change Science Program, University of Technology Sydney, Department of Energy and Environment, Integrated Marine Observing System (IMOS), National Environment Science Program (NESP TWQ Hub).

Appendix A: Process list of B3p0

The processes described in this paper are for version B3p0, which is invoked with a configuration file listing the processes in each of the domains `water`, `sediment` and `epibenthic`:

```
water
{
tfactor
viscosity
moldiff
values_common
remineralization
microphytobenthos_spectral_grow_wc
phytoplankton_spectral_grow_wc(small)
phytoplankton_spectral_grow_wc(large)
trichodesmium_mortality_wc
trichodesmium_spectral_grow_wc
phytoplankton_spectral_mortality_wc(small)
phytoplankton_spectral_mortality_wc(large)
zooplankton_mortality_wc(small)
zooplankton_mortality_wc(large)
zooplankton_large_carnivore_spectral_grow_wc
zooplankton_small_spectral_grow_wc
nitrification_wc
p_adsorption_wc
carbon_chemistry_wc
gas_exchange_wc(carbon,oxygen)
light_spectral_wc(H,HPLC)
massbalance_wc
}
epibenthos
{
tfactor_epi()
values_common_epi()
macroalgae_spectral_grow_epi()
seagrass_spectral_grow_epi(Zostera)
seagrass_spectral_grow_epi(Halophila)
seagrass_spectral_grow_epi(Deep)
coral_spectral_grow_bleach_epi()
```

```
coral_spectral_carb_epi(H)
macroalgae_mortality_epi()
seagrass_spectral_mortality_proto_epi(Zostera)
seagrass_spectral_mortality_proto_epi(Halophila)
seagrass_spectral_mortality_proto_epi(Deep)
massbalance_epi()
light_spectral_uq_epi(H)
diffusion_epi()
}
sediment
{
tfactor
viscosity
moldiff
values_common
remineralization
light_spectral_sed(HPLC)
microphytobenthos_spectral_grow_sed
carbon_chemistry_wc()
microphytobenthos_spectral_mortality_sed
phytoplankton_spectral_mortality_sed(small)
phytoplankton_spectral_mortality_sed(large)
zooplankton_mortality_sed(small)
zooplankton_mortality_sed(large)
trichodesmium_mortality_sed
nitrification_denitrification_sed
p_adsorption_sed
massbalance_sed()
}
```

or alternatively with a call in the configuration file: `PROCESSFNAME B3p0`.

Other processes in the `process_library` can be validly called, but their scientific description is not given in this paper. The header in the source code for each process file gives detail about it use within the code, such as any arguments that it requires (for example `seagrass_spectral_grow_epi` requires the seagrass type as an argument).

Appendix B: Code architecture

This paper is a scientific description of the EMS ecological library (`/EMS/model/lib/ecology`). The ecological library consists primarily of a set of routines describing individual processes. The model chooses which processes it will include based on a configuration file (App. A provides the configuration file for B3p0). The model equations are primarily derivatives of the ecological state variables, and have been split in this paper into separate processes (such as a phytoplankton growth), thus aligning with the code (such as `phytoplankton_spectral_grow_wc.c`). This object-based approach allows individual processes to be included / excluded in a configuration file without re-writing the model code.

Within a process file, the routine containing the ecological derivatives is `<process_name>_calc`, and within that routine the ecological derivatives are stored within the array `y1`. Each element in the array `y1` stores the derivatives of a state variable. The index to the array for each state variable is determined within each process initialisation routine, `<process_name>_init`, and stored in the processes' workspace `ws`. In the case of nitrate, for example, the derivative held in `y1` will be the sum of the derivatives calculated in multiple processes (such as each autotrophic growth process, nitrification, denitrification, and each grazing and mortality process). The array of derivatives is then used by the model's adaptive integrator to update the model state, as held in the array `y`.

Some components of the ecological model are updated only once every time step without the derivatives being calculated. These include the optical and carbon chemistry model state variables. In these cases, the state variables, which are stored in the array `y`, are updated directly and this is done in either the routine `<process_name>_precalc` or `<process_name>_postcalc`.

Appendix C: State (prognostic) variables

The below tables list the ecologically-relevant physical variables (Table C1), 10 dissolved (Table C2), 20 microalgal (Table C3), 2 zooplankton (Table C4), 7 non-living inorganic particulate (Table C5), 7 non-living organic particulate (Table C6) and 7 epibenthic plant (Table C7) and 5 coral polyp (Table C8) and 4 reaction centre (Table C9) state variables. All state variables that exist in the water column layers have an equivalent in the sediment layers (and are specified by `<variable name>_sed`). The dissolved tracers are given as a concentration in the porewater, while the particulate tracers are given as a concentration per unit volume (see Sec. 10.3.2).

Name	Symbol	Units	Description
Temperature (temp)	T	°C	Water temperature
Salinity (salt)	S	PSU	Water salinity
Sea level elevation (eta)	η	m	Sea level elevation relative to mean sea level
Porosity (porosity)	ϕ	-	Fraction of the volume made up of water
Bottom shear stress (ustrcw_skin)	τ	N m^{-2}	Shear stress due to currents and waves
Sand ripple height (PHYSRIPH)	-	m	Physical dimension used for estimating bottom roughness due to ripples according to Grant and Madsen (1982)
Solar zenith (Zenith)	θ_{air}	radians	Solar zenith angle is the angle between the zenith and the centre of the Sun's disc, taking a value of zero with the sun directly above, and $\pi/2$ when at, or below, the horizon.

Table C1. Long name (and variable name) in model output files, symbol and units used in this document, and a description of ecologically-relevant physical state and diagnostic variables.

Name	Symbol	Units	Description
Total alkalinity (alk)	A_T	mol kg^{-1}	Concentration of ions that can be converted to uncharged species by a strong acid. The model assumes A_T =[HCO_3^-] + [CO_3^{2-}], often referred to as carbonate alkalinity. Alkalinity and DIC together quantify the equilibrium state of the seawater carbon chemistry.
Nitrate (NO3)	[NO_3^-]	mg N m^{-3}	Concentration of nitrate. In the absence of nitrite [NO_2^-] in the model, nitrate represents [NO_3^-] + [NO_2^-].
Ammonia (NH4)	[NH_4^-]	mg N m^{-3}	Concentration of ammonia.
Dissolved Inorganic Phosphorus (DIP)	P	mg P m^{-3}	Concentration of dissolved inorganic phosphorus, also referred to as orthophosphate or soluble reactive phosphorus, SRP, composed chiefly of HPO_4^{2-} ions, with a small percentage present as PO_4^{3-}.
Dissolved inorganic carbon (DIC)	DIC	mg C m^{-3}	Concentration of dissolved inorganic carbon, composed chiefly at seawater pH of HCO_3^-, with a small percentage present as CO_3^{2-}.
Dissolved oxygen (Oxygen)	[O_2]	mg O m^{-3}	Concentration of oxygen.
Chemical Oxygen Demand (COD)	COD	mg O m^{-3}	Concentration of products of anoxic respiration in oxygen units. This represents products such as hydrogen sulfide, H_2S, that are produced during anoxic respiration and which, upon reoxidation of the water, will consume oxygen.
Dissolved Organic Carbon (DOR_C)	O_C	mg C m^{-3}	The concentration of carbon in dissolved organic compounds.
Dissolved Organic Nitrogen (DOR_N)	O_N	mg N m^{-3}	The concentration of nitrogen in dissolved organic compounds.
Dissolved Organic Phosphorus (DOR_P)	O_P	mg P m^{-3}	The concentration of phosphorus in dissolved organic compounds.

Table C2. Long name (and variable name) in model output files, symbol and units used in this document, and a description of all dissolved state variables. When the concentration of an ion is given, the chemical formulae appears in [ ] brackets.

Name	Symbol & Units	Description
Phytoplankton N (*_N)	B [mg N m^{-3}]	Total structural biomass of nitrogen of the phytoplankton population. All microalgae have a C:N:P ratio of the structural material of 106:16:1. Thus the mass of phosphorus in the structural material of a population with a biomass B is given by: $\frac{1}{16}\frac{31}{14}B$ and the mass of carbon by: $\frac{106}{16}\frac{12}{14}$ B. The number of cells is given by B/m_N.
Phytoplankton N reserves (*_NR)	BR_N^* [mg N m^{-3}]	Total non-structural biomass of nitrogen of the phytoplankton population. Phytoplankton N reserves divided by Phytoplankton N is a number between 0 and 1 and represents the factor by which phytoplankton growth is inhibited due to the internal reserves of nitrogen.
Phytoplankton P reserves (*_PR)	$\frac{1}{16}\frac{31}{14}BR_P^*$ [mg P m^{-3}]	Total non-structural biomass of phosphorus of the phytoplankton population. Phytoplankton P reserves divided by (Phytoplankton N $\times \frac{1}{16}\frac{31}{14}$) is a number between 0 and 1 and represent the factor by which phytoplankton growth is inhibited due to the internal reserves of phosphorus.
Phytoplankton I reserves (*_I)	$\frac{1060}{16}\frac{1}{14}BR_I^*$ [mmol photon m^{-3}]	Total non-structural biomass of fixed carbon of the phytoplankton population, quantified in photons. Phytoplankton I reserves divided by (Phytoplankton N $\times \frac{1060}{16}\frac{1}{14}$) is a number between 0 and 1 and represent the factor by which phytoplankton growth is inhibited due to the internal reserves of energy (or fixed carbon).
Phytoplankton chlorophyll (*_Chl)	nc_iV [mg m^{-3}]	Concentration of the chlorophyll a pigment of the population. The four phytoplankton classes have two pigments, a chlorophyll a-based pigment and an accessory pigment. As the pigment concentration adjusts to optimise photosynthesis, including the presence of the accessory pigment, the intracellular content, c_iV, represents only the chlorophyll a-based pigment. As the model does not distinguish between mono-vinyl and di-vinyl forms of chlorophyll, this c_i represents either form, depending on the phytoplankton type.

Table C3. Long name (and variable name) in model output files, symbol and units used in this document, and description of all microalgae state variables in the model. The model contains four categories of phytoplankton (category shown as * in left column, and given in brackets in following list): small (PhyS), $r < 2$ μm phytoplankton; large (PhyL): $r > 2\mu$m phytoplankton; *Trichodesmium* (Tricho): nitrogen fixing phytoplankton; and benthic microalgae (MPB): fast-sinking diatoms that are suspended primarily in the top layer of sediment porewaters. The elemental ratio of phytoplankton including both structural material and reserves is given by: C:N:P = $106(1+R_C^*) : 16(1+R_N^*) : (1+R_P^*)$. In the model description (this document) we have more correctly described fixed carbon as carbon reserves, while in the model outputs they are represented quantified as energy reserves. The relationship is 1 mg C of carbon reserves is equal to $(1060/106)/12.01$ mmol photons of energy reserves.

Name	Symbol	Units	Description
Zooplankton N (ZooS_N, ZooL_N)	Z	[mg N m^{-3}]	Total biomass of nitrogen in animals. With only small and large zooplankton categories resolved, small zooplankton represents the biomass of unicellular fast growing animals (protozoans) and large zooplankton represents the biomass of all other animals (metazoans). All zooplankton have a C:N:P ratio of 106:16:1. Thus the mass of phosphorus of a population with a biomass Z is given by: $\frac{1}{16}\frac{31}{14}Z$ and the mass of carbon by: $\frac{106}{16}\frac{12}{14}$ Z.

Table C4. Long name (and variable name) in model output files, symbol, unit used in this document, and description of zooplankton state variables in the model.

Name	Symbol	Units	Description
Fine Sediment (FineSed)	$FineSed$	[kg m^{-3}]	Identical to Mud-mineral, except that it is initialised to zero in the model domain, and enters only from the catchments.
Dust (Dust)	$Dust$	[kg m^{-3}]	Very small sized, re-suspending particles with a sinking velocity of 1 m d^{-1} and mass-specific optical properties based on observations in Gladstone Harbour.
Mud-mineral (Mud-mineral)	$Mud_{\mathrm{non-CaCO_3}}$	[kg m^{-3}]	Small sized, re-suspending particles with a sinking velocity of 17 m d^{-1}, and mass-specific optical properties based on observations in Gladstone Harbour.
Mud-carbonate (Mud-carbonate)	$Mud_{\mathrm{CaCO_3}}$	[kg m^{-3}]	Small sized, re-suspending particles with a sinking velocity of 17 m d^{-1}, and mass-specific optical properties based on observations of suspended carbonates at Lucinda Jetty.
Sand-mineral (Sand-mineral)	$Sand_{\mathrm{non-CaCO_3}}$	[kg m^{-3}]	Medium sized, re-suspending particles with a sinking velocity of 173 m d^{-1} and mass-specific optical properties based on observations in Gladstone Harbour.
Sand-carbonate (Sand-carbonate)	$Sand_{\mathrm{CaCO_3}}$	[kg m^{-3}]	Medium sized, re-suspending particles with a sinking velocity of 173 m d^{-1} and mass-specific optical properties based on observations of suspended carbonates at Lucinda Jetty.
Gravel-mineral (Gravel-mineral)	$Gravel_{\mathrm{non-CaCO_3}}$	[kg m^{-3}]	Large, non-resuspending particles.
Gravel-carbonate (Gravel-carbonate)	$Gravel_{\mathrm{CaCO_3}}$	[kg m^{-3}]	Large, non-resuspending particles.

Table C5. Long name (and variable name) in model output files, symbol, unit used in this document, and description of all inorganic particulate state variables in the model.

Name	Symbol	Units		Description
Particulate Inorganic Phosphorus (PIP)	PIP	[mg m^{-3}]	P	Phosphorus ions that are absorbed onto particles. It is considered a particulate with the same properties as Mud.
Immobilised Particulate Inorganic Phosphorus (PIPI)	$PIPI$	[mg m^{-3}]	P	Phosphorus that is permanently removed from the system through burial of PIP.
Labile Detritus Nitrogen Plank (DetPL_N)	D_{Red}	[mg m^{-3}]	N	Concentration of N in labile (quickly broken down) organic matter with a C:N:P ratio of 106:16:1 derived from living microalgae, zooplankton, coral host tissue and zooxanthellae with the same C:N:P ratio. Thus the mass of phosphorus in D_{Red} is given by: $\frac{1}{16}\frac{31}{14}D_{Red}$ and the mass of carbon by: $\frac{106}{16}\frac{12}{14}D_{Red}$.
Labile Detritus Nitrogen Benthic (DetBL_N)	D_{Atk}	[mg m^{-3}]	N	Concentration of N in labile (quickly broken down) organic matter with a C:N:P ratio of 550:30:1 derived from living seagrass and macroalgae with the same C:N:P ratio. Thus the mass of phosphorus in D_{Atk} is given by: $\frac{1}{30}\frac{31}{14}D_{Atk}$ and the mass of carbon by: $\frac{550}{30}\frac{12}{14}D_{Atk}$.
Refractory Detritus Carbon (DetR_C)	D_C	[mg m^{-3}]	C	Concentration of carbon as particulate refractory (slowly breaking down) material. It is sourced only from the breakdown of labile detritus, and from rivers.
Refractory Detritus Nitrogen (DetR_N)	D_N	[mg m^{-3}]	N	Concentration of nitrogen as particulate refractory (slowly breaking down) material. It is sourced only from the breakdown of labile detritus, and from rivers.
Refractory Detritus Phosphorus (DetR_P)	D_P	[mg m^{-3}]	P	Concentration of phosphorus as particulate refractory (slowly breaking down) material. It is sourced only from the breakdown of labile detritus, and from rivers.

Table C6. Long name (and variable name) in model output files, symbol, unit used in this document, and description of all particulate detrital state variables in the model.

Name	Symbol	Description
Macroalgae (MA)	MA [g N m^{-2}]	Concentration of nitrogen biomass per m^2 of macrolagae. Macroalgae (or seaweed) grows above all other benthic plants (corals, seagrasses, benthic microalgae). It is parameterised as a non-calcifying leafy algae, with a C:N:P ratio of 550:30:1, and a formulation for calculating the percentage of the bottom covered as $1 - \exp(-\Omega_{MA}\ MA)$. In the model, in the absence of both calcifying macroalgae (particularly *Halimeda*) and unicellular epiphytes, macroalgae represents the biomass of all seaweeds and epiphytes.
Seagrass (SG)	SG [g N m^{-2}]	Concentration of nitrogen biomass per m^2 of a seagrass form parameterised to be similar to *Zostera*. This form captures light after it has passed through macroalgae and before it passes through *Halophila*. This form is better adapted to high light, low nutrient conditions than *Halophila* as a result of a deeper root structure and being able to shade it. See macroalgae for elemental ratio and bottom cover.
Halophila (SGH)	SGH [g N m^{-2}]	Concentration of nitrogen biomass per m^2 of a seagrass form parameterised to be similar to *Halophila ovalis*. This form captures light after it has passed through the *Zostera* seagrass form. The *Halophila ovalis* form is batter adapted to low light conditions than *Zostera*, having a faster growth rate and lower minimum light requirement. See macroalgae for elemental ratio and bottom cover.
Deep seagrass (SGD)	SGD [g N m^{-2}]	Concentration of nitrogen biomass per m^2 of a seagrass form parameterised to be similar to *Halophila deciphens*. This form captures light after it has passed through the *Zostera* and *Halophila ovalis* seagrass form.
*root N	$*ROOT\_N$ [g N m^{-2}]	Concentration of nitrogen biomass per m^2 in the roots of seagrass type * (SG, SGH or SGD). While this biomass in reality exists in multiple depths in the sediments, and in the model accesses multiple layers for nutrient uptake, it is quantified in the epibenthic compartment.

Table C7. Long name (and variable name) in model output files, units, symbol used in this document, and description of macroalgae and seagrass state variables in the model. The order in the above table corresponds to their vertical position, and therefore the order in which they access light. Benthic microalage, being suspended in porewaters, is consider as a particulate in Table C5.

Name	Symbol	Description
Coral host N (CH_N)	CH [g N m^{-2}]	Concentration of nitrogen biomass per m^2 of coral host tissue in the entire grid cell. Unlike other epibenthic variables, corals area is assumed to exist in communities that are potentially smaller than the grid size. The fraction of the grid cell covered by corals is given by A_{CH}. Thus the biomass in the occupied region is given by CH/A_{CH}. The percent coverage of the coral of the bottom for the whole cell is given by $A_{CH}\,(1-\exp(-\Omega_{CH}\ CH/A_{CH}))$. With only one type of coral resolved, CH represents the biomass of all symbiotic corals. Since the model contains no other benthic filter-feeders, CH best represent the sum of the biomass of all symbiotic filter-feeding organisms such as corals, sponges, clams etc. C:N:P is 106:16:1.
Coral symbiont N (CS_N)	CS [mg N m^{-2}]	Concentration of nitrogen biomass per m^2 of coral symbiont cells, or zooxanthellae. To determine the density of cells, use $n = CS/m_N$. The percentage of the bottom covered is given by $\frac{\pi}{2\sqrt{3}} n\pi r_{zoo}^2$ where πr^2 is the projected area of the cell, n is the number of cells, and $\pi/(2\sqrt{3}) \sim 0.9069$ accounts for the maximum packaging of spheres. C:N:P is 106:16:1.
Coral symbiont chl (CS_Chl)	nc_iV [mg chl m^{-2}]	Concentration of chlorophyll biomass per m^2 of coral symbiont cells.
Coral symbiont diadinoxanthin (CS_Xp)	nx_pV [mg pig m^{-2}]	Concentration of the photosynthetic xanthophyll cycle pigment per m^2 of coral symbiont cells.
Coral symbiont diatoxanthin (CS_Xh)	nx_hV [mg pig m^{-2}]	Concentration of heat dissipating xanthophyll cycle pigment biomass per m^2 of coral symbiont cells.

Table C8. Long name (and variable name) in model output files, units, symbol used in this document, and description of coral state variables in the model.

Name	Symbol	Description
Symbiont oxidised RC (CS_Qox)	Q_{ox} [mg N m^{-2}]	Concentration of symbiont reaction centres in an oxidised state per m^2, residing in the symbiont, of in the entire grid cell.
Symbiont reduced RC (CS_Qred)	Q_{red} [mg N m^{-2}]	Concentration of symbiont reaction centres in a reduced state per m^2, residing in the symbiont, of in the entire grid cell.
Symbiont inhibited RC (CS_Qin)	Q_{in} [mg N m^{-2}]	Concentration of symbiont reaction centres in an inhibited state per m^2, residing in the symbiont, of in the entire grid cell.
Symbiont reactive oxygen (CS_RO)	$[ROS]$ [mg N m^{-2}]	Concentration of reactive oxygen per m^2, residing in the symbiont, of in the entire grid cell.

Table C9. Long name (and variable name) in model output files, units, symbol used in this document, and description of coral reaction state variables in the model.

Appendix D: Parameter values used in eReefs biogeochemical model (B3p0).

The below five tables of parameters are specified for each run, and can be automatically generated by the EMS software after a simulation from the parameter file. At model initialisation the model produces a file `ecology_setup.txt` that contains a list of all the parameter values used, both those specified in the parameter file, and those using model defaults.

For a more information see Robson et al. (2018).

Description	Name in code	Symbol	Value	Units
Reference temperature	Tref	T_{ref}	2.000000e+01	Deg C
Temperature coefficient for rate parameters	Q10	$Q10$	2.000000e+00	none
Nominal rate of TKE dissipation in water column	TKEeps	ϵ	1.000000e-06	$m^2\ s^{-3}$
Atmospheric CO2	xco2_in_air	pCO_2	3.964800e+02	ppmv
Concentration of dissolved N2	N2	$[N_2]_{gas}$	2.000000e+03	mg N m^{-3}
DOC-specific absorption of CDOM 443 nm	acdom443star	$k_{CDOM,443}$	1.300000e-04	m^2 mg C^{-1}

Table D1. Environmental parameters in eReefs biogeochemical model (B3p0).

Description	Name in code	Symbol	Value	Units
Chl-specific scattering coef. for microalgae	bphy	b_{phy}	2.000000e-01	m^{-1}(mg Chla m^{-3})$^{-1}$
Nominal N:Chl a ratio in phytoplankton by weight	NtoCHL	$R_{N:Chl}$	7.000000e+00	g N(g Chla)$^{-1}$
Maximum growth rate of PL at Tref	PLumax	μ_{PL}^{max}	1.400000e+00	d^{-1}
Radius of the large phytoplankton cells	PLrad	r_{PL}	4.000000e-06	m
Natural (linear) mortality rate, large phytoplankton	PhyL_mL	$m_{L,PL}$	1.000000e-01	d^{-1}
Natural (linear) mortality rate in sed., large phyto.	PhyL_mL_sed	$m_{L,PL,sed}$	1.000000e+01	d^{-1}
Maximum growth rate of PS at Tref	PSumax	μ_{PL}^{max}	1.600000e+00	d^{-1}
Radius of the small phytoplankton cells	PSrad	r_{PS}	1.000000e-06	m
Natural (linear) mortality rate, small phyto.	PhyS_mL	$m_{L,PS}$	1.000000e-01	d^{-1}
Natural (linear) mortality rate in sed., small phyto.	PhyS_mL_sed	$m_{L,PS,sed}$	1.000000e+00	d^{-1}
Maximum growth rate of MB at Tref	MBumax	μ_{MPB}^{max}	8.390000e-01	d^{-1}
Radius of the MPB cells	MBrad	r_{MPB}	1.000000e-05	m
Natural (quadratic) mortality rate, MPB (in sed)	MPB_mQ	$m_{Q,MPB}$	1.000000e-04	d^{-1}(mg N m^{-3})$^{-1}$
Ratio of xanthophyll to chl a of PS	PSxan2chl	$\Theta_{xan2chl,PS}$	5.100000e-01	mg mg $^{-1}$
Ratio of xanthophyll to chl a of PL	PLxan2chl	$\Theta_{xan2chl,PL}$	8.100000e-01	mg mg $^{-1}$
Ratio of xanthophyll to chl a of MPB	MBxan2chl	$\Theta_{xan2chl,MPB}$	8.100000e-01	mg mg $^{-1}$
Maximum growth rate of Trichodesmium at Tref	Tricho_umax	μ_{MPB}^{max}	2.000000e-01	d^{-1}
Radius of Trichodesmium colonies	Tricho_rad	r_{MPB}	5.000000e-06	m
Sherwood number for the Tricho dimensionless	Tricho_Sh	Sh_{Tricho}	1.000000e+00	none
Linear mortality for Tricho in sediment	Tricho_mL	$m_{L,Tricho}$	1.000000e-01	d^{-1}
Quadratic mortality for Tricho due to phages in wc	Tricho_mQ	$m_{Q,Tricho}$	1.000000e-01	d^{-1}(mg N m^{-3})$^{-1}$
Critical Tricho above which quadratic mortality applies	Tricho_crit		2.000000e-04	mg N m^{-3}
Minimum density of Trichodesmium	p_min	$\rho_{min,Tricho}$	9.000000e+02	kg m^{-3}
Maximum density of Trichodesmium	p_max	$\rho_{max,Tricho}$	1.050000e+03	kg m^{-3}
DIN conc below which Tricho N fixes	DINcrit	DIN_{crit}	1.000000e+01	mg N m^{-3}
Ratio of xanthophyll to chl a of Trichodesmium	Trichoxan2chl	$\Theta_{xan2chl,Tricho}$	5.000000e-01	mg mg $^{-1}$
Minimum carbon to chlorophyll a ratio	C2Chlmin	θ_{min}	2.000000e+01	wt/wt

Table D2. Phytoplankton parameters in eReefs biogeochemical model (B3p0).

Description	Name in code	Symbol	Value	Units
Maximum growth rate of ZS at Tref	ZSumax	μ_{max}^{ZS}	4.000000e+00	d^{-1}
Radius of the small zooplankton cells	ZSrad	r_{ZS}	5.000000e-06	m
Swimming velocity for small zooplankton	ZSswim	U_{ZS}	2.000000e-04	m s^{-1}
Grazing technique of small zooplankton	ZSmeth		rect	none
Maximum growth rate of ZL at Tref	ZLumax	μ_{max}^{ZL}	1.330000e+00	d^{-1}
Radius of the large zooplankton cells	ZLrad	r_{ZL}	3.200000e-04	m
Swimming velocity for large zooplankton	ZLswim	U_{ZL}	3.000000e-03	m s^{-1}
Grazing technique of large zooplankton	ZLmeth		rect	none
Growth efficiency, large zooplankton	ZL_E	E_{ZL}	4.260000e-01	none
Growth efficiency, small zooplankton	ZS_E	E_{ZS}	4.620000e-01	none
Natural (quadratic) mortality rate, large zooplankton	ZL_mQ	$m_{Q,ZL}$	1.200000e-02	d^{-1}(mg N m^{-3})$^{-1}$
Natural (quadratic) mortality rate, small zooplankton	ZS_mQ	$m_{Q,ZS}$	2.000000e-02	d^{-1}(mg N m^{-3})$^{-1}$
Fraction of growth inefficiency lost to detritus, large zoo.	ZL_FDG	γ_{ZL}	5.000000e-01	none
Fraction of mortality lost to detritus, large zoo.	ZL_FDM	N/A	1.000000e+00	none
Fraction of growth inefficiency lost to detritus, small zoo.	ZS_FDG	γ_{ZS}	5.000000e-01	none
Fraction of mortality lost to detritus, small zooplankton	ZS_FDM	N/A	1.000000e+00	none

Table D3. Zooplankton parameters in eReefs biogeochemical model (B3p0).

Description	Name in code	Symbol	Value	Units
Fraction of labile detritus converted to refractory detritus	F_LD_RD	ζ_{Red}	1.900000e-01	none
Fraction of labile detritus converted to DOM	F_LD_DOM	ϑ_{Red}	1.000000e-01	none
fraction of refractory detritus that breaks down to DOM	F_RD_DOM	ϑ_{Ref}	5.000000e-02	none
Breakdown rate of labile detritus at 106:16:1	r_DetPL	r_{Red}	4.000000e-02	d^{-1}
Breakdown rate of labile detritus at 550:30:1	r_DetBL	r_{Atk}	1.000000e-03	d^{-1}
Breakdown rate of refractory detritus	r_RD	r_R	1.000000e-03	d^{-1}
Breakdown rate of dissolved organic matter	r_DOM	r_O	1.000000e-04	d^{-1}
Respiration as a fraction of umax	Plank_resp	ϕ	2.500000e-02	none
Oxygen half-saturation for aerobic respiration	KO_aer	K_{OA}	2.560000e+02	mg O m^{-3}
Maximum nitrification rate in water column	r_nit_wc	$\tau_{nit,wc}$	1.000000e-01	d^{-1}
Maximum nitrification rate in water sediment	r_nit_sed	$\tau_{nit,sed}$	2.000000e+01	d^{-1}
Oxygen half-saturation for nitrification	KO_nit	$K_{O_2,nit}$	5.000000e+02	mg O m^{-3}
Rate at which P reaches adsorbed/desorbed equilibrium	Pads_r	τ_{Pabs}	4.000000e-02	d^{-1}
Freundlich Isothermic Const P adsorption to TSS in wc	Pads_Kwc	$k_{Pads,wc}$	3.000000e+01	mg P kg TSS^{-1}
Freundlich Isothermic Const P adsorption to TSS in sed	Pads_Ksed	$k_{Pads,sed}$	7.400000e+01	mg P kg TSS^{-1}
Oxygen half-saturation for P adsorption	Pads_KO	$K_{O_2,abs}$	2.000000e+03	mg O m^{-3}
Exponent for Freundlich Isotherm	Pads_exp	N/A	1.000000e+00	none
Maximum denitrification rate	r_den	τ_{denit}	8.000000e-01	d^{-1}
Oxygen half-saturation constant for denitrification	KO_den	$K_{O_2,denit}$	1.000000e+04	mg O m^{-3}
Rate of conversion of PIP to immobilised PIP	r_immob_PIP	τ_{Pimm}	1.200000e-03	d^{-1}

Table D4. Detritus parameters in eReefs biogeochemical model (B3p0).

Description	Name in code	Symbol	Value	Units
Sediment-water diffusion coefficient	EpiDiffCoeff	D	3.000000e-07	$m^2\ s^{-1}$
Thickness of diffusive layer	EpiDiffDz	h	6.500000e-03	m
Maximum growth rate of MA at Tref	MAumax	μ_{MA}^{max}	1.000000e+00	d^{-1}
Natural (linear) mortality rate, macroalgae	MA_mL	ζ_{MA}	1.000000e-02	d^{-1}
Nitrogen-specific leaf area of macroalgae	MAleafden	Ω_{MA}	1.000000e+00	$m^2\ g\ N^{-1}$
Respiration as a fraction of umax	Benth_resp	ϕ	2.500000e-02	none
net dissolution rate of sediment without coral	dissCaCO3_sed	d_{sand}	1.000000e-03	$mmol\ C\ m^{-2}\ s^{-1}$
Grid scale to reef scale ratio	CHarea	A_{CH}	1.000000e-01	$m^2\ m^{-2}$
Nitrogen-specific host area of coral polyp	CHpolypden	Ω_{CH}	2.000000e+00	$m^2\ g\ N^{-1}$
Max. growth rate of Coral at Tref	CHumax	μ_{CH}^{max}	5.000000e-02	d^{-1}
Max. growth rate of zooxanthellae at Tref	CSumax	μ_{CS}^{max}	4.000000e-01	d^{-1}
Radius of the zooxanthellae	CSrad	r_{CS}	5.000000e-06	m
Quadratic mortality rate of coral polyp	CHmort	ζ_{CH}	1.000000e-02	$(g\ N\ m^{-2})^{-1}\ d^{-1}$
Linear mortality rate of zooxanthellae	CSmort	ζ_{CS}	4.000000e-02	d^{-1}
Fraction of coral host death translocated.	CHremin	f_{remin}	5.000000e-01	-
Rate coefficent for particle uptake by corals	Splank	S_{part}	3.000000e+00	$m\ d^{-1}$
Maximum daytime coral calcification	k_day_coral	k_{day}	1.320000e-02	$mmol\ C\ m^{-2}\ s^{-1}$
Maximum nightime coral calcification	k_night_coral	k_{night}	6.900000e-03	$mmol\ C\ m^{-2}\ s^{-1}$
Carbonate sediment dissolution rate on shelf	dissCaCO3_shelf	d_{shelf}	1.000000e-04	$mmol\ C\ m^{-2}\ s^{-1}$
Age tracer growth rate per day	ageing_decay	n/a	1.000000e+00	$d\ d^{-1}$
Age tracer decay rate per day outside source	anti_ageing_decay	Φ	1.000000e-01	d^{-1}
Bleaching ROS threshold	ROSthreshold	ϕ_{ROS}	5.000000e-04	$mg\ O\ cell^{-1}$
Xanthophyll switching rate coefficient	Xanth_tau	τ_{xan}	8.333333e-04	s^{-1}
Ratio of RCII to Chlorophyll a	chla2rcii	A_{RCII}	2.238413e-06	$mol\ RCII\ g\ Chl^{-1}$
Stoichiometric ratio of RCII units to photons	photon2rcii	m_{RCII}	1.000000e-07	$mol\ RCII\ mol\ photon^{-1}$
Maximium zooxanthellae expulsion rate	ROSmaxrate	γ	1.000000e+00	d^{-1}
Scaling of DetP to DOP, relative to N	r_RD_NtoP	r_{RD_NtoP}	2.000000e+00	-
Scaling of DOM to DIP, relative to N	r_DOM_NtoP	r_{DOM_NtoP}	1.500000e+00	-
Radius of Trichodesmium colonies	Tricho_colrad	$r_{Trichocolony}$	5.000000e-06	m

Table D5. Benthic parameters in eReefs biogeochemical model (B3p0), excluding seagrass

Description	Name in code	Symbol	Value	Units
Maximum growth rate of SG at Tref	SGumax	μ_{SG}^{max}	4.000000e-01	d^{-1}
Half-saturation of SG N uptake in SED	SG_KN	$K_{SG,N}$	4.200000e+02	mg N m^{-3}
Half-saturation of SG P uptake in SED	SG_KP	$K_{SG,P}$	9.600000e+01	mg P m^{-3}
Natural (linear) mortality rate aboveground seagrass	SG_mL	ζ_{SG_A}	3.000000e-02	d^{-1}
Natural (linear) mortality rate belowground seagrass	SGROOT_mL	ζ_{SG_B}	4.000000e-03	d^{-1}
Fraction (target) of SG biomass below-ground	SGfrac	$f_{below,SG}$	7.500000e-01	-
Time scale for seagrass translocation	SGtransrate	$\tau_{tran,SG}$	3.330000e-02	d^{-1}
Nitrogen-specific leaf area of seagrass	SGleafden	Ω_{SG}	1.500000e+00	m^2 g N^{-1}
Seagrass seed biomass as fraction of 63 % cover	SGseedfrac	$f_{seed,SG}$	1.000000e-02	-
Sine of nadir Zostera canopy bending angle	SGorient	$\sin\beta_{blade,SG}$	5.000000e-01	-
Compensation irradiance for Zostera	SGmlr	$E_{comp,SG}$	4.500000e+00	mol m^{-2}
Maximum depth for Zostera roots	SGrootdepth	$z_{root,SG}$	-1.500000e-01	m
Critical shear stress for SG loss	SG_tau_critical	$\tau_{SG,shear}$	1.000000e+00	N m^{-2}
Time-scale for critical shear stress for SG loss	SG_tau_time	$\tau_{SG,time}$	4.320000e+04	s
Maximum growth rate of SGH at Tref	SGHumax	μ_{SGH}^{max}	4.000000e-01	d^{-1}
Half-saturation of SGH N uptake in SED	SGH_KN	$K_{SGH,N}$	4.200000e+02	mg N m^{-3}
Half-saturation of SGH P uptake in SED	SGH_KP	$K_{SGH,P}$	9.600000e+01	mg P m^{-3}
Nitrogen-specific leaf area of SGH	SGHleafden	Ω_{SGH}	1.900000e+00	m^2 g N^{-1}
Natural (linear) mortality rate, aboveground SGH	SGH_mL	ζ_{SGH_A}	6.000000e-02	d^{-1}
Natural (linear) mortality rate, belowground SGH	SGHROOT_mL	ζ_{SGH_B}	4.000000e-03	d^{-1}
Fraction (target) of SGH biomass below-ground	SGHfrac	$f_{below,SGH}$	5.000000e-01	-
Time scale for Halophila translocation	SGHtransrate	$\tau_{tran,SGH}$	3.330000e-02	d^{-1}
Halophila seed biomass as fraction of 63 % cover	SGHseedfrac	$f_{seed,SGH}$	1.000000e-02	-
Sine of nadir Halophila canopy bending angle	SGHorient	$\sin\beta_{blade,SGH}$	1.000000e+00	-
Compensation irradiance for Halophila	SGHmlr	$E_{comp,SGH}$	2.000000e+00	mol m^{-2}
Maximum depth for Halophila roots	SGHrootdepth	$z_{root,SGH}$	-8.000000e-02	m
Critical shear stress for SGH loss	SGH_tau_critical	$\tau_{SGH,shear}$	1.000000e+00	N m^{-2}
Time-scale for critical shear stress for SGH loss	SGH_tau_time	$\tau_{SGH,time}$	4.320000e+04	s

Table D6. Seagrass parameters in eReefs biogeochemical model (B3p0).

Description	Name in code	Symbol	Value	Units
Maximum growth rate of SGD at Tref	SGDumax	μ_{SGD}^{max}	4.000000e-01	d^{-1}
Half-saturation of SGD N uptake in SED	SGD_KN	$K_{SGD,N}$	4.200000e+02	mg N m^{-3}
Half-saturation of SGD P uptake in SED	SGD_KP	$K_{SGD,P}$	9.600000e+01	mg P m^{-3}
Nitrogen-specific leaf area of SGD	SGDleafden	Ω_{SGD}	1.900000e+00	m^2 g N^{-1}
Natural (linear) mortality rate, aboveground SGD	SGD_mL	ζ_{SGD_A}	6.000000e-02	d^{-1}
Natural (linear) mortality rate, belowground SGD	SGDROOT_mL	ζ_{SGD_B}	4.000000e-03	d^{-1}
Fraction (target) of SGD biomass below-ground	SGDfrac	$f_{below,SGD}$	2.500000e-01	-
Time scale for deep SG translocation	SGDtransrate	$\tau_{tran,SGD}$	3.330000e-02	d^{-1}
Deep SG seed biomass as fraction of 63 % cover	SGDseedfrac	$f_{seed,SGD}$	1.000000e-02	-
Sine of nadir deep SG canopy bending angle	SGDorient	$\sin\beta_{blade,SGD}$	1.000000e+00	-
Compensation irradiance for deep SG	SGDmlr	$E_{comp,SGD}$	1.500000e+00	mol m^{-2}
Maximum depth for deep SG roots	SGDrootdepth	$z_{root,SGD}$	-5.000000e-02	m
Critical shear stress for deep SG loss	SGD_tau_critical	$\tau_{SGD,shear}$	1.000000e+00	N m^{-2}
Time-scale for shear stress for deep SG loss	SGD_tau_time	$\tau_{SGD,time}$	4.320000e+04	s

Table D7. Deep seagrass parameters in eReefs biogeochemical model (B3p0).